ISSN: 0128-7680

Pertanika Journal of SCIENCE & TECHNOLOGY

VOLUME 8 NO.1
JANUARY 2000

A scientific journal published by Universiti Putra Malaysia Press

Pertanika Journal of Science & Technology

About the Journal

Pertanika, the poineer journal of UPM, began publication in 1978. Since then, it has established itself as one of the leading multidisciplinary journals in the tropics. In 1992, a decision was made to streamline Pertanika into three journals to meet the need for specialised journals in areas of study aligned with the strengths of the univeristy. These ara **(i) Pertanika Journal of Tropical Agricultural Science, (ii) Pertanika Journal of Science and Technology (iii) Pertanika Journal of Social Science and Humanities**.

Aims and Scope

Pertanika Journal of Science and Technology welcomes full papers and short communications in English or Bahasa Melayu in the fields of chemisty, physics, mathematics and statistics, engineering, environmental control and management, ecology and computer science. It is published twice a year in January and July.

Articles must be reports of research not previously or simultaneously published in other scientific or technical journals.

Communications are notes of a significant finding intended for rapid publication. It should not exceed five double-spaced typerwritten pages and must be accompanied by a letter from the author justifying its publication as a communication.

Reviews are critical appraisals of literature in areas that are of interest to a broad spectrum of scientists and researchers. Review papers will be published upon invitation.

Submission of Manuscript

Three complete clear copies of the manuscript are to be submitted to

The Chief Editor
Pertanika Journal of Science and Technology
Universiti Putra Malaysia
43400 UPM Serdang, Selangor Darul Ehsan
MALAYSIA
Tel: 89486101 Ext: 1326; Fax (603)89416172

Proofs and Offprints

Page proofs, illustration proofs, the copy-edited manuscript and an offprint order form will be sent to the author. Proofs must be checked very carefully within the specified time as they will not be proofread by the Press editors.

Authors will receive 20 offprints of each article. Additional copies can be ordered from the Secretary of the Editorial Board by filling out the offprint order form.

Published by Universiti Putra Malaysia Press
ISSN No.: 0128-7680

Pertanika Journal of Science & Technology

Volume 8 No. 1, 2000

Contents

ISSN: 0128-7680
Pertanika J. Sci. & Technol. **8(1)**: 1 - 18 (2000)

Diffusion Coefficient Estimations by Thin-Channel Column Inverse Gas Chromatography : Preliminary Experiments

Mohd. Ghazali Mohd. Nawawi
Department of Chemical Engineering
Faculty of Chemical & Natural Resources Engineering
Universiti Teknologi Malaysia
Skudai, Johor, Malaysia

Received 27 May 1998

ABSTRAK

Suatu turus saluran-cetek kromatografi gas telah direkabentuk dan diguna untuk menentukan pekali resapan air dan isopropanol dalam fasa polimer melalui teknik kromatografi gas songsang. Teknik ini adalah suatu teknik yang mudah, cepat dan berkesan sebagai gantian kepada kaedah erapan dan nyaherapan bagi menentukan pekali resapan bagi bahan telapan dalam berbagai filem membran polimer; teknik ini terutamanya berguna apabila masalah yang berkaitan dengan ketidakseimbangan taburan polimer menghadkan ketepatan pengukuran oleh kromatografi gas songsang. Suatu lapisan membran kitosan yang homogen telah disediakan melalui teknik tuang larutan dan digunakan sebagai fasa tetap sebagai lapisan polimer yang sekata dalam turus kromatografi gas. Penemuan awal menunjukkan bahawa pekali resapan air adalah lebih tinggi daripada pekali resapan isopropanol dan pekali resapan bertambah dengan suhu turus. Kesan saiz bahan telapan pada pekali resapan juga telah dikaji ke atas suatu siri alkohol : metanol, etanol dan isopropanol. Keputusannya mencadangkan pekali resapan dipengaruhi oleh saiz bahan telapan.

ABSTRACT

A thin-channel gas chromatography column was designed and used to measure diffusion coefficients of water and isopropanol in polymer phase via inverse gas chromatography (IGC) technique. The thin-channel column inverse gas chromatography technique proved to be a simple, fast and efficient alternative to sorption and desorption methods for measuring diffusion coefficients of permeants in thin polymer membranes films; the technique is especially useful when the problems associated with the irregularity of polymer distribution severely limit the accuracy of IGC measurement. Thin homogeneous chitosan membranes prepared by the solution casting technique were used as the stationary phase to provide a relatively uniform layer of polymer phase in the gas chromatography column. The diffusion coefficient of water was higher than that of isopropanol and diffusion coefficients of the permeants increased with column temperature. The effects of permeants size on diffusion coefficients were investigated on a series of alcohols: methanol, ethanol and isopropanol. The diffusion coefficients were inversely related to the permeants size.

Keywords: thin-channel column, gas chromatography, inverse gas chromatography, chitosan, membrane, isopropanol, water, diffusion coefficient

INTRODUCTION

Gas chromatography (GC) has become well established as an alternative for studying the interaction of polymers with volatile solutes years ago [1,2,3]. In a typical application, the polymer is used as the stationary phase in a chromatography column. The solute or probe is vaporized and injected into a carrier gas flowing through the column. As the probe is swept through the column, it can interact with the polymer via adsorption or absorption. The retention time of the probe and the shape of the elution profile (i.e. chromatographic peak) will reflect the strength and nature of the interactions that occur between the polymer and the solute and can be used to study those interactions. Such an experiment is sometimes referred to as inverse gas chromatography (IGC), to differentiate it from the more common analytical application of gas chromatography.

In general, IGC has been used primarily for the measurement of solution thermodynamic parameters. When an IGC experiment is carried out at temperatures significantly higher than the glass transition temperature of the polymeric stationary phase, the retention time will be determined by the solubility of that component in the polymer. Consequently, measurements of retention time can be used to calculate such useful parameters as Henryís law constant, the activity coefficient, and various solution model interaction parameters. In comparison with bulk equilibrium methods (gravimetric sorption/desorption) for thermodynamic measurements, IGC offers several advantages. The foremost among these is speed: a single IGC experiment can be completed in minutes; a vapor sorption experiment may require hours or days to complete.

In principle, IGC experiments can also be used to obtain information about the diffusion of the solute in the polymer phase. It has long been recognized that mass-transport limitations in the stationary phase result in significant spreading and distortion of a chromatography peak. A number of researchers have attempted to exploit this phenomenon as a means of measuring the diffusion coefficient of the solvent in the stationary phase [3-6]. In all of these studies, packed-column chromatography was used and diffusion coefficient estimates were extracted from the elution curve data using the van Deemter equation. None of these efforts has provided a convincing demonstration that the method can be used to obtain meaningful information; difficulties inherent in the use of a packed column make it nearly impossible to relate the measured elution curve to the diffusion coefficient. The major limitation is the irregular distribution of polymer within the column, which prohibits the application of realistic models for stationary phase transport processes. The van Deemter analysis assumes a uniform distribution of polymer. In any real packed column, the distribution will not be uniform and will be difficult to characterize. Pawlisch and Laurence [7,8] developed a modified mathematical model for the diffusion of solutes at infinite dilution in thin, uniform polymer films coated on glass capillary columns. Measurements were made for benzene, toluene, and ethylbenzene in polystyrene for 110° – 140 °C. The resulting values of the

diffusion coefficients were in good agreement with extrapolated values from sorption experiments [9,10].

In a pervaporation process, diffusion coefficients of permeating components in polymers in general depend strongly on the state of swelling of the polymer because of the plasticizing action of the liquid on the segmental motions of the polymer. In general, two methods have been widely used to obtain diffusion coefficients: the absorption experiment method [11,12] and the desorption experiment [13 - 15]. The two methods are based on the unsteady state process and are complicated. The experimental results are very sensitive to the accuracy of measurements. Fels and Huang [14] and Rhim and Huang [15] tried to determine the diffusion coefficients of organic components in polyethylene from desorption experiments and applied the resulting diffusion coefficients to their equations for predicting the behavior of the pervaporation process. However, the results of the comparison of the calculated data with the experimental data were not fully satisfactory. Despite the advantages and despite the widespread use of IGC, to date no attempts to utilize the use of gas chromatography to determine diffusion coefficients applicable to pervaporation process have been reported in the literature.

In this study we report the estimation of diffisuvities, methanol, ethanol, and isopropanol in the stationary column membrane made from chitosan using inverse gas chromatography method. Effects of temperature and permeant size on diffusivity have been established. A significant improvement for the diffusivity measurements by the IGC method specifically applicable to the falt-sheet pervaporation membranes have been achieved. The technique uses a specially designed column based on the concept of a thin-channel columns where a highly uniform polymer membrane is used as the stationary phase. The thin-channel column offers great improvement over the conventional packed columns where the irregularity of the coating severely limits measurement accuracy. Such a column may be used in preference to the capillary column for diffusivity studies of solutes especially in membrane research since the same membrane used in the separation processes may be employed as the stationary phase in the column.

Theory

Diffusion processes on gas chromatographic columns lead to broadening of the chromatographic peak. In traditional gas chromatography, the peak broadening is directly related to the resolving power of the columns and as such has received extensive theoretical interest [2,16]. There are two major factors that contribute to peak broadening: diffusion of the injected compound (probe) in the carrier gas and diffusion of the probe in the stationary phase. The former is characterized by the gas-phase mutual diffusion coefficient, D_g, and the latter factor is related to the liquid-phase mutual diffusion coefficient, D_L.In the case of IGC experiments, where a polymer is the stationary phase, D_L is a polymer-probe diffusion coefficient.

We will follow the standard chromatographic approach in expressing the distribution of a probe on the column by means of the height equivalent to a

theoretical plate (HETP), *H*. HETP is related to the number of theoretical plates *N* and to the physical length of the column *L* as

$$H = \frac{L}{N} \tag{1}$$

The measurements of effective diffusion coefficients were based on the well known equation developed by van Deemter et al. [17] for a gas chromatographic column:

$$H = \mathrm{A} + \frac{B}{u} + Cu \tag{2}$$

where u is the linear velocity of carrier gas and A, B and C are constants of the column, gases and operating conditions.

On packed columns, A is called the eddy diffusion term and is related to the size of the support particles and the irregularity of packing. The constant B describes the time-dependent factors; only the longitudinal diffusion of the probe, along the stream of the carrier gas, contributes significantly to B. The third term in eqn. (2) is related to peak broadening, which is due to solute/ stationary phase resistance to mass transfer within the column. The constant C is given by

$$C = \frac{8}{\pi} \frac{K}{(1 + K)^2} \frac{d^2}{D_L} \tag{3}$$

where d is the thickness of the stationary phase, D_L is the solute diffusion coefficient in the liquid phase, and K is the partition ratio given by

$$K = \frac{t_r - t_m}{t_m} \tag{4}$$

where t_r and t_m are the retention time to peak minimum of the probe molecule and a non-interacting material such as methane.

The simple version of the van Deemter equation, eqn. (3), does not consider broadening effects due to the non-instantaneous equilibration of vapor phase across the column by molecular or hydrodynamic mass transfer [18]. Trans-column diffusion in the gas phase is assumed to be fast compared with diffusion through the stationary phase. Furthermore, the assumptions used to derive the C term are unrealistic for most practical gas chromatography columns where the geometry of the column packing is very complex. Giddings [19] has developed a nonequilibrium treatment which enables calculation of peak dispersion in more complex cases by redefining the C term to take account, various dispersion factors. In the case of uniform film thickness, Giddings results are the same as that for the van Deemster C term but with the constant $8/\pi$ replaced by *2/3*. So eqn. (3) which becomes,

$$C = \frac{2}{3}\frac{K}{(1+K)^2}\frac{d^2}{D_L} \tag{5}$$

Equation (2) is only valid for describing the elution of symmetric peaks, which requires that mass-transfer resistances be small but not negligible. Equation (2) then becomes

$$H = A + \frac{B}{u} + \frac{2}{3}\frac{K}{(1+K)^2}\frac{d^2}{D_L}u \tag{6}$$

The determination of D_L involves the measurement of H at several relatively high flow rate, where the term B/u is negligible and A remains suitably small. The slope obtained in a plot of H versus u enables one to calculate D_L, since K can be directly obtained from these experiments. Thus

$$H = \frac{2}{3}\frac{K}{(1+K)^2}\frac{d^2}{D_L}u \tag{7}$$

From plate theory, it can be shown that for a column producing Gaussian-shaped peaks, H is related to the peak width or variance by [2]

$$H = L\left(\frac{\sigma_t}{t_r}\right)^2 = \frac{L}{5.54}\left(\frac{W_{1/2}}{t_r}\right)^2 \tag{8}$$

where σ_t^2 is the variance of the peak and $W_{1/2}$ is the peak width at half the peak height.

MATERIALS AND METHODS

Chitosan flakes of Flonac-N grade were obtained from Kyowa Technos Co. Ltd. Japan. Reagent grade acetic acid was purchased from Canlab, Canada. Isopropanol, ethanol and methanol obtained from Commercial Alcohols Inc. Canada were of reagent grade. Gases used for the operation of the chromatograph were supplied by Praxair, Kitchener, Ontario. A high-purity helium was used as the carrier gas, dry-grade compressed air and hydrogen were used for the flame ionization detector (FID), and methane was used as the non-interacting material.

A Hewlett Packard 5890 Series II gas chromatography equipped with both Flame Ionization Detector (FID) and Thermal Conductivity Detector (TCD) was used for the inverse gas chromatography experiments. *Fig. 1* gives a schematic of the apparatus. A hydration system is used to saturate the carrier gas with water vapour in order to swell the stationary phase to a certain extent. The flow rate of the carrier gas was controlled by a thermostated precision needle valve and was measured by soap bubble flowmeter. A 10-µl Hamilton syringe was used to inject the probes. A specially designed column is used and will be further discussed in the next section.

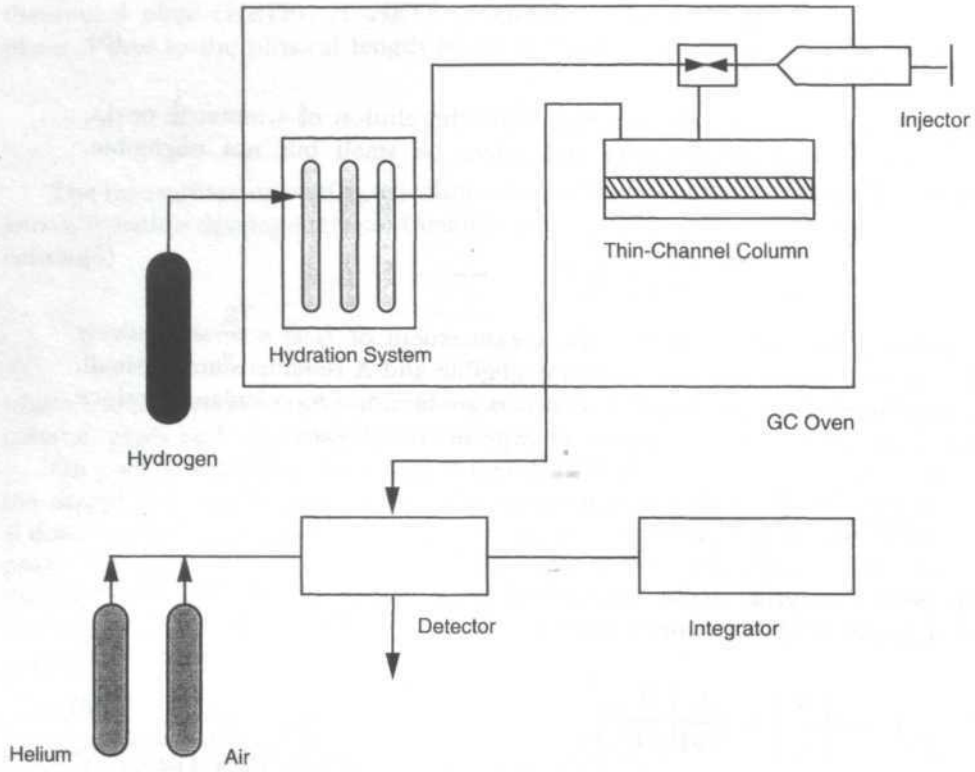

Fig 1. A schematic diagram of the apparatus used for the IGC: (1) GC oven; (2) thin-channel column; (3) hydration system; (4) detector; (5) integrator; (6) injector; (7) hydrogen; (8) helium; (9) air.

The Thin-Channel Column

The column was designed based on the concept of a spiral thin-channel system normally used for a cross-flow ultrafiltration unit. *Fig. 2* gives a schematic of the column. The column consists of two parts: the top part or the thin-channel plate and the bottom part where the stationary phase was placed. The parts were sealed together with bolts and nuts. The finished column had a thin-channel with dimensions of 3 mm in depth, 3 mm in width and 126 cm in length. The solute concentration-time profile was observed by the detector from the introduction of the solute at the injection point to its emergence at the outlet. The stationary phase which was actually a thin layer of homogeneous dense chitosan membrane was prepared according to the preparation of the pervaporation membranes [16].

Theoretically, this thin-channel gas chromatography column features a significant improvement over the more conventional packed columns. Firstly, a thin layer of dense membrane can be used as the stationary phase; in general, casting a dense membrane layer is less difficult and less time-consuming than

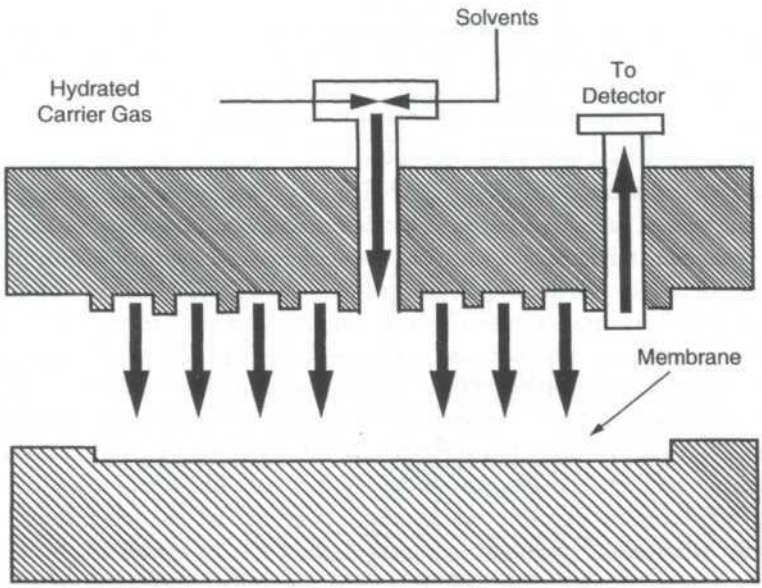

Fig 2. A schematic diagram of thin-channel GC column

preparing a packed column or coating the inner wall of a small tube. Secondly, the thickness of the stationary phase can easily be adjusted. Thirdly, the membrane can be directly cast onto the column, and most importantly, a more regular polymer distribution can be obtained.

Stationary Phase Preparation

The stationary phase consists of a thin layer of chitosan dense membrane. The membrane was prepared from a homogeneous 0.5 wt. % chitosan in acetic acid aqueous casting solution. The procedure (*Fig. 3*) involved dissolution of chitosan polymer in acetic acid to form the casting solution, casting of the polymer solution onto a glass plate to form a membrane film, treatment in sodium hydroxide solution to regenerate chitosan, washing to remove traces of alkaline solution, and drying in air to evaporate the solvent.

Experimental Procedure

The procedure for obtaining an elution curve was simple. After the GC reached stable, steady-state operations, a small amount of solvent, in liquid or vapour state, was injected into the carrier gas depending on the type of detector used, flame ionization (FID) or thermal conductivity detector (TCD). FID is only sensitive to organic substances, whereas TCD is sensitive to both organic substances and water. Vapour samples were injected into the carrier gas at the injection point (*Fig. 4*) to obtain elution curves and retention times of the probes in the swollen stationary phase and FID was used to measure the amount of solvent in the carrier gas leaving out of the column. The injection unit was

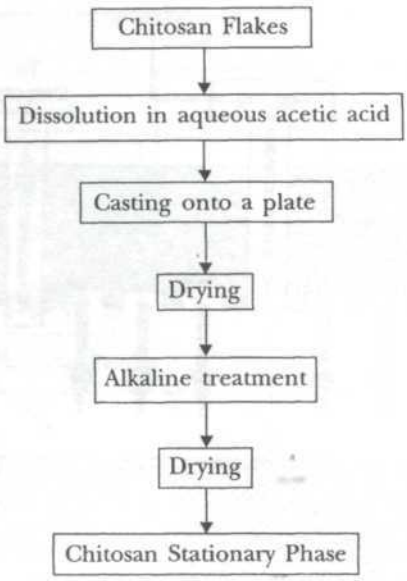

Fig. 3 Sequence of preparation of chitosan film stationary phase

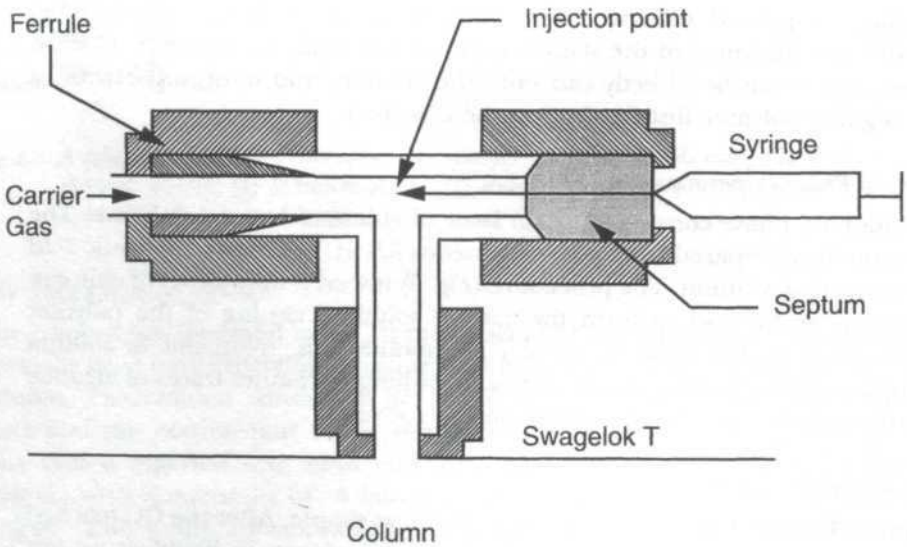

Fig 4. A schematic of the injection point of the thin-channel column

designed using a Swagelok T fitting (with an outside diameter of 3.18 mm and inside diameter of approximately 3 mm) which was directly connected to the column to minimize dead spaces or mixing. Sudden diameter changes of the fitting at the injection point that may create dead spaces or mixing was minimized. The injection unit was used in which the needle of the syringe can

be extended to the head of the column to further reduce dead spaces or mixing at the injection point. Similar design was used at the outlet point; a Swagelok fitting with an inside diameter of 3 mm allowed the column to be fastened directly to the detector.

In contrast, liquid samples were injected into the carrier gas to obtain elution curves and to determine retention times of the probes in dry stationary phase and TCD was used to measure the amount of solvent in the carrier gas leaving out the column. The liquid samples were injected through a heated injection point at 200 °C to ensure complete vaporization of the liquids. The carrier gas flow outlet flow rate was measured using a soap bubble flow meter.

The output from the gas chromatographic detector was fed to a Hewlett Packard HP 3396 Series II integrator. The experimental determination of $W_{1/2}$ and t_r was performed in triplicate for each flow rate and temperature, and an average plate height, H, was calculated. The linear portion of a graph of H vs.u was used to calculate C in the van Deemter equation (2). The value of the diffusion coefficient in the polymer membrane was calculated from C using eqn. (3). The thickness of the membrane was measured manually by using a Mitutoyo MDC Series 293 digimatic micrometer.

Measurement of Variance of Peak on Slightly Asymmetrical Peaks

When the eluted peak has a symmetrical, Gaussian profile, both the plate height, H, and the peak variance, st are easily measured. However, peaks are seldom perfectly symmetrical and the methods used to determine the necessary parameters depends very much on the degree of the asymmetry of the peaks. In this study, a simple method was used to estimate peak variance from tailed peaks obtained from the chromatogram of the solutes. This method of finding the variance involved drawing tangents on the strip-chart chromatogram through the points of inflection, i.e., steepest-slope tangents on the sides of the peak. In *Fig. 5*, the tangents are shown as intersecting the baseline at "initial" and "final" peak times, t_i and t_f. The peak variance was determined by using the equation (2)

$$\sigma_t = \frac{1}{2}\left(t_+ + t_-\right) \tag{8}$$

RESULTS AND DISCUSSION

The thin-channel column with the chitosan membrane stationary phase was used to investigate the partition coefficients of water and isopropanol. *Fig. 6* shows the effects of carrier gas velocity, u, on the partition coefficient K for both water and isopropanol at 30 °C. The small variations (near-zero slope) of K with u indicate that the partition coefficients of water and isopropanol are not dependent on the carrier gas velocity. Hence, we are justified to use the van Deemter equation to estimate diffusion coefficients of water and isopropanol in chitosan stationary phase using the thin-channel column.

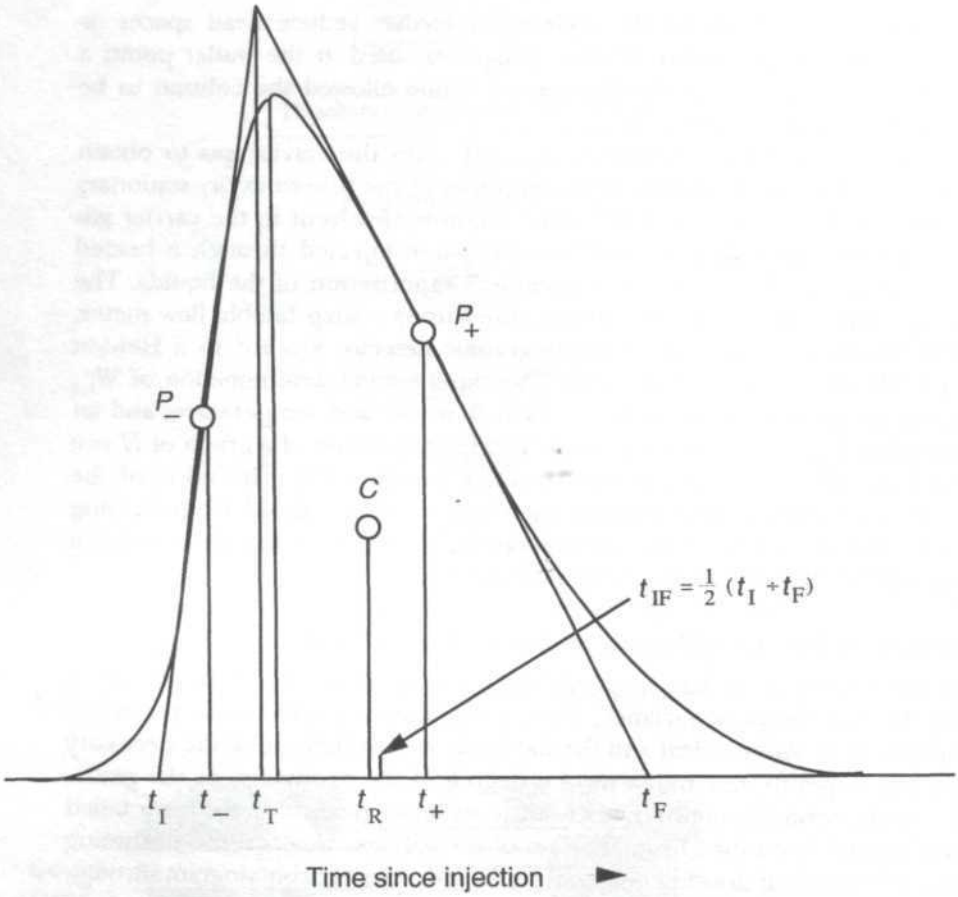

Fig 5. Times on peak concentration profile measured from mass center of injection profile, P- and P+ are the points of inflection

The thin-channel column GC technique was used to study the partition coefficients and diffusion coefficients of isopropanol, ethanol, methanol and water in the stationary phase chitosan membrane. The results of a series of experiments to measure the amount of peak spreading as a function of flow rate at room temperature are shown in *Fig. 7.* At sufficiently high flow rates, *H* increases linearly with u, with gradient C given by the simple van Deemter expression where applicable. In general, the plate heights for these experiments on polymer stationary phases are much higher than the 0.5 - 2 mm values for *H* aimed for in analytical gas chromatography [18]. High plate heights may be rationalized by considering the nature of the chitosan polymer with a glass transition temperature, T_g of about 101 °C [20]. At room temperature, chitosan contains crystalline regions which are not penetrated by the probe molecule and amorphous or rubbery regions. The rate of diffusion through this material is much slower than through the usual liquid stationary phases used in gas

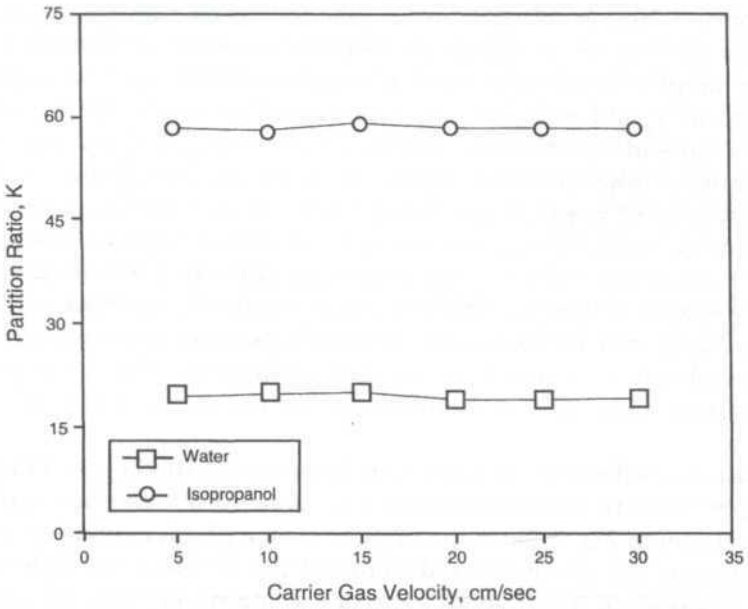

Fig 6. Partition coefficients of water and isopropanol as a function of the linear carrier gas velocity

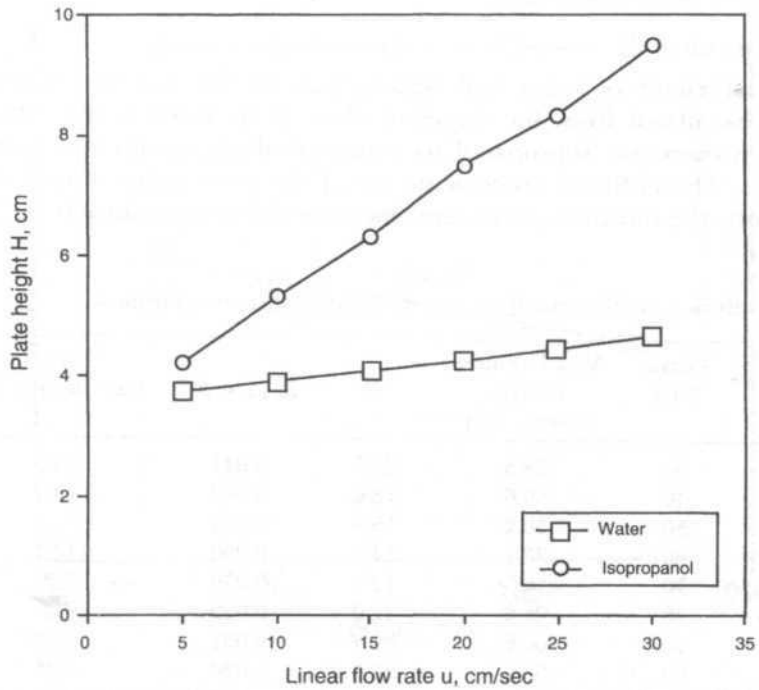

Fig 7. van Deemter curves for the thin-channel column with chitosan film stationary phase

chromatography. At temperatures below T_g, the molecular movements of the chitosan chains are limited to segmental vibrations at about a relatively fixed position. The amptitude of segmental vibration increases with increasing temperature up to T_g and at T_g; the chain segments have sufficient energy to perform rotational and translational motions or short-range diffusion motion. The plate heights of isopropanol are higher than that of water indicating that the rate of diffusion of isopropanol through the chitosan stationary phase is slower than that of water. This is not unexpected because water molecule is smaller than isopropanol molecule and generally, highly hydrophilic chitosan stationary phase exhibits stronger affinity to water relative to isopropanol. Note that this is consistent with the results obtained in the pervaporation experiments with isopropanol/water mixtures where the permeation flux of water is significantly higher than that of isopropanol for the entire range of feed composition.

The diffusion coefficients of water and isopropanol in the dry chitosan membrane at 30 °C were determined from the slope of the corresponding H versus u plots shown in *Fig. 7*. Since the slope of such a plot is equivalent to the C term in equation (2), the numerical values of the diffusion coefficients of water and isopropanol in the chitosan stationary phase could be calculated for the corresponding K values. The results are tabulated in Table 1. As expected, the diffusion coefficient of water in the chitosan membrane is larger than that of isopropanol.

Effects of Temperature

Diffusion coefficients of water and isopropanol for the chitosan stationary phase were calculated from the slopes of H vs. u. In Table 1, the diffusion coefficients of water and isopropanol are summarized along with the operating temperatures. The diffusion coefficients are of the same order of magnitude and apparently the diffusion coefficients increase with temperature from 30 to

TABLE 1
Diffusion coefficients from gas chromatography measurements

Probe	Temp. (°C)	Van Deemter C term (see 3 10^2)	K	$K/(1+K)^2$	D_L (cm^2/sec) 3 10^7
Water	30	28.5	20.7	0.044	1.03
	40	30.6	18.0	0.050	1.07
	50	30.2	16.6	0.054	1.17
	60	33.1	14.6	0.060	1.21
	70	36.5	12.3	0.070	1.28
Isopropanol	30	95.2	32.0	0.029	0.20
	40	66.6	29.7	0.032	0.32
	50	53.3	25.6	0.036	0.45
	60	48.4	21.9	0.042	0.58
	70	47.5	17.2	0.052	0.73

70 °C. An increase in temperature provides energy for a general increase in segmental motion. If the energy density is sufficient, the polymer may pass through structural transitions such as the T_g, which further affects the diffusion process. Above T_g, in the rubbery state, the segmental motion is rapid but molecular motion is still restricted by chain entanglements. As temperature increases, the degree of entanglement decreases and molecular slip increases. The effects of an increase in temperature may also be expressed in terms of the increase in free volume directly related to the bulk expansion of the polymer due to the increased segmental motions.

As shown in *Fig. 8*, the temperature dependence of diffusion coefficients, D_L over small temperature ranges can be represented by an Arrhenius type relation:

$$D_L = D_0 \exp\left(-\frac{E_a}{RT}\right) \tag{9}$$

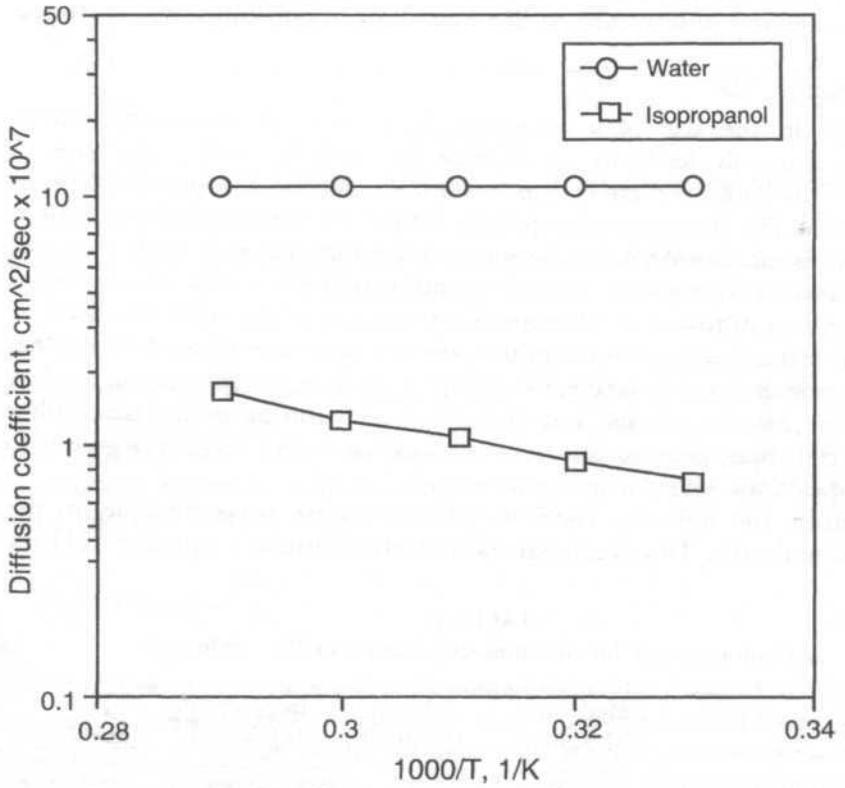

Fig 8. Arrhenius plots of diffusion coefficients for water and isopropanol in the chitosan stationary phase

where D_o is a constant, E_a the activation energy for diffusion, R the gas constant, and T_g the operating temperature. The activation energy for diffusion for water and isopropanol can be calculated from the slopes of Fig. 8 and are summarized in Table 2. The activation energy for diffusion of isopropanol is higher than that for water, which suggests that the water molecules require less energy than isopropanol does to facilitate diffusion through the stationary phase. Note that the difference in the activation energy for each probe may arise from several factors including molecular size and probe/stationary phase interaction. Interestingly, activation energy for diffusion of isopropanol through the swollen stationary phase is lower than that through the dry stationary phase. This indicates that the diffusion of isopropanol is also affected by the nature of the stationary phase; the presence of sorbed water in the water swollen stationary phase apparently decreases the energy required for the diffusion of isopropanol. Water apparently depresses the T_g of the chitosan membrane and changes the properties of the stationary phase induced by plasticisation and swelling processes. Note that plasticisation and swelling of the stationary phase caused by prolonged exposure to water saturated carrier gas are both reversible processes. The amorphous chitosan polymer exhibits a significant change from glass-like behaviour when dry to soft, rubbery-like behaviour when swollen and *vice-versa.*

Effect of Penetrant Size

An increase in the size of a penetrant in a series of chemically similar penetrants generally leads to an increase in solubility and a decrease in diffusion coefficients. The effect of penetrant size on the diffusion coefficients is illustrated in *Fig. 9* at various temperatures for a series of alcohols: methanol, ethanol and isopropanol. As can be seen, as the size of the alcohols increases from methanol to isopropanol, the corresponding diffusion coefficients decrease. The decrease in diffusion coefficients is a reflection of the need to create or utilize a critical activation volume in the polymer stationary phase proportional to that of the penetrant molecule; the size of the hole required to accommodate the molecule, the length and the size of the path the molecule must follow during its diffusion, and the free volume available to the polymer segment to exchange positions with the probe molecules.

Therefore, the diffusion coefficient shows inverse proportionality to the size of the molecule. This result agrees well with Einstein's equation [21] for

TABLE 2
Activation energy for diffusion determined by IGC technique

	Methanol (KJ/kgmol)	Ethanol (kJ/kgmol)	Isopropanol (kJ/kgmol)	Water (kJ/kgmol)
Dry Stationary Phase	0.854	0.901	1.097	0.515
Swollen Stationary Phase	0.333	0.507	0.715	–

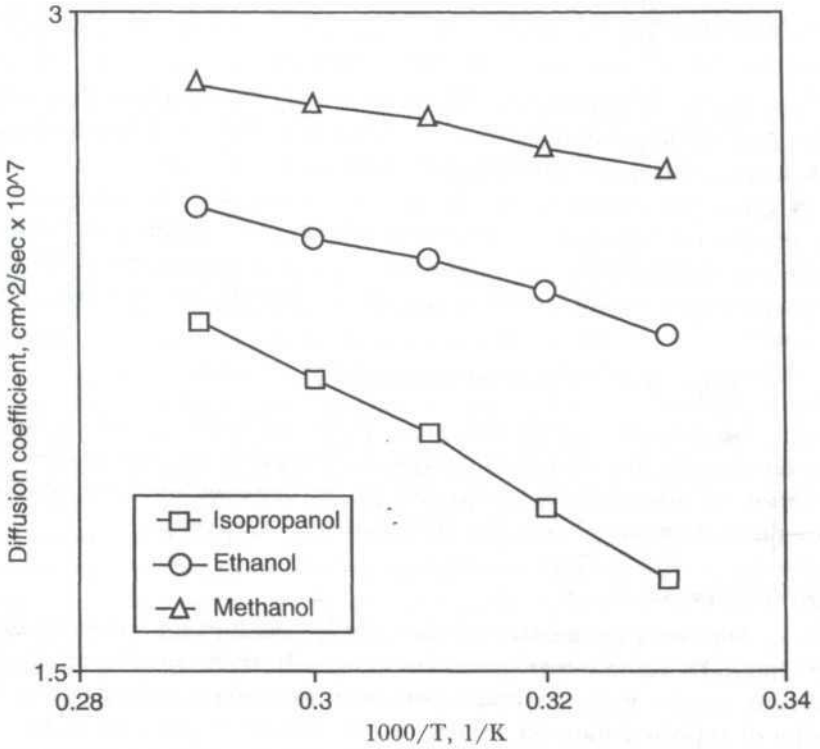

Fig 9. Arrhenius plots of diffusion coefficients of methanol, ethanol and isopropanol

the diffusion coefficient relating to the chain length of the solvent which has the form

$$D = RT/f \tag{10}$$

where f is called the friction factor and is directly proportional to the chain length. The validity of such a relationship has also been confirmed by other workers [22,23]. According to Fujita's free volume theory [24], the thermodynamic diffusion coefficient, D, is related to the free volume by the following expression:

$$D = ART\exp\left(-\frac{B}{f}\right) \tag{11}$$

where A and B are parameters that are assumed to be independent of diffusant concentration and temperature. However, A is a pre-exponential factor which depends on the properties of the diffusant and the polymer, whereas B is a constant characterizing the size of the hole needed for a diffusion jump. The fractional free volume of the pure polymer is denoted by f.

On the basis of eqn. (10), the following equation can be written for the diffusion coefficient at zero penetrant concentration, D_L:

$$D_L = ART\exp\left(-\frac{B}{f_L}\right) \tag{12}$$

where f_L is the fractional free volume of the pure polymer. Hence, increasing the diffusant size will, in general, cause an increase in B and possibly a decrease in A, which in turn decreases the diffusion coefficient.

Table 3 gives the summary of the activation energy for diffusion of methanol, ethanol and isopropanol calculated from the corresponding Arrhenius plot of diffusion coefficients. The apparent activation energy for diffusion increases proportional to the relative size of the penetrants and have the following order;

Isopropanol > ethanol > methanol

Evidently, the presence of sorbed water in the stationary phase causes a significant decrease in the activation energy. As previously discussed, swelling and plastization of the chitosan stationary phase increase the free volume available to the system to enhance the diffusion of the solvents.

Accuracy of Measurements

It is difficult to determine the accuracy of the diffusion coefficients measurements by the thin-channel column inverse gas chromatography technique. Comparison of the present results with literature data was somewhat difficult, due to unavailability of reported data on similar probe/stationary phase systems and different temperature range involved. Generally, the diffusion coefficients for polymer/probe systems lie in the range of 10^{-6} to 10^{-9} cm^2/sec [25]. The overall accuracy of the diffusion coefficients measured by the thin-channel column IGC method, as evidenced by the linearity of the Arrhenius plot of the diffusion coefficients indicated by the numerical value of the regression coefficient of determination, R^2, (see Table 3) was reasonably good.

In this work, no apparent sample-size dependent effects on the retention times were observed. Tailing and asymmetric peaks were minimal. This supports our belief that the thin-channel column "*coated*" with the chitosan membrane layer was sufficiently well-prepared, and apparatus effects were small and negligible, and that adsorption was minimized. Therefore, it was assumed that thermodynamic equilibrium was achieved in the column, and hence we were

TABLE 3
Diffusion activation energy of a series of alcohols determined by thin-channel column inverse gaschromatography technique

Chitosan Stationary Phase	Activation Energy, kJ/kgmol		
	MeOH	EtOH	i-PrOH
Dry	0.85	0.90	1.91
Swollen	0.51	0.62	1.08

justified in using the van Deemter equation to calculate the diffusion coefficients with a high degree of accuracy. The design of the column parameters can be adjusted, within limits, to suit certain purposes and the thickness of the polymer film can be readily varied to allow for the study of a range of diffusion coefficients of components in polymeric membranes.

CONCLUSION

A spiral thin-channel column was designed and used for the study of diffusion in chitosan stationary phase based on inverse gas chromatography technique. The following conclusions can be drawn from this work:

(1) The uniquely designed column presents a reliable alternative to the conventional packed and capillary columns, for the measurements of diffusion coefficients by inverse gas chromatography technique.
(2) Inverse gas chromatography technique provides a simple, fast and objective alternative to estimate the diffusion in polymer membrane.
(3) The measured diffusion coefficients are dependent on both temperature and molecular size; the diffusion coefficients increase with an increase in temperature and decrease with an increase in molecular size of the probes.
(4) The diffusion coefficients in water swollen stationary phase are generally higher than those obtained in dry stationary phase; the sorbed water affects the diffusion of alcohols through the polymer film.

REFERENCES

LAUB, R.J. and R.L. PECSOK. 1978. *Physicochemical Applications of Gas Chromatography.* New York: Wiley.

CONDER, J.R and C.L.YOUNG. 1979. *Physicochemical Measurement by Gas Chromatography.* New York: Wiley.

BRAUN, J.M. and J.E. GUILLET. 1975. Studies of polystyrene in the region of the glass transition temperature by inverse gas chromatography. *Macromolecules* **8**: 883.

TAIT, P.J.T. and A.M. ABUSHIHADA. 1979. The use of a gas chromatographic technique for the study of diffusion in polymer. *J. Chromatogr. Sci.* **17**: 219.

KONG, J.M. and S.J. HAWKES. 1975. Diffusion in uncrosslinked silicones. *Macromolecules* **8**: 148.

GALIN, M. and M.C. RUPPRECHT. 1978. Study by gas-liquid chromatography of the interactions between linear or branched polystyrenes and solvents in the temperature range 60-200 °C. *Polymer* **19**: 506.

PAWLISCH, C., A. MACRIS and R.L. LAURENCE. 1987. Solute diffusion in polymers. I. The use of Capillary Column Inverse Gas Chromatography. *Macromolucules* **20**: 1564

PAWLISCH, C.,A. MACRIS and R.L.LAURENCE. 1980. Solute diffusion in polymers, II. *Macromolecules* **20**:

DUDA, J.L. and J.S. VRENTAS. 1968. Diffusion in atactic polystyrene above the glass transition point. *J. Polym. Sci.* A-2, **(6)**: 675.

DUDA, J.L., Y.C. Ni and J.S. VRENTAS. 1978. Diffusion of ethylbenzene in molten polystyrene. *J. Appli. Polym. Sci.* **22**: 689.

CRANK, J. and G.S. PARK. 1968. *Diffusion in Polymers.* New York: Academic Press.

CRANK, J. 1979. The *Mathematics of Diffusion.* 2nd edn Oxford University Press.

MCCALL, D.W. 1957. Diffusion in ethylene polymers. I. Desorption kinetics for a thin slab. *J. Polym. Sci.* 26: 151.

FELS, M. and R.Y.M. HUANG. 1970. Diffusion coefficient of liquids in polymer membranes by a desorption method. *J. Appl. Polym. Sci.*, **14**: 523.

RHIM, J.W. and R.Y.M. HUANG. 1989. On the prediction of separation factor and permeability in the separation of binary mixtures by pervaporation. *J. Membrane Sci.* **46**: 335.

SCHUPP, O.E. 1968. Gas chromatography. In *Technique of Organic Chemistry,* eds. E.S. Perry and A. Weissberger. New York: Interscience.

VAN DEEMTER, J.J., F.J. ZUIDERWEG and A. KLINKENBERG. 1956. Longitudinal diffusion and resistance to mass transfer as causes of nonideality in chromatography. *Chem. Eng. Sci.* **5**: 271.

LITTLEWOOD, A.B. 1970. *Gas Chromatography.* 2nd edn. New York: Academic Press.

GIDDINGS, J.C. 1965. *Dynamics of Chromatography.* Part 1. New York: Marcel Dekker Inc.

GHAZALI, M.N. 1997. Pervaporation Dehydration of Isopropanol/Water Mixtures Using Chitosan Membranes. Ph.D Thesis, University of Waterloo, CA.

BIRD, R.B., W.E. STEWARDT and E.N. LIGHTFOOT. 1960. *Transport Phenomena.* New York: Wiley.

PRAGER, S. and F. LONG. 1951. Diffusion of hydrocarbon vapor into polyisobutylene. *J. Am. Chem. Soc.* **73**: 4072.

PRAGER, S. E. BAGLEY, and F. LONG. 1953. Equilibrium sorption data for polyisobutylene hydrocarbon systems, *J. Am. Chem. Soc.* **75**: 1255.

FUJITA, H. 1961. Diffusion in polymer-diluent systems. *Fortschr. Hocpolym. Forsch.* **3**: 1.

PRICE, F.P., P.T. GILMORE, E.L. THOMAS and R.L. LAURENCE. 1978. Polymer/polymer diffusion. I. Experimental technique. *J. Polym. Sci., Polym. Sypm.* **63**: 33.

ISSN: 0128-7680
Pertanika J. Sci. & Technol. **8(1)**: 19 - 29 (2000)

One-Dimensional Consolidation of Kelang Clay

Mohd Raihan Taha, Jimjali Ahmed and Sofian Asmirza
Dept. of Civil and Structural Engineering
Universiti Kebangsaan Malaysia
43600 UKM Bangi Selangor, Malaysia

Received 23 June 1998

ABSTRAK

Satu kajian mengenai kelakuan pengukuhan lempung Kelang dibentangkan dalam kertas kerja ini. Sampel tanah yang diambil dari kawasan yang berhampiran dengan Pelabuhan Kelang menunjukkan bahawa lempung tersebut boleh dibahagikan kepada lempung marin di sebelah atas dan lempung sungai di sebelah bawah. Perbezaan awal ini adalah berdasarkan kehadiran kelompang laut pada bahagian atas dan bahan ini tidak didapati pada lapisan bawah. Telah ditunjukan bahawa kedua lempung ini mempunyai ciri pengukuhan serta lain-lain ciri geoteknik asas yang berbeza. Sejarah pengukuhan menunjukkan bahawa lempung Kelang adalah terkukuh normal dan dikelaskan sebagai lempung kebolehmampatan tinggi. Tekanan tanggungan atas akibat tanah tambak mestilah diabaikan untuk memperolehi nisbah pengukuhan lebih yang sebenar. Telah didapati juga bahawa sekaitan yang diberikan oleh Terzaghi dan Peck (1967) memberikan anggaran yang terbaik bagi index mampatan terutamanya bagi lempung marin.

ABSTRACT

A study on the consolidation behaviour of Kelang clay is presented in this paper. The soil samples taken near the Port of Kelang showed that the clay can be divided into upper marine and the lower river clays. The initial distinction was based on the existence of sea shells in the upper deposits and none in the lower deposits. It has been shown that these two clays have different consolidation properties as well as other basic geotechnical characteristics. Consolidation history indicated that Kelang clay is normally consolidated and may be classified as a high compressibility clay. The overburden pressure due to fill must be neglected in order to obtain the true overconsolidation ratio. It was also found that the correlation given by Terzaghi and Peck (1967) provided the best estimates for the compression index, particularly that of the marine clay.

Keywords: consolidation, Kelang clay, marine clay, river clay, Malaysian clay, Malaysian soil

INTRODUCTION

The rapid growth of industrialisation requires an extensive construction of infrastructure in Malaysia. In addition to new projects, the maintenance and upgrading of facilities also provided significant input to the overall development. Some of the major areas that are receiving impetus for such developments include the coastal regions where ports and highways are located. These areas of quartenary age consist mainly of soft clays, peat and other soft organic deposits. It poses major construction and maintenance problems due to low

bearing capacity and high deformation behaviour (Chin 1967, Mustafa and Wan Badaruzzaman 1989, and Mohamad and Chin 1990).

In general, theory of consolidation deals with the response of soil systems to imposed load and predicts stresses and displacements of the loaded soil as a function of space and time. This theory, since its introduction by Terzaghi in 1923, has formed the foundation of modern geotechnical engineering. The concept is fundamental to the practice of geotechnical engineering where the interaction of soil and water dominates. Although consolidation is used for estimating settlements, it has also played key roles in analysing stability of slopes, design of piled foundations, laboratory tests, etc. (Schiffman *et al.* 1984).

An extensive study has been undertaken to study, characterise and predict the bahaviour of Kelang clay. This was undertaken so that future structures can be designed and constructed safely and economically. The consolidation study presented in this paper formed part of the goals towards achieving this endeavour.

Site Geology and Basic Geotechnical Properties

Generally, the thickness of the soft clay deposits in the Southeast Asian region (which includes countries such as Malaysia, Indonesia, Singapore, Thailand, etc.) ranged from very shallow thin layers to depths of 40 m. It is then followed by layering of sand, peat and other soft clay deposits finally reaching the quartzite bedrock at about 80 m below the surface (Cox 1970; Ting and Chan 1971; Bibi 1971; Ting and Ooi 1977; and Bosch 1988). These deposits were formed about 10,000 years ago due to change in sea level. The geological environment for the rise and fall of sea level in Peninsular Malaysia was elaborated on by Tjia (1975 and 1977).

DATA

The soil sample used in this study was obtained near the port of Kelang. In the Kelang area, the soft clay deposits ranged between 20 to 40 m in thickness (Bibi 1971). Below these layers of sand, clay and organic deposits follow. At certain locations, the organic deposits may reach 6 m in thickness. A similar profile was observed some 200 km to the north along the coast (Britt and Ratcliff 1970).

RESULTS AND DISCUSSION

A borehole profile of the subsurface soil is shown in *Fig 1.* In actual fact two clay layers existed in the profile, i.e. marine and river clays. They are differentiated by the existence of corals and sea shells which is the distinguished feature of the marine clays (Ahmed 1992). The sea shells were found to increase in number with depth until 15.8 m where the marine species formed a boundary of about 10 cm thick. Below this depth no marine specimens were observed. Small wooden chips and decayed roots were traced throughout the borehole. Thin layers of sand/silt were also found in the river clay.

Most clays are either greenish or bluish in colour except in the upper 2.25 m which are dark gray in colour. The gray colour was possibly developed due to oxidation of sulphur and iron in the clay as a result of it being exposed to atmosphere. Dennet (1932) observed that the in-situ blue clay turned to gray and finally reddish-yellow in 9 months. The existence of the dark gray clay at depths of 18 m, 21 m, and 24 m illustrates the deposition of the clay layer with respect to the dramatic rise and fall of sea level beginning some 10,000 years ago (Ahmed 1992). The clay fractions for both deposits ranged between 27 to 48%. The main clay minerals were montmorillonite (42%), illite (24%), kaolinite (21%) and microcline (13%). The microline is a mineral which will eventually turn to kaolinite giving the total kaolinite 34%.

The index properties of the Kelang clay are also shown in *Fig 1.* The average values of the Atterberg's limits and unit weights are given in Table 1. The water contents of the marine clay were very close to the liquid limit with all liquid limit values below 84%. In the Casagrande's plasticity chart, the soil fall in the left CH (high plasticity clays) region with most points lies just above the A-line. The river clays have liquid limits in excess of 84% and are located on the right CH region. Similar observations were made by Jaadil (1991).

TABLE 1
Average values of some geotechnical properties of Kelang clay

Clay type	Water content w_n (%)	Liquid limit LL (%)	Plastic limit PL (%)	Unit weight kN/m³	G_s
Marine	71	71	32	15.48	2.64
River	88	103	41	14.42	2.61

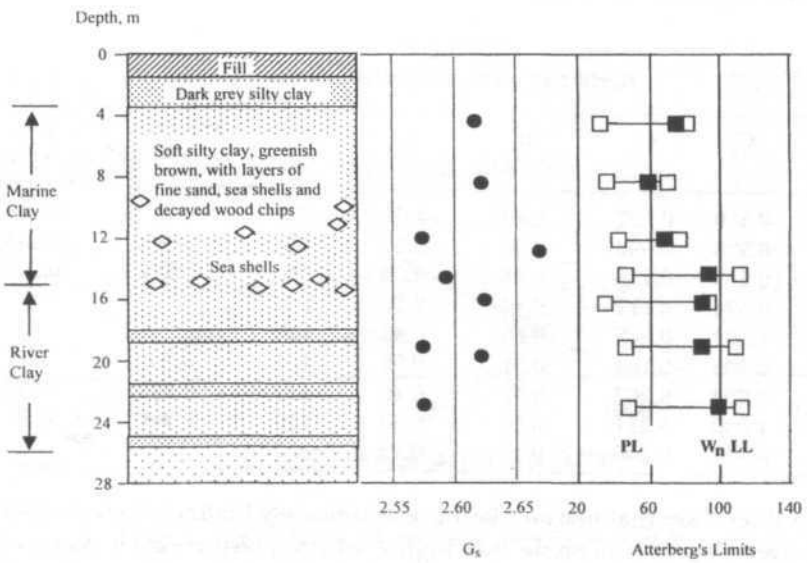

Fig 1. Depth profile, specific gravity (G_s) and Atterberg's limit of the clay deposit

Consolidation Behaviour

Fig. 2 shows a typical plot of *e-log* σ_{vc} curve of the marine clay sample. It illustrates a slightly concaving curve as it reaches the virgin compression line demonstrating some sensitivity. Vane shear test results indicated a sensitivity value of 1.7 to 6.5 indicating low to medium sensitive clays.

The typical consolidation curve of the river clay is shown in *Fig. 3*. It also shows a concave upon reaching the virgin line. For both clays, beyond the preconsolidation pressure, the compressibility decreases continuously with the increase in effective vertical stress. The main difference to that of the marine clay is that the initial void ratio of the river clay is significantly higher. The coefficient of volume change, m_v which increases and then reduces in the virgin line is the same for both clays. The coefficient of consolidation, c_v, also decreases after reaching the past maximum pressure, σ_{vm}. This indicates that the sample is not disturbed or slightly disturbed. Thus the approximation of the σ_{vm} can be considered reliable.

Consolidation test parameters for all tests are given in Table 2. The values of σ_{vm} and c_v were obtained using the Casagrande's method. The c_v and m_v parameters are the mean values in virgin compression. The table is divided into two because it was initially assumed that the upper marine clay and the lower river clay have different properties. This table provides further proof to this hypothesis. The compression and rebound indices (C_c and C_r, respectively) for river clay are twice those of the marine clays. The modified compression and rebound indices ($C_{c\varepsilon}$ and $C_{r\varepsilon}$, respectively) show that the values are consistent or almost constant for the upper marine clay. However, it increases with depth for the river clay. This analysis omits the results for depth of 15.65 m because the values obtained were way off line due to difficulties in obtaining the void ratio caused by the existence of many sea shells.

TABLE 2
Results of 1-D consolidation tests

Depth (m)	C_c	C_r	m_v (m^2/MN)	c_v (m^2/yr)	σ'_{vc} (kPa)	$C_{c\varepsilon}$= $C_c/(1+eo)$	$C_{r\varepsilon}$= $C_r/(1+eo)$
4.09	0.610	0.102	0.49	1.55	34	0.2	0.045
8.10	0.525	0.098	0.47	3.51	45	0.2	0.045
12.28	0.587	0.113	0.48	6.03	90	0.205	0.047
Average	0.574	0.111	0.48	3.70			
15.65	1.102	0.249	0.66	0.48	105		
16.10	0.705	0.164	0.51	0.55	100	0.20	0.05
19.10	0.934	0.262	0.52	0.45	110	0.27	0.075
23.01	1.049	0.311	0.54	0.50	130	0.305	0.09
Average	0.947	0.246	0.56	0.49			

The c_v values show that marine clay have significantly higher values compared to that of river clay. It is possible that high c_v of the marine clay is due to the fine sand layers. However, the m_v values show similarities with the river clays

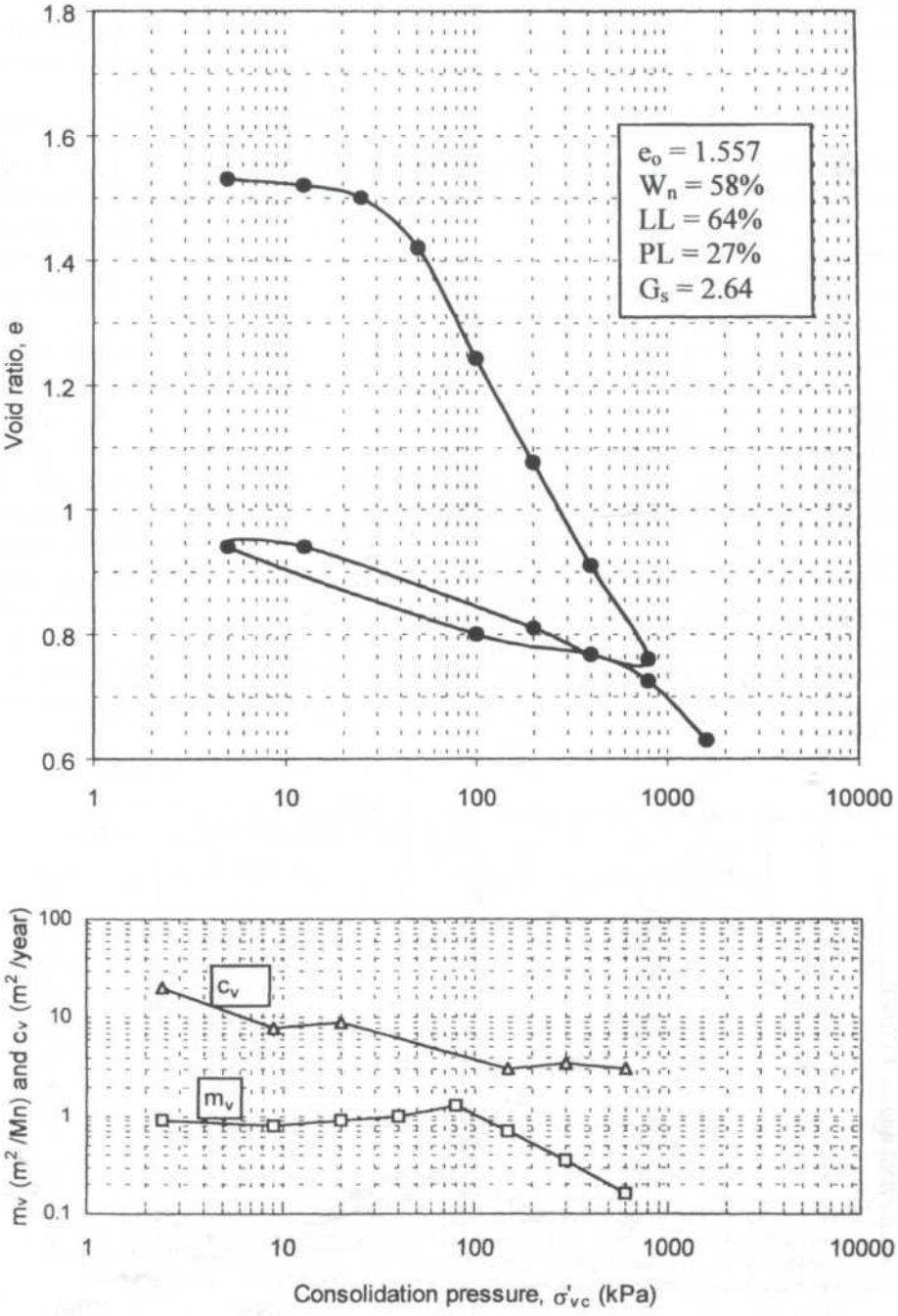

Fig 2. Consolidation test results for samples at 8.10 m

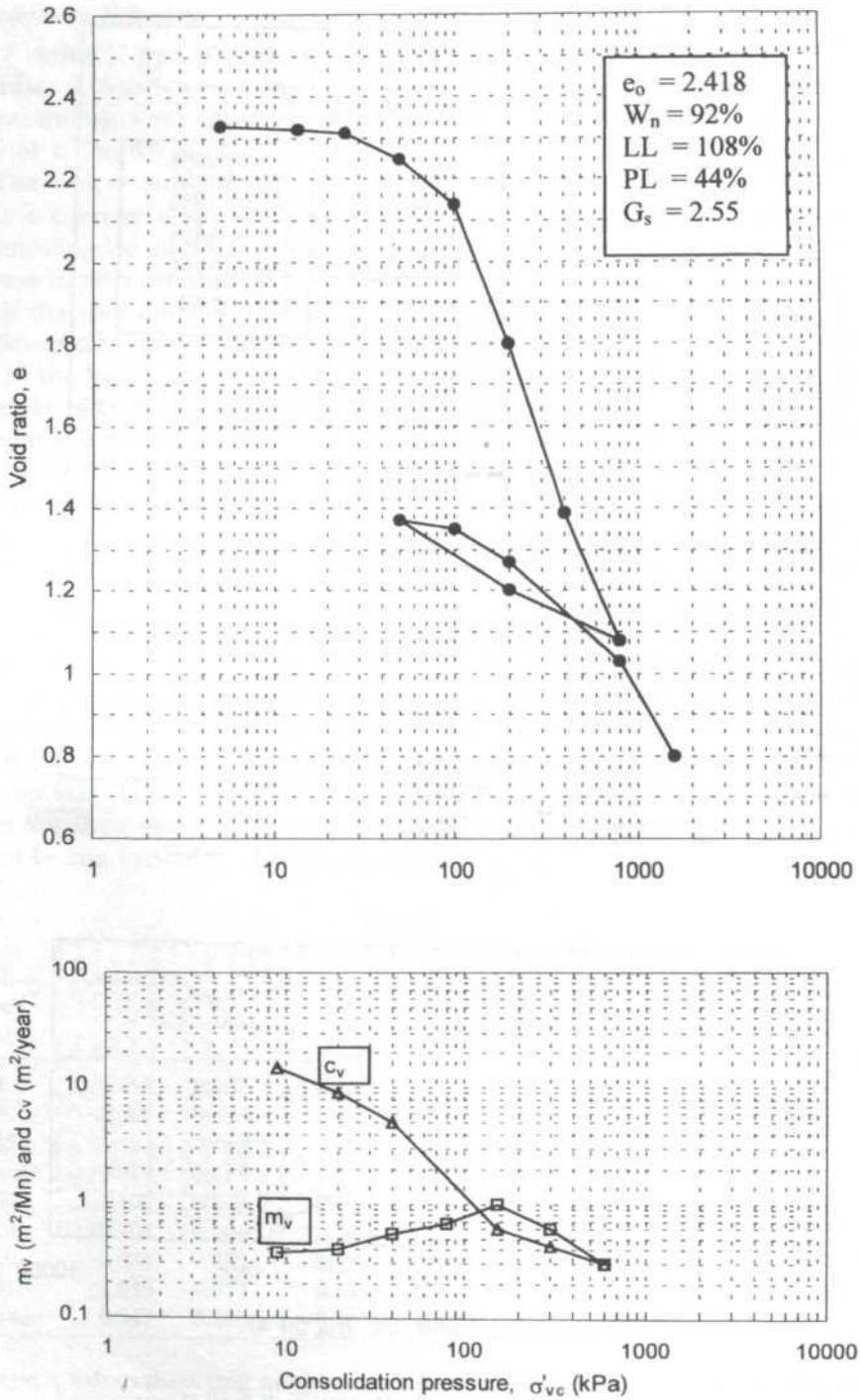

Fig 3. Consolidation test results for samples at 19.10 m

having higher indices. Based on Head (1984), Kelang clays (marine and river clay) may be classified as clay with high compressibility and it is most probably a normally consolidated clay.

Estimation of Consolidation History

Fig. 4 shows the plot of past maximum pressure, σ'_{vm}, against depth. The two white circles represents minimum and maximum probable values and the black circles represent the most probable values. These are estimated from *e-log* σ'_{vc} plots at the respective depths (Ahmed 1992). The overburden pressure, σ'_{vo} was calculated based on assumptions that the groundwater table is at 2.3 m and using unit densities from Table 1. The line on the right is the calculated σ'_{vo} incorporating filled areas and the left is without the fill. It can be seen that σ'_{vm} may lie anywhere on and between these two lines.

In order to predict which line represents the actual σ'_{vo}, *Fig. 5* (US Navy, 1971) illustrates the correlation between c_v and LL that has been used. Using LL, *Fig. 1* and c_v in Table 2, the results obtained showed that the samples were practically undisturbed. In general, there was no remoulding and all points lie above the line for remoulded samples (refer to *Fig. 5*). One point, however, is located outside/above the upper line, indicating a probable overconsolidation. This is the value which lies close to the right line (depth 12.28 m). Since all other σ'_{vm} are closer to the left line except two points, the more appropriate line which represents σ'_{vo} is the left line, *i.e.* the line which ignores the fill. However, it must be mentioned that the fill should not be ignored especially

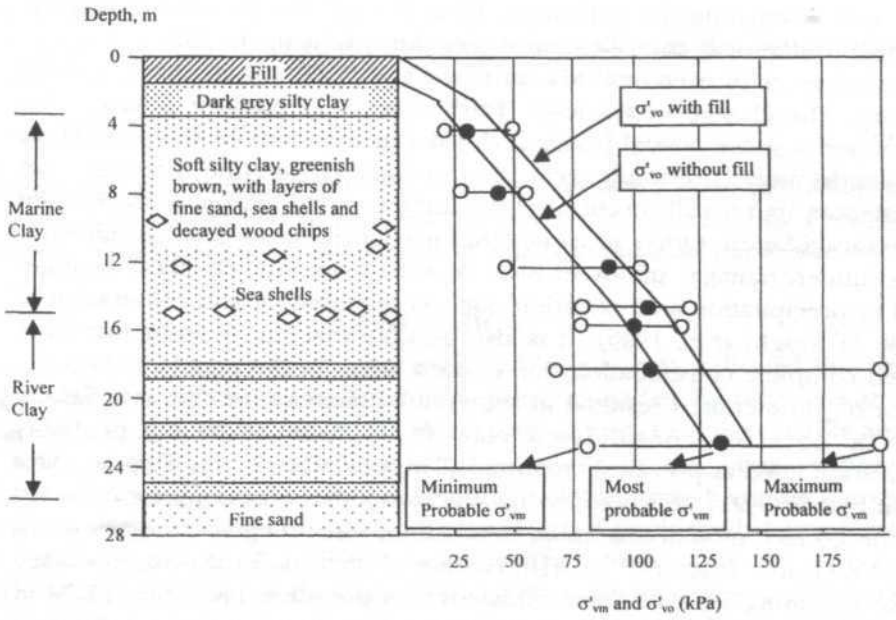

Fig 4. Estimation of σ'_{vm} *and* σ'_{vo} *of Kelang clay*

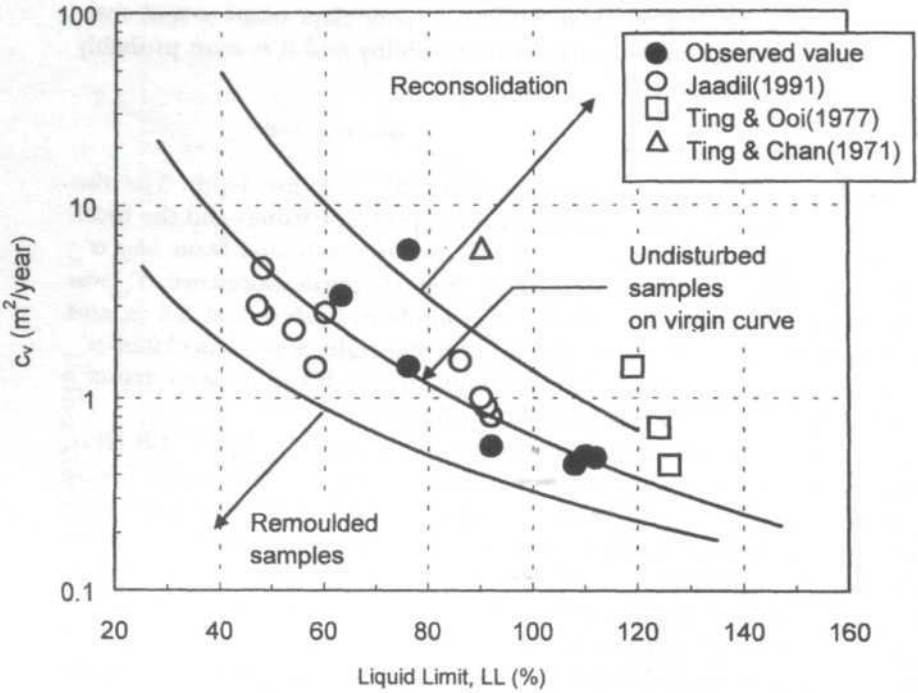

Fig 5. Relationship between c_v and LL (after U.S. Navy1971)

when one is calculating the settlement. Thus, it must also be realised that the clay is still undergoing consolidation under the weight of the fill.

The existence of overconsolidated deposits at 12.28 m and 15.65 m is not surprising. The change in sea level (Fairbridge 1961) made it possible that there existed a stable coastal beach at this depth sometime in the past. Thus, these depths were previously near the surface. Desiccation (drying) and consolidation, that usually occur near the surface, could have possibly resulted in overconsolidation. Other processes that may attribute to overconsolidation include underdrainage, minor erosion of sediments and chemical changes caused by precipitation and oxidation, such as cementation and colouration of the clay (Terzaghi *et al.* 1996). It is also possible that the deposits may have achieved complete consolidation due to sand layers in the profile.

The σ'_{vo} line chosen resulted in the establishment of the fact that Kelang clay is a normally consolidated clay as opposed to being probably underconsolidated as previously reported (Ting and Chan 1971; Ting and Ooi 1977 and Jaadil 1991). It is possible that the consolidation tests were conducted on disturbed or remoulded samples. In addition, when the data from Ting and Chan (1971) and Ting and Ooi (1977) were plotted in *Fig. 5*, the results fell into the reloading zone (overconsolidated). On the other hand the results of Jaadil (1991) showed that the clay was in the undisturbed zone indicating normally consolidated soil. Jaadil (1991) conducted the *LL* tests on oven dried

soil which might have affected the results. All three researchers also have the *e-log* σ curves indicating remoulded samples, i.e. lines which do not curve as it approaches the virgin compression and does not show a clear σ'_{vm}.

Compression Index Relationships

There are many empirical relationships between compression index and basic soil properties such as water content, initial void ratio, liquid limit and plasticity index. The relationships can provide a quick estimation of the compressibility of clay prior to complete results from consolidation tests. By far, the most common formula links compression index and liquid limit and only a few of these models will be discussed in this paper. The earliest relationship between compression index and liquid limit was provided by Skempton (1944). The formula was based on test on remoulded clays and is not appropriate for comparison. Thus, it will not be used for further discussion.

Terzaghi and Peck (1967) obtained a relationship for normally consolidated clay with low to medium plasticity such that:

$$C_c = 0.009\ (LL\text{-}10) \tag{1}$$

This relationship is shown in *Fig. 6.* For the data obtained in this study, it can be concluded that the formula is excellent for LL up to 110%. Beyond this, the relationship underestimates C_c. Since the water content of the marine clay is lower than 84% and river clay more than 84 %, therefore the formula will have a better correlation for the marine clay. In general, however, since the formula has a reliability of about 30%, it can be concluded that the formula fits very well for Kelang clay.

Huat *et al.* (1995) obtained the following relationship for clay in the region of west coast of Selangor (Kelang is located in this zone):

$$C_c = 0.005\ (LL+71.8) \tag{2}$$

This line has also been plotted in *Fig. 6.* It does provide a good estimation of the C_c; however, it can be observed that the correlation provided by Terzaghi and Peck (1967) gives a better estimate of this consolidation parameter.

CONCLUSION

The consolidation tests and analysis conducted in this study indicated that the Kelang clay is normally consolidated as opposed to earlier findings that it is underconsolidated. Furthermore, the clay is divided into the upper marine and the lower river clays. The existence of sea shells in the upper deposits distinguished the two profiles. Test results also indicated that the upper marine clay has a sensitivity range of low to medium. It has a significantly lower initial void ratio compared to that of the river clay. The compression and rebound indices of the river clay are also higher for the river clay indicating greater total compressibility of this deposit. The coefficient of consolidation, however, showed that it is significantly higher for the marine clays. Analysis of data

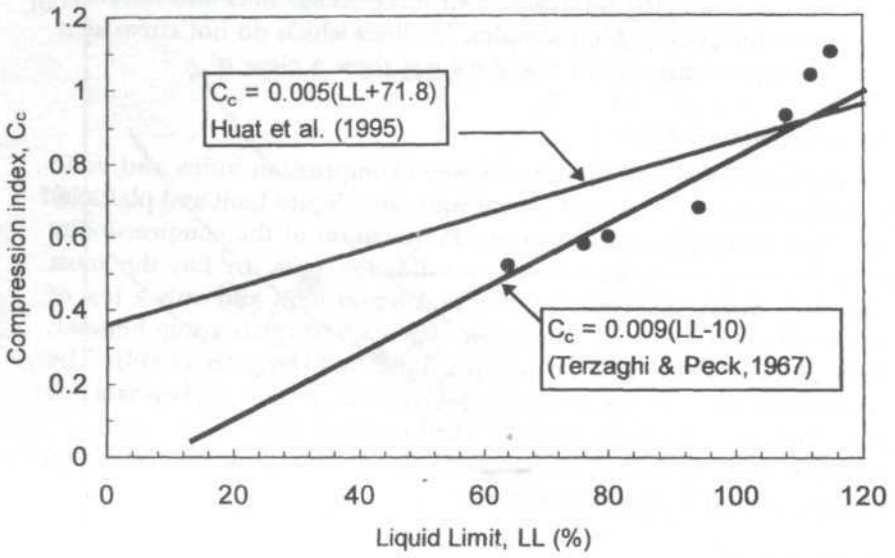

Fig 6. Relationship between C_c and LL

revealed that the relationship provided Terzaghi and Peck (1967) gives an excellent estimate for the compression index from liquid limit values particularly that of the marine clay. Similarly, relationship forwarded by Huat *et al.* (1995) also provided good estimates.

REFERENCES

AHMED, J. 1992. Strength and Deformation Behaviour of Kelang Clay. MSc Thesis. Universiti Kebangsaan Malaysia.

BIBI, M. 1971. Klang-Langat delta, Selangor, West Malaysia, quarternary sediments, clay minerals and foraminera. BSc (Hons) Thesis. Universiti Malaya.

BOSCH, J.H.A. 1988. The quartenary deposits in coastal plains of Peninsular Malaysia, Geological Survey of Malaysia, Quartenary Geology Section, Report No. OG/1.

BRITT, G.B., and E. RAWCLIFF. 1970. Piling and pile tests on a number of sites in Malaya. In *Proc. 2nd Southeast Asian Conf. on Soil Engineering*, p. 93-105. Singapore.

CHIN, F.K. 1967. The design and construction of tidal control structures in coastal clays, *Proc. 1st Southeast Asian Conf. on Soil Mechanics*, p. 261-267. Bangkok.

COX, J.B. 1970. A Review of the Engineering Characteristics of the Recent Marine Clays in South-East Asia, *Research Report No. 6*, Asian Institute of Technology, Bangkok.

DENNET, J.H. 1932. The western coastal alluvial soils. *Malay. Agri. J.* **20**: 298-303.

FAIRBRIDGE, R.W, 1961. Eustatic changes in sea level. Physics and chemistry of the earth 4:99-185.

HEAD, K.H. 1984. Manual of Soil Laboratory Testing 2, ELE Int. Limited.

HUAT, B.B.K., K. OTHMAN and A.A. JAFFAR. 1995. Geotechnical properties of Malaysian marine clays. *J. Inst. Engineers Malaysia* **56**: 23-33.

JAADIL, J. 1991. Deformation Behaviour of Kelang Clay in 1-Dimensional Consolidation, MSc Thesis, Universiti Kebangsaan Malaysia, 203 p.

MOHAMAD, R., and C.W. CHIN. 1990. Geotechnical design aspects for widening low embankments on soft grounds. *PLUS Seminar on Geotechnical Aspects of the North-South Expressway.* p. 177-185.

MUSTAFA, A., and W.H. WAN BADARUZZAMAN. 1989. Transformation of existing pile to raft foundation as a solution to settlement problems. *Proc. 2nd Int'l. Conf. on Foundations and Tunnels.* p. 245-252.

SCHIFFMAN, R.L., V. PANE and R.E. GIBSON. 1984. The theory of one-dimensional consolidation of saturated clays: IV - An overview of the non-linear finite strain sedimentation and consolidation. In *Sedimentation Consolidation Models:Predictions, and Validation*, ed. R.N. Yong and F.C. Townsend, p. 1-29 ASCE.

SKEMPTON, A.W. 1944. Notes on the compressibility of clays. *Quart. J. of the Geological Soc. of London* **100**: 119-135.

TERZAGHI, K., and R.B PECK. 1967. *Soil Mechanics in Engineering Practice.* 2nd Edn. New York: John Wiley and Sons.

TERZAGHI, K., R.B. PECK and G. MESRI. 1996. *Soil Mechanics in Engineering Practice.* 3rd Edn. New York: John Wiley and Sons.

TJIA, H.D. 1975. Additional dates of raised shorelines in Malaysia and Indonesia. *Sains Malaysiana* **4(2)**: 69-84.

TJIA, H.D. 1977. Sea level variations during the last six thousand years in Peninsular Malaysia. *Sains Malaysiana* **6(2)**: 171-183.

TING, W.H., and S.F. CHAN. 1971. Bearing capacity of bakau timber piles in the coastal alluvium of West Malaysia. *Proc. 4th Regional Conf. on Soil Mech. and Found. Eng.* p. 317-322.

TING, W.H., and T.A. OOI. 1977. Some properties of the coastal alluvia of Peninsular Malaysia. *Proc. Intl. Symposium on Soft Clay*, p. 89-101. Bangkok.

US NAVY. 1971. Soil mechanics, foundations, and earth structures. *NAVFAC Design Manual DM-7.*

ISSN: 0128-7680
Pertanika J. Sci. & Technol. **8(1)**: 31 - 40 (2000)

Pencirian Resonan Plasmon Permukaan dan Penggunaan Saput Tipis Emas sebagai Lapisan Aktif Sensor Optik

Rosmiza Mokhtar, Mohd. Maarof Moksin
dan W. Mahmood Mat Yunus
Jabatan Fizik, Fakulti Sains dan Pengajian Alam Sekitar
Universiti Putra Malaysia,
43400 UPM Serdang, Selangor, Malaysia

Received 29 Disember 1999

ABSTRAK

Ciri-ciri resonan plasmon permukaan (SPR) saput tipis logam emas pada pelbagai ketebalan dibincangkan. Pengukuran telah dilakukan pada filem berketebalan antara 50.98 nm – 92.38 nm dan ketebalan lapisan emas yang sesuai untuk sensor optik SPR ditentukan bernilai ≈ 50 nm yang menghasilkan nilai keterpantulan yang minimum dan resonan yang tajam. Penggunaan sensor optik jenis ini juga diuji untuk pengukuran peratus etanol dalam air suling. Garis tentu ukur didapati bersifat linear dengan sensitiviti direkodkan sebagai 9 3 10^{-2}/(% isipadu ethanol) untuk kepekatan larutan etanol 15%.

ABSTRACT

The characterizations of a surface plasmon resonance (SPR) of gold thin film at various film thickness are discussed. The measurements have been carried out for film thickness from 50.98 nm to 92.38 nm and the suitable thickness of gold film for SPR optical sensor was found as ≈ 50 nm which produces minimum reflectivity and sharp resonance. The potential application of the SPR as an optical sensor has been explored in measuring small percentage of ethanol in distilled water. The calibration curve was linear with the sensitivity recorded as 9 3 10^{-2}/(%vol. ethanol) for the concentration of ethanol in water 15%.

Keywords: data acquisition system, autotronic, draft requirement, energy requirement, crop production systems

PENGENALAN

Resonan plasmon permukaan (SPR) adalah ayunan ketumpatan cas bebas yang merambat sepanjang antara muka dua medium yang bersifat logam dan dielektrik. Untuk satu nilai frekuensi tertentu plasmon-polariton permukaan yang merambat di sepanjang permukaan sesuatu bahan konduktor biasanya logam nipis, umumnya memiliki momentum lebih besar dari foton dalam medium dielektrik. Oleh itu gandingan foton dengan plasmon untuk menghasilkan resonan plasmon-polariton biasanya dapat dilakukan dengan gandingan prisma (Raether 1988, Sadowski dan rakan-rakan 1991). Kaedah gandingan ini melibatkan prisma yang selaput dengan selaput tipis logam, dan telah digunakan sebagai sensor optik yang cukup sensitif (Sambles dan rakan 1991, Weber dan rakan-rakan 1975, Kano dan Kawata 1994, Namira dan rakan-

rakan 1995, Dougherty 1993). Dalam kebanyakan kajian yang melibatkan plasmon permukaan, logam emas dan perak kerap kali digunakan. Ini kerana logam perak menghasilkan resonan yang tajam dan logam emas pula bersifat lebih stabil di udara serta tidak bertindak balas dengan kebanyakan sampel kimia dan biologi (Kretschmann and Raether 1971, De-Bruijn dan rakan-rakan 1992).

Dalam kajian ini, prisma berindeks biasan tinggi digunakan sebagai substrat. Jumlah cahaya yang dipantulkan dari substrat akan bertambah dengan pertambahan sudut tuju sehingga pada satu sudut tertentu di mana semua cahaya dipantulkan. Sudut ini dikenali sebagai sudut genting, θ_c. Bagi prisma yang disaput dengan satu lapisan nipis logam (seperti emas atau perak), wujud satu sudut yang lebih besar daripada sudut genting ini di mana cahaya tidak dipantulkan sepenuhnya. Merujuk kepada Rajah (1a), komponen vektor gelombang, k yang selari dengan permukaan saput tipis boleh ditulis sebagai

$$k_x = nk_o \sin \theta \qquad (1)$$

dengan n adalah indeks biasan prisma, k_o adalah vektor nombor gelombang dalam ruang bebas dan θ adalah sudut tuju dalaman (sudut dalam dielektrik; prisma). Untuk kes $\theta > \theta_c$ (sudut kritikal prisma), nilai $k_x > k_o$. Bila keadaan ini dipenuhi, sinar cahaya akan dapat menembusi lapisan logam dan berganding dengan plasmon permukaan pada antara muka logam dengan udara/cecair. Dengan mengubah nilai θ kita akan dapati satu nilai θ tertentu di mana berlaku $k_x > k_{spr}$. Bila keadaan ini dipenuhi, plasmon-polariton permukaan teruja dan berayun dan berlaku pantulan minimum. Sudut di mana pantulan minimum ini berlaku dikenali sebagai sudut resonan plasmon permukaan, θ_{spr}. Fenomena

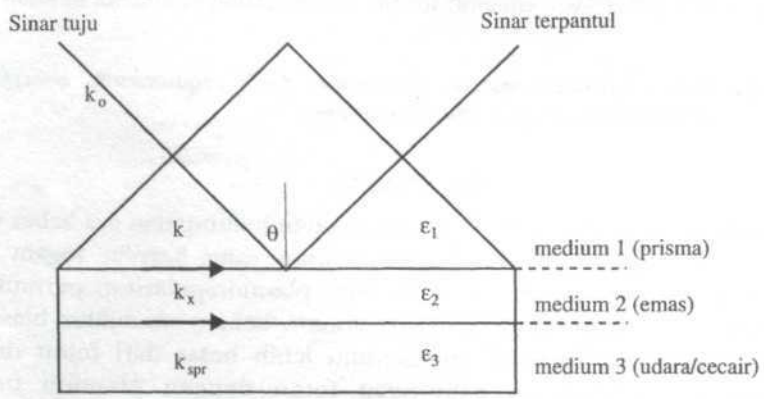

Rajah 1a: Susunan uji kaji menunjukkan gandingan prisma plasmon permukaan di mana meidum ke-2 bertindak sebagai lapisan aktif sensor optik.

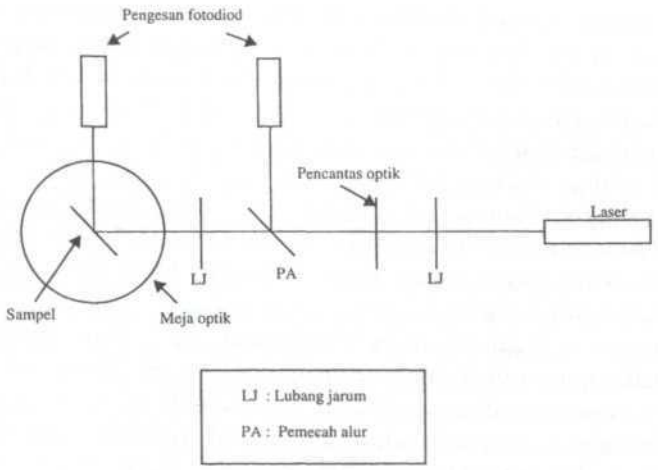

Rajah 1b: Menunjukkan susunan peralatan dan teknik pencerapan data ujikaji.

inilah yang dikenali sebagai resonan plasmon permukaan (SPR). Kerana SPR bersifat gelombang TM, pengujian plasmon ini hanya dapat dilakukan dengan menggunakan sinar cahaya terkutub P (komponen medan elektrik selari dengan satah tuju) sahaja dengan persamaan serakan ditulis sebagai (De-Bruijn dan rakan-rakan 1992)

$$k_{spr} = k\sqrt{\frac{\varepsilon_m \varepsilon_d}{\varepsilon_m + \varepsilon_d}} \qquad (2)$$

di mana ε_m dan ε_d ialah ketelusan logam (medium ke-2) dan ketelusan medium dielektrik (medium ke-3).

Objektif kajian ini adalah untuk menentukan ketebalan selaput tipis logam emas yang sesuai digunakan sebagai lapisan logam yang aktif dalam penggunaan kaedah ini sebagai satu sensor optik untuk menentukan kuantiti etanol dalam larutan.

KAEDAH DAN UJI KAJI

Dalam kajian ini, terdapat dua kategori sampel iaitu sampel logam (medium aktif) dan sampel larutan (medium tidak aktif). Logam yang digunakan sebagai selaput tipis adalah emas tulen (99.999%, VG Microtech, U.K.) yang selaput pada permukaan prisma bersudut 60° menggunakan teknik percikan (Polaron E5100) pada tekanan 10^{-3} torr. Dengan kaedah ini selaput tipis logam emas dalam julat ketebalan (50-93) nm dapat disediakan untuk kajian pencirian resonan plasmon permukaan dan sekaligus menentukan ketebalan logam emas yang sesuai untuk digunakan sebagai sensor optik. Kajian juga dijalankan untuk menguji kestabilan selaput tipis logam emas terhadap kesan persekitaran.

Untuk tujuan ini, sampel selaput tipis emas dibiarkan di udara pada suhu bilik dengan relatif kelembapan ~70% dan seterusnya pengukuran pencirian plasmon diulangi selepas hari ke-16. Sampel larutan yang digunakan dalam kajian ini adalah larutan etanol (James Burrough (F.A.D.) Ltd.). Untuk uji kaji ini, sebanyak tiga sampel larutan etanol disediakan iaitu 5.0%, 10.0% dan 15.0% etanol dalam air suling. Peratus kandungan etanol dirujuk dengan nisbah kedua-dua isipadu yang berkaitan, iaitu isipadu etanol dan air suling. Satu sel khas (3.31 cm^3) dibina untuk menempatkan sampel larutan. Sel ini diletakkan bersebelahan permukaan prisma yang selaput dengan filem tipis emas agar larutan etanol bersentuhan dengan permukaan selaput tipis emas. Dalam kertas ini, fenomena resonan plasmon permukaan digunakan sebagai asas sensor optik untuk menentukan peratus organik etanol dalam air suling. Sampel ini dipilih kerana mudah disediakan dan kaedah ini juga merupakan asas penentuan ketulenan sesuatu larutan menggunakan kaedah sensor optik.

Ujikaji dilakukan dengan mengukur keterpantulan sinar alur laser HeNe (632.8 nm, 10 mWatt(RS 109P)) sebagai fungsi kepada sudut tuju θ. Isyarat sinar tuju dan sinar pantulan dikesan oleh fotodiod (Newport HC-302) sementara pemprosesan isyarat dilakukan dengan menggunakan penguat terkunci (SR530). Sinar alur laser (632.8 nm) terkutub P disinarkan dengan satah tuju tegak dengan permukaan sampel. Rajah (1b) menunjukkan susunan radas uji kaji yang mengandungi prisma di atas meja optik, laser, polarizer dan pengesan fotodiod. Untuk setiap sampel, pencerapan data keterpantulan dilakukan bagi setiap pertambahan θ = 0.1°. Kejituan putaran sudut θ ialah < 0.01°. Putaran meja sampel dan pengesan dilakukan dengan kawalan bermotor (Newport-MM3000) dan komputer peribadi IBM/386. Dalam kes ini, pengesan fotodiod berputar dua kali sudut putaran sampel untuk memastikan alur terpantul jatuh pada permukaan pengesan fotodiod pada setiap langkah putaran sampel. Sudut resonan plasmon, θ_{spr} ditunjukkan oleh nilai keterpantulan minimum, R_{spr} yang memenuhi kaitan (1) dan (2).

HASIL DAN PERBINCANGAN

Keterpantulan sinar terkutub P sebagai fungsi kepada sudut tuju, θ untuk gandingan prisma boleh dijelaskan oleh persamaan Fresnel. Untuk sistem yang terdiri dari tiga medium, persamaan Fresnel boleh ditulis seperti berikut:

$$\left|r_{123}\right|^2 = \left|\frac{r_{12} + r_{23}\exp(2ik_2d)}{1 + r_{12}r_{23}\exp(2ikd)}\right| \qquad (3)$$

dengan $$r_{ij} = \frac{\varepsilon_j k_i - \varepsilon_i k_j}{\varepsilon_j k_i + \varepsilon_i k_j} \qquad (4)$$

ε dan r_{ij} masing-masing mewakili ketelusan medium dan keterpantulan Fresnel untuk antara muka tunggal sementara k adalah nombor gelombang dan ditulis sebagai (Robertson dan Fullerton 1989):

$$k_i = \frac{\omega}{c}\left(\varepsilon_i - \varepsilon_i \sin^2\theta_i\right)^{1/2} \quad (5)$$

dengan i = 1, 2 dan 3. Tandaan 1, 2 dan 3 masing-masing dirujuk kepada prisma, selaput tipis logam dan medium gas/cecair (lihat Rajah 1a). Dengan menggunakan kaedah cuba jaya data uji kaji kepada persamaan Fresnel (3), nilai ketelusan dan ketebalan lapisan logam emas dengan udara ditentukan bernilai; -10.48+i2.14, -10.51+i1.98, -10.73+i1.93, -10.97+i2.33 dan -10.52+i3.04 dengan ketebalan masing-masing direkodkan sebagai 50.98, 60.79, 61.53, 73.22 dan 92.38 nm. Plot keterpantulan optik sebagai fungsi kepada sudut tuju untuk kes ini ditunjukkan pada Rajah 2. Rajah (2a) menjelaskan persetujuan yang baik antara data ujikaji dengan data teori yang dikira menggunakan parameter cuba jaya yang diperolehi. Ciri plasmon terhadap ketebalan lapisan logam emas ditunjukkan oleh Rajah (2b) di mana pemalar ketelusan nyata berubah dalam

Rajah 2a

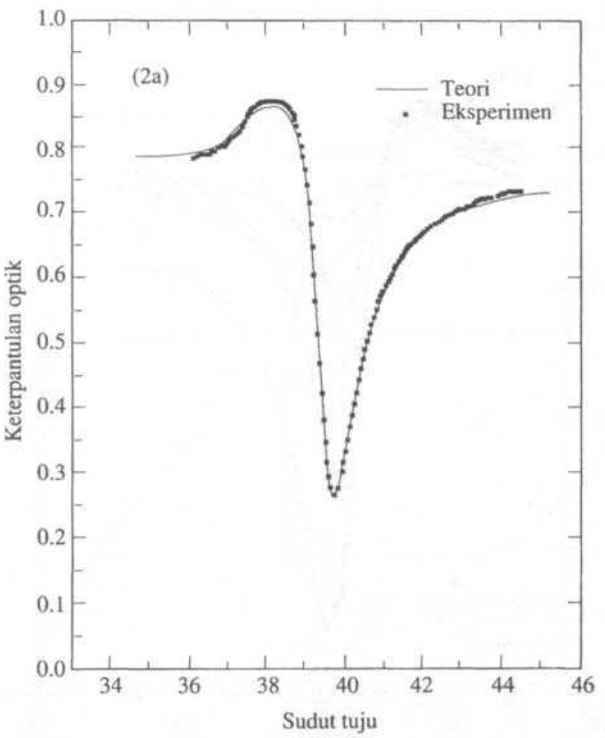

Rajah 2a: Plot keterpantulan optik sebagai fungsi kepada sudut tuju, θ menjelaskan persetujuan nilai teori dengan data uji kaji. Simbol empat segi (■) adalah data uji kaji manakala garis selanjar adalah nilai teori;

lengkungan (-10.48 ↔ -10.97) dan pemalar ketelusan khayal berubah dari 1.93 kepada 3.04. Dalam kajian ini, perubahan kedua pemalar tersebut tidak dapat menjelaskan pergantugan nilai ketelusan logam emas kepada ketebalan sampel secara total, kerana telah dikenal pasti bahawa pemalar optik selaput tipis logam bergantung juga kepada parameter penyediaan dan keadaan persekitaran (Bryan-Brown 1991). Pemalar optik juga didapati tidak berubah setelah dibiarkan terdedah selama 16 hari kepada persekitaran suhu bilik 25°C dengan kelembapan relatif 70%. Parameter penyediaan sampel dalam kajian ini (teknik percikan Polaron E5100) yang tidak dapat dikawal dengan tepat boleh mengakibatkan kemungkinan parameter penyediaan berbeza antara satu sama lain. Walaupun pergantungan pemalar dielektrik kepada ketebalan sampel dalam hal ini tidak berlaku secara total, tetapi hasil kajian ini menunjukkan kesan ketebalan adalah ketara terhadap pemalar dielektrik khayal dan keterpantulan minimum (R_{spr}). Pergantungan R_{spr} sebagai fungsi kepada ketebalan lapisan logam emas

Rajah 2b

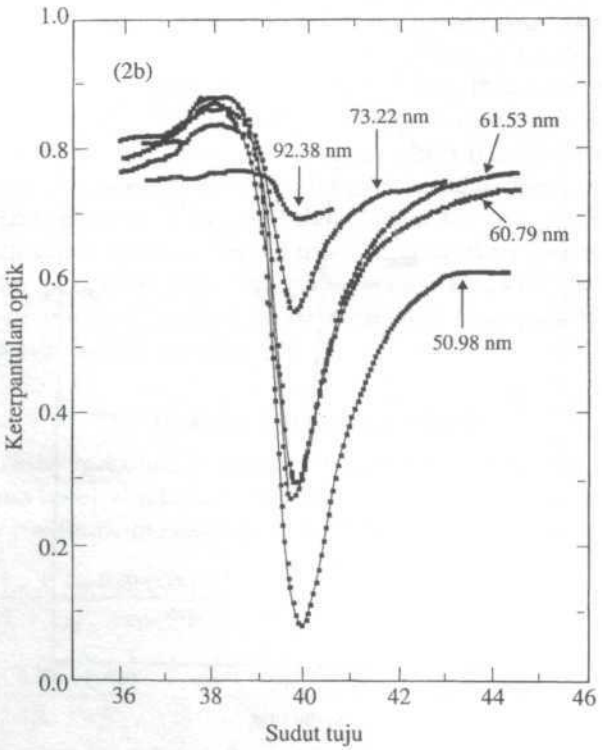

Rajah 2b: Plot keterpantulan optik sebagai fungsi kepada sudut tuju θ , menunjukkan lengkung keterpantulan optik pada pelbagai nilai ketebalan sampel logam emas.

ditunjukkan pada Rajah 3, di mana keterpantulan minimum, R_{spr} bertambah daripada 0.080% kepada 0.695% bila ketebalan sampel bertambah dari 50.80 nm kepada 92.38 nm. Plot kecil dalam Rajah 3 di sudut bawah sebelah kanan menunjukkan perubahan pemalar dielektrik khayal sebagai fungsi kepada ketebalan sampel. Hasil kajian ini menjelaskan kesesuaian logam emas sebagai lapisan aktif sensor optik resonan plasmon permukaan (SPR) dengan ketebalan yang sesuai adalah ≈ 50 nm. Pada nilai ketebalan ini juga dapat diperhatikan bahawa lengkung resonan adalah tajam dan merupakan satu kebaikan dalam penentuan θ untuk sensor optik. Untuk ketebalan < 50 nm, didapati lapisan emas yang disediakan dengan kaedah ini (teknik percikan Polaron E5100) tidak menunjukkan daya lekat yang baik terhadap substrat kaca. Sampel berketebalan < 50 nm juga didapati tidak bersifat homogen yang baik. Oleh yang demikian tidak sesuai digunakan sebagai lapisan aktif sensor optik (SPR) terutama untuk pengukuran pada sampel-larutan yang berketumpatan tinggi seperti susu getah atau madu.

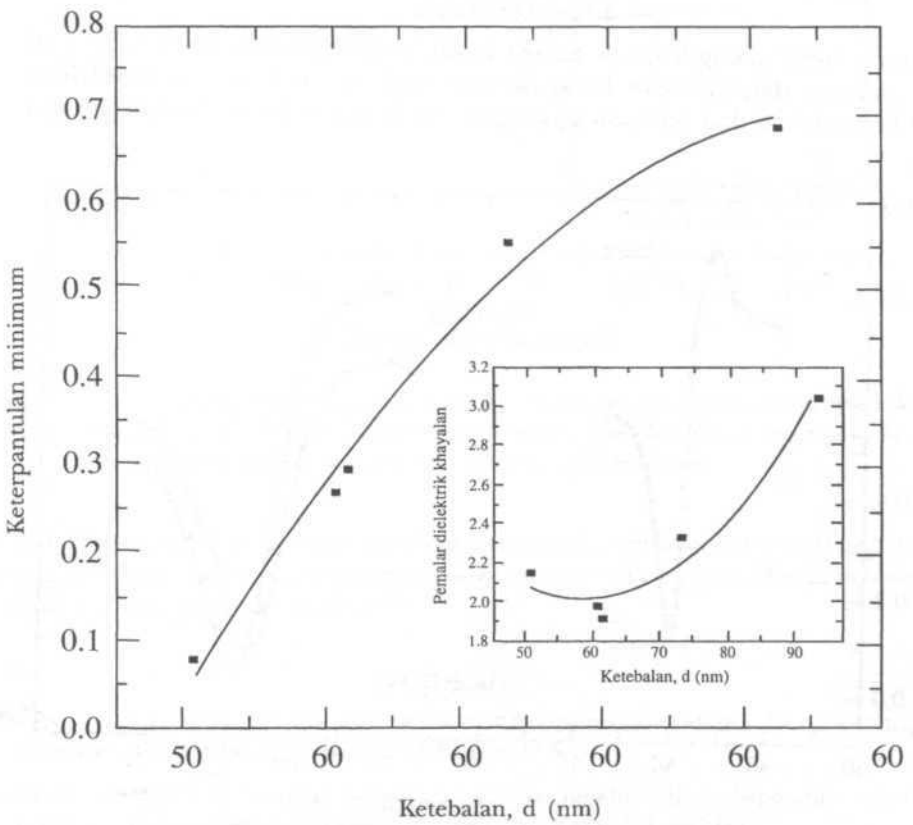

Rajah 3. Perkaitan keterpantulan optik minimum, R_{spr} dengan ketebalan sampel lapisan emas. Plot kecil di sudut bawah sebelah kanan menunjukkan plot nilai pemalar dielektrik khayalan terhadap ketebalan sampel.

Dengan menggunakan ketebalan optimum ≈ 50 nm, satu sel sensor optik direka bentuk untuk menentukan peratus etanol dalam air suling (0 - 15% isipadu). Rajah 4 menunjukkan perubahan lengkung peratus keterpantulan optik sebagai fungsi kepada sudut tuju, θ untuk tiga kes berikut; lapisan emas-udara, lapisan emas-air suling, dan lapisan emas-etanol. Sudut plasmon resonan, θ_{spr} didapati berganjak ke sebelah kanan (θ lebih besar) bila medium ketiga (Rajah 1a) bertambah tumpat. Plot θ_{spr} lawan peratus kepekatan etanol dalam air suling ditunjukkan oleh Rajah 5 dengan kecerunan garis (dirujuk sebagai sensitiviti sensor SPR) adalah direkodkan sebagai $9\ 3\ 10^{-2}$/(% isipadu ethanol). Plot kecil di sudut bawah sebelah kanan pada Rajah 5 menunjukkan satu alternatif lain di mana peratus isipadu etanol dapat ditentukan, iaitu dengan memplot nilai keterpantulan minimum (R_{spr}) sebagai fungsi kepada kepekatan larutan. Dengan resolusi putaran sudut tuju dalam kajian 0.01°, teknik ini berkemampuan menentukan peratus isipadu etanol dalam air sehingga kepada <1%.

PENGHARGAAN

Pengarang ingin mengucapkan terima kasih kepada Jabatan Fizik, Universiti Putra Malaysia dan Malaysia Toray Science Foundation kerana menyediakan segala kemudahan dan bantuan kewangan untuk kajian ini dijalankan dengan

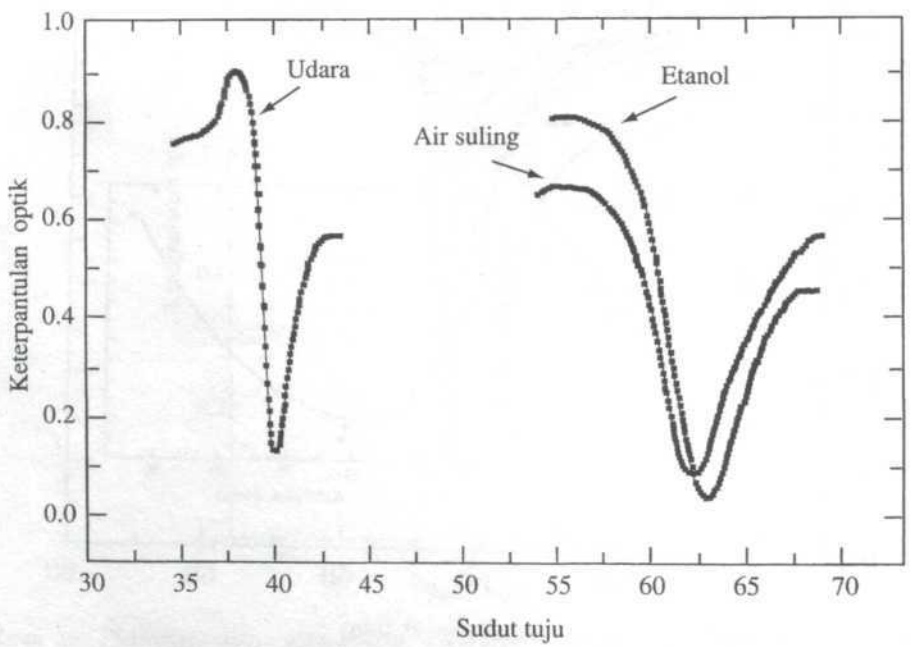

Rajah 4. Resonan plasmon permukaan untuk tiga sampel, iaitu; (a) emas-udara; (b) emas-air suling; dan (c) emas-etanol. Sudut resonan plasmon berganjak kepada sudut tuju yang lebih besar bila indeks biasan medium ke-3 bertambah.

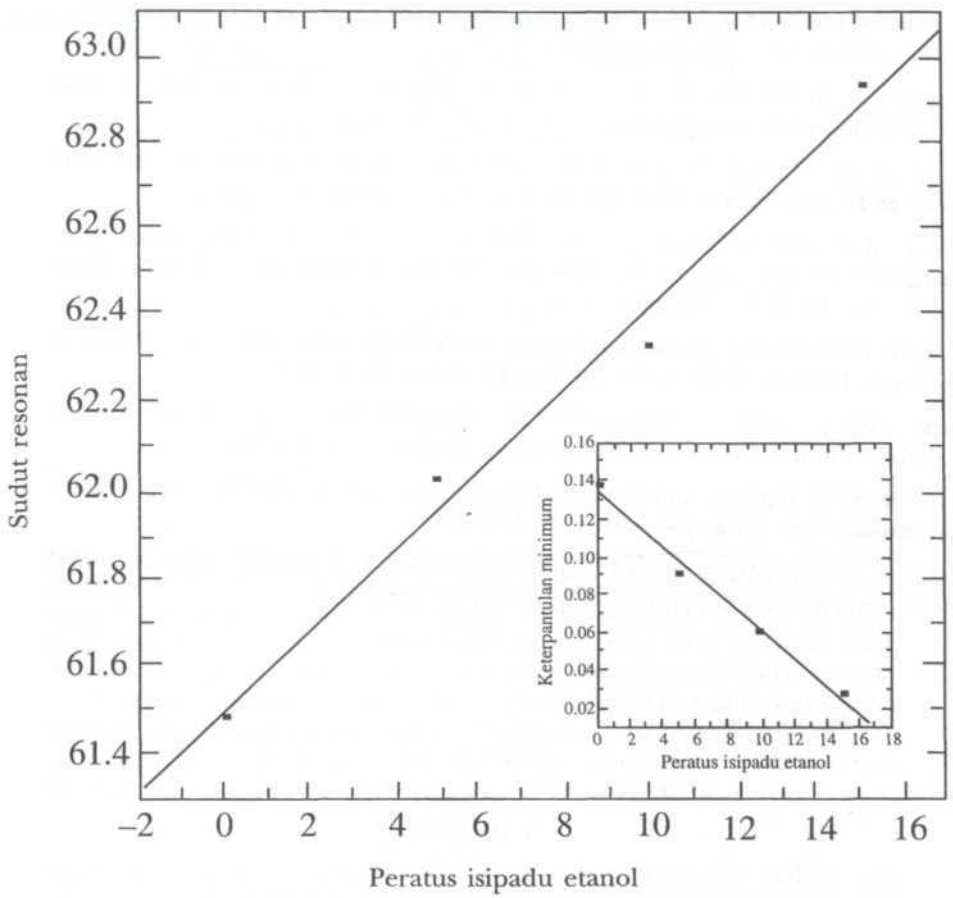

Rajah 5. Perkaitan linear antara sudut resonan, θ_{spr} dengan peratus isipadu etanol dalam air suling. Plot kecil di sudut bawah sebelah kanan menjelaskan kaitan linear yang baik juga boleh ditunjukkan oleh plot keterpantulan optik minimum.

jayanya. Pengarang (Cik Rosmiza Mokhtar) juga ingin merakamkan penghargaan kepada Kerajaan Malaysia kerana membiayai program Pengajian Master selama 2 tahun melalui program PASCA.

RUJUKAN

BRYAN-BROWN, G.P. 1991. Optical Excitation of Electromagnetic Modes Using Grating Coupling, Ph.D. Thesis, University of Exeter, U.K.

DOUGHERTY, G. 1993. A compact optoelectronic instrument with a disposable sensor based on surface plasmon resonance. *Meas. Sci. Technol.* **4**: 697-699.

DE-BRUIJN, H.E., R.P.H. KOOYMAN and J. GREVE. 1992. Choice of metal and wavelength for surface plasmons sensors: some considerations. *Appl. Opt.* **31**: 440-442.

KANO, H. and S. KAWATA. 1994. Surface plasmon sensor for absorption-sensitivity enhancement. *Appl. Opt.* **33**: 5166-5170.

KRETSCHMANN, E., and H. RAETHER. 1971. The determination of optical constants of metal by excitation of surface plasmons. *Z. Phys.* **241**: 313-321.

NAMIRA, E., T. HAYASHIDA, T. ARAKAWA. 1995. Surface plasmon resonance for the detection of some biomolecules. *Sensors and Actuators* **B 24**: 142-144.

ROBERTSON, W.M. and E. FULLERTON. 1989. Re-examination of the surface-plasma-wave technique for determining the dielectric constant and thickness of metal films. *J. Opt. Soc. Am.* **B 6**: 1584-1589.

RAETHER, H. 1988. Surface plasmons on Smooth and Rough Surfaces and on Grating in Springer Tracts in Modern Physics; Vol. III Berlin: Springer Verlag.

SADOWSKI, J.W., J. LEKKALA, I. VIKAHOLM. 1991. Biosensors based on surface plasmon excited in non-noble metals. *Biosensors and Bioelectronics* **6**: 439-444.

SAMBLES, J.R., G.W. BRADBERY and F. YANG, -1991. Optical excitation of surface plasmons: an introduction. *Contemporary Phys.* **32**: 173-183.

WEBER, W.H., and S.L. MCCARTHY. 1975. Surface plasmon resonance as a sensitive optical probe of metal-film properties. *Phys. Rev.* B **12**: 5643-5650.

ISSN: 0128-7680
Pertanika J. Sci. & Technol. 8(1): 41 - 54 (2000)

Analisis Pengawalan Pemberat Rangkaian Neural Perambatan-Balik untuk Pengecaman Aksara Jawi

Ramlan Mahmod dan Khairuddin Omar
Jabatan Sains Komputer
Fakulti Sains Komputer dan Teknologi Maklumat
Universiti Putra Malaysia
43400 Serdang Selangor

Jabatan Sains dan Pengurusan Sistem
Fakulti Teknologi dan Sains Maklumat
Universiti Kebangsaan Malaysia
43600 Bangi Selangor

Received 27 August 1996

ABSTRAK

Satu daripada beberapa faktor yang mempengaruhi keupayaan ***Rangkaian Neural*** (atau ringkasnya **RN**) dalam fasa pengecaman adalah nilai mula yang diberi kepada pemberat semasa fasa latihan. Rangkaian yang telah dilatih boleh terperangkap ke dalam *minimum tempatan* apabila nilai mula pemberat tidak ditentukan dengan betul. Kertas ini membentangkan analisis terhadap keupayaan rangkaian untuk mengecam aksara Jawi setelah ia dilatih menggunakan kaedah pengawalan pemberat yang berlainan. Tiga kaedah yang biasa digunakan ialah *sifar*, *rawak* dan *rawak Nguyen-Widrow*. Kertas ini membincangkan kesan ketiga-tiga kaedah ini terhadap keupayaan pengecaman rangkaian.

ABSTRACT

One of the factors that influences the recognition ability of a neural network is the initial values given to the weight vector during the training phase. The network may be trapped into a local minima if the initial weights are not chosen carefully. This paper presents an analysis of the ability of the network to recognise Jawi characters after it was trained using different methods of weight initialization. Three most common methods are zero, random and Nguyen-Widrow random. This paper presents the effect of these three methods on the ability of the network's recognition.

Keywords: Rangkaian neural, perambatan-balik, Rawak Nguyen-Widrow, pengecaman corak

PENGENALAN

Perambatan-balik adalah tatacara *kecerunan berasas-turunan* untuk mensetkan pemberat bagi satu **RN** multi-lapis rambatan ke hadapan yang juga dikenali sebagai *perseptron multi-lapis*. Bagaimanapun *perambatan-balik* hanyalah satu cara menganggarkan tatacara kecerunan turunan sebagaimana biasa ia dilaksanakan, Ruck *et al* (1992), iaitu, ralat kuasadua yang dikira itu diperuntukkan kepada permukaan ralat yang hanya didefinasikan oleh vektor latihan semasa dan bukan vektor latihan secara keseluruhan. Begitu juga tatacara ini sangat

bergantung kepada nilai awal pemberat yang diberikan, iaitu sama ada dengan memberikan nilai sifar kepada seluruh pemberat atau secara rawak dalam julat nilai tertentu. Kertas ini memaparkan satu analisis perbandingan pelbagai nilai pemberat awal seperti yang dinyatakan tadi termasuk menggunakan kaedah pemberat awal Nguyen-Widrow. Satu perbandingan kaedah nilai awal yang manakah yang dikatakan paling baik akan dipaparkan dengan menggunakan data sintasis. Di dalam kertas ini kami mengutarakan pencaman corak huruf-huruf tunggal Jawi sebagai aplikasi utama.

Bahagian berikut menjelaskan secara ringkas latarbelakang RN. Bahagian berikutnya menjelaskan implementasi bagi rangkaian ini dengan aplikasinya kepada aksara Jawi. Hasil simulasi dipaparkan di dalam bahagian selanjutnya. Akhir sekali hasil ujikaji ini disimpulkan di bahagian kesimpulan.

LATAR BELAKANG

Bahagian ini menjelaskan paradigma RN seperti senibina *perseptron multi-lapis*, *fungsi pengaktifan*, model *latihan perambatan-balik*, dan *algoritma*nya.

Senibina Perseptron Multi-Lapis

Senibina *perseptron multi-lapis* adalah lanjutan daripada *perseptron satu-lapis*, yang dikaji oleh Rosenblatt pada pertengahan 1950'an. *Perseptron multi-lapis* bermakna terdapat lebih daripada satu lapisan nod-nod yang terhubung sepenuhnya di antara lapisan-lapisan itu. Rajah 1 menunjukkan struktur *perseptron multi-lapis*.

Setiap nod dalam Rajah 1a digambarkan oleh bulatan berlorek di dalam Rajah 1b, yang melaksanakan perjumlahan input berpemberat dan seterusnya digunakan oleh *fungsi pengaktifan tak-linear* dalam Rajah 1c untuk mendapatkan nilai output untuk setiap nod pada lapisan yang seterusnya. Rangkaian tadi menunjukkan terdapat satu lapisan tersembunyi, iaitu satu lapisan yang bukan lapisan input atau lapisan output. Rangkaian itu mempunyai M unit nod input, H nod pada lapisan tersembunyi, dan N nod output. Lapisan input tidak dikira sebagai satu lapisan, iaitu hanya lapisan yang menggunakan *fungsi pengaktifan tak-linear* sahaja dikira sebagai satu lapisan. Ini bermakna lapisan pertama bermula di lapisan tersembunyi. Senibina RN jenis *perseptron multi-lapis* akan digunakan dalam kertas ini.

Fungsi Pengaktifan

Pelbagai *fungsi pengaktifan* boleh digunakan. Fungsi yang sering digunakan ialah *fungsi Sigmoid* (lengkok bentuk-S), (Fauset 1994); dan (Ramlan dan Khairuddin 1996). Fungsi ini tak-linear dan boleh dicari terbitannya. Dua bentuk fungsi tersebut ialah *fungsi logistik* dan *fungsi tangen hiperbola* yang mempunyai sifat-sifat yang sama di antara keduanya. Kedua-duanya mempunyai kebaikan terutama didalam kegunaan RN yang dilatih oleh *perambatan-balik*, kerana terdapat hubungan yang mudah di antara nilai fungsi pada satu titik dan nilai terbitannya (boleh mendapatkan terbitannya) pada titik tadi boleh mengurangkan beban pengiraan ketika latihan. Fungsi ini juga bersifat global,

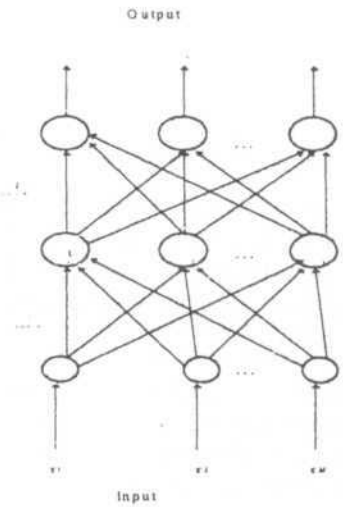

Rajah 1a. Senibina rangkaian multi-lapis

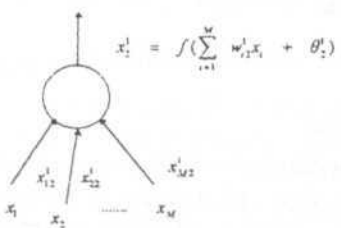

Rajah 1b.Butiran terperinci tentang nod

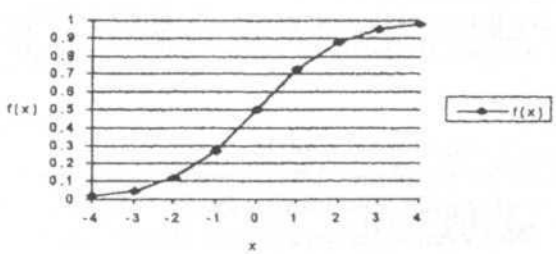

Rajah 1c. Fungsi pengaktifan sigmoid perpaduan

iaitu kesan nilai fungsi pada satu titik dan nilai terbitannya adalah terhadap julat $-\infty$ hingga $+\infty$ dan sangat berguna untuk tujuan pengkelasan yang fungsi outputnya bernilai 0 atau 1 atau -1. Berikut diberikan fungsi Sigmoid Binari yang sering digunakan:

$$f(x) = \frac{1}{1+\exp(-\sigma x)}$$

dan terbitannya diberikan oleh

$$f(x) = \sigma(x)[1- f(x)]$$

Fungsi sigmoid yang julatnya adalah dari 0 hingga 1 sering digunakan untuk RN jika output dikehendaki adalah berbentuk binari atau berada dalam julat di antara 0 dan 1. Sebaliknya jika julat berada di antara –1 dengan 1 adalah lebih baik ditukar kepada bentuk bipolar dan kemudian gunakan fungsi sigmoid bipolar, Fausett(1994) seperti berikut:

$$g(x) = 2f(x)-1 = \frac{2}{2+\exp(-\sigma x)} - 1$$

$$= \frac{1-\exp(-\sigma x)}{1+\exp(-\sigma x)}$$

dan terbitannya diberikan oleh:

$$g'(x) = \frac{\sigma}{2}[1+ g(x)][1 - g(x)]$$

Fungsi pengaktifan yang digunakan didalam kertas ini adalah dari jenis bipolar.

Model Latihan Perambatan-balik

Perambatan-balik adalah kaedah kecerunan menurun untuk melatih pemberat dalam *Perseptron multi-lapis* dan juga dikenali sebagai petua *delta teritlakkan,* Ruck et al(1992). Latihan bagi rangkaian ini melibatkan tiga peringkat: *menghantar corak isyarat input latihan kehadapan, pengiraan dan merambat balik ralat yang dikira,* dan *kemaskini semua pemberat,* Fausett(1994).

Untuk sebarang masalah yang diberi, terdapat satu set vektor latihan katalah X, dalam keadaan untuk setiap $x \in X$, maka terdapat vektor yang dikehendaki d D, dengan D adalah set output yang bersekutu dengan vektor latihan dalam X.

Katalah ralat semasa E_p didefinasikan oleh:

$$E_p = \frac{1}{2}\left(d_p - z_p\right)^T \left(d_p - z_p\right)$$

$$= \frac{1}{2}\sum_{k=1}^{N}\left(d_{k,p} - z_{k,p}\right)^2 \qquad (1)$$

dengan $d_{k,p}$ adalah komponen ke k daripada p vektor output yang dikehendaki d_p, dan $z_{k,p}$ adalah komponen ke k daripada vektor output z_p sebenar apabila p latihan x_p^l menjadi input kepada p*erseptron multi-lapis.*

Katakan jumlah ralat E_T didefinasikan seperti berikut:

$$E_T = \sum_{p=1}^{P} E_p$$

dengan P adalah *kekardinalan* bagi X. Ambil ingatan bahawa E_T adalah fungsi bagi kesemua set latihan dan juga pemberat dalam rangkaian. *Petua perambatan-balik* didefinasikan sebagai berikut:

$$\Delta w(t) = -\eta \frac{\partial E_p}{\partial w} + \alpha \Delta w(w-1) \qquad (2)$$

dengan η, adalah *kadar pembelajaran*, iaitu suatu nilai positif yang kecil, α adalah faktor *momentum* yang juga mempunyai nilai positif yang kecil, dan w mewakili pemberat. Di dalam persamaan di atas, $\Delta w(t)$ adalah perubahan pemberat yang dikira pada masa t. Apabila sebutan *momentum* digunakan ($\alpha \neq 0$), petua latihan ini disebut *kaedah momentum*. Apabila nilai α dalam (2) sama dengan sifar, ia disebut *perambatan-balik sertamerta* kerana ia mengira kecerunan berdasarkan vektor latihan tunggal. Terdapat variasi lain iaitu *perambatan-balik berkelompok*, yang mengira perubahan pemberat menggunakan kecerunan berdasarkan kepada *ralat total* E_T. Untuk masalah yang melibatkan pemaparan keputusan, maka kaedah *perambatan-balik serta-merta* digunakan.

Pilihan Pengawalan Pemberat dan Pincang

Pilihan untuk mengawalkan pemberat adalah sangat penting dan memberi kesan kepada rangkaian sama ada telah mencapai tahap *ralat minimum yang sejagat* dan, jika sekalipun telah mencapai tahap tersebut adakah ia menumpu dengan cepat. Persoalan ini akan cuba digarab dengan memilih beberapa kaedah mengawalkan nilai pemberat. Bahagian berikut akan membicarakan kaedah-kaedah tersebut.

PENGAWALAN PEMBERAT SIFAR

Dalam kaedah ini semua pemberat diawalkan dengan nilai sifar, ini termasuklah nilai awal pemberat *pincang*.

PENGAWALAN PEMBERAT RAWAK

Kaedah ini sangat bergantung kepada *fungsi pengaktifan* yang digunakan. *Fungsi sigmoid* yang digunakan didalam rangkaian ini mempunyai batas atas dan batas bawah. Dengan alasan ini, adalah sangat penting supaya tidak memilih suatu nilai yang akan menghasilkan nilai *fungsi pengaktifan*nya bersamaan dengan sifar. Ini termasuklah nilai terbitannya. Begitupun nilai awalnya juga tidak boleh terlalu besar, atau isyarat input awal kepada unit tersembunyi atau unit output hendaklah berada di dalam julat yang membolehkan nilai terbitan *fungsi sigmoid* itu dengan suatu nilai yang kecil. Dengan perkataan lain, jika nilai awal pemberat terlalu kecil, input bersih kepada unit tersembunyi atau

unit output akan menghampiri sifar. Nilai yang dicadangkan ialah suatu nilai rawak yang berada di antara julat -0.5 dan 0.5 ataupun nilai julat yang berpatutan. Pelbagai *fungsi rawak* boleh digunakan untuk menjana nombor-nombor dalam julat -0.5 dan 0.5. Dalam kajian ini, kami tidak membuat analisis terhadap setiap fungsi rawak secara terperinci sebelum membuat pilihan. Kami hanya mengambil satu daripada fungsi rawak yang kerap digunakan dan rumus fungsi tersebut adalah seperti di bawah:

```
rawak = (float) ((rand()%5000)/10000.00).
```

yang rand() adalah adalah fungsi pratakrif dalam bahasa pengaturcaraan C. Ia berfungsi menjanakan nombor rawak berada di antara -5000 dan 5000 sahaja.

PENGAWALAN PEMBERAT RAWAK NGUYEN-WINDROW

Kaedah ini boleh digunakan untuk mengawalkan nilai pemberat dan *pincang*nya dan dikatakan boleh menumpu cepat berbanding dengan pengawalan rawak biasa, Fausett(1994). Dalam kaedah ini sedikit ubahsuai terhadap perambatan ralat dan ubahsuai ini berasaskan analisa geometri iaitu melihat tindakbalas di antara neuron di lapisan tersembunyi dengan satu unit input; dan kemudian dikembangkan kepada beberapa unit input. Pemberat untuk lapisan di antara unit-unit tersembunyi dengan unit-unit output diawalkan dengan nilai yang berada di antara -0.5 dan 0.5. Manakala pemberat untuk lapisan di antara unit-unit tersembunyi dengan unit-unit input diubahsuaikan supaya dapat memperbaiki kebolehan proses pembelajarannya. Pembolehubah-pembolehubah dan rumus yang digunakan ialah η adalah bilangan unit input, manakala p *adalah* bilangan unit tersembunyi, dan β adalah faktor skala:

$$\beta = 0.7(p)^{1/n}$$

Tatacara untuk kaedah ini adalah seperti berikut:

Langkah 0: Untuk setiap unit tersembunyi ($j = 1, 2, ..., p$):

Langkah 1: Awalkan Vektor Pemberat (VP) nya dengan (dari unit input):

$v_{i,j}$ (*lama*) = nombor rawak di antara -0.5 dan 0.5 (atau dalam julat tertentu selain daripada sifar).

Langkah 2: Kira $\left\| v_j(lama) \right\|$

Langkah 3: Awalkan semula dengan:

$$v_{i,j} = \frac{\beta v_{i,j}(lama)}{\left\| v_j(lama) \right\|}$$

dan setkan pincang $v_{0,j}$ = nombor rawak di antara $-\beta$ dan β.

Langkah 4: Uji syarat berhenti.

IMPLEMENTASI

Pengkodan Data

Corak input dan tindak balas atau outputnya yang digunakan ketika latihan hendaklah diwakilkan dalam bentuk yang tertentu dan sesuai untuk diproses di dalam RN. *Perwakilan dwikutub* dikatakan mempunyai ciri-ciri yang sangat baik jika dibandingkan dengan *perwakilan perduaan*, (Fausett 1994). Oleh itu, corak input dan corak output yang berbentuk *perwakilan dwikutub* ini telah digunakan di dalam semua latihan yang dilakukan. Pertimbangkan huruf-huruf Jawi tunggal seperti yang diberikan di dalam Rajah 2.

Sebanyak 7 corak input telah digunakan didalam *algoritma latihan*. Kita akan menggunakan rangkaian ini untuk mengkelaskan setiap *vektor input* itu sama ada dipunyai atau tidak dipunyai oleh setiap 7 kelas kategori. Rangkaian akan mempunyai 7 unit output untuk mengkelaskan setiap unit input. Vektor input mempunyai saiz corak pixel 8x8, atau 64-tutupan. Setiap corak '.' diwakilkan dengan nilai 1 manakala corak ' ' pula diwakilkan dengan –1, seperti yang digambarkan di dalam Rajah 2a.

Menukarkan corak dua dimensi kepada satu vektor input dilakukan dengan mudah, iaitu dengan hanya mencantumkan baris-baris, iaitu baris pertama akan diikuti baris kedua dan seterusnya, sebagai contoh corak, huruf 'Alif' akan menjadi

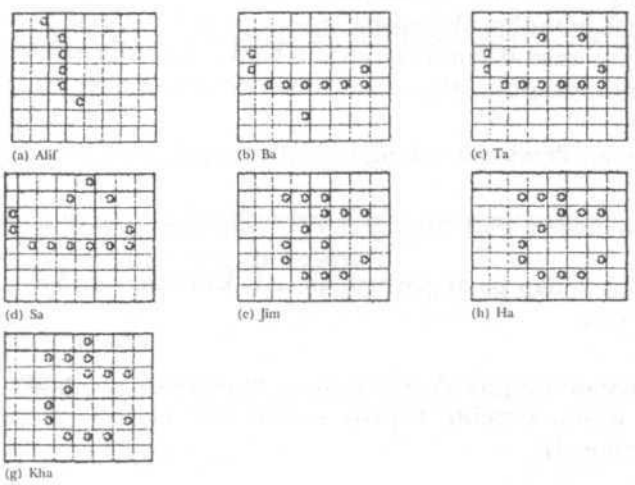

Rajah 2. Contoh huruf Jawi

-1 1 -1 -1 -1 -1 -1 -1,
-1 -1 1 -1 -1 -1 -1 -1,
-1 -1 1 -1 -1 -1 -1 -1,
-1 -1 1 -1 -1 -1 -1 -1,
-1 -1 1 -1 -1 -1 -1 -1,
-1 -1 1 -1 -1 -1 -1 -1,
-1 -1 -1 -1 -1 -1 -1 -1,
-1 -1 -1 -1 -1 -1 -1 -1.

Rajah 2a. Perwakilan huruf 'Alif' dalam bentuk perwakilan dwikutub

-1 1 -1 -1 -1 -1 -1 -1, -1 -1 1 -1 -1 -1 -1 -1, -1 -1 1 -1 -1 -1 -1 -1, -1 -1 1 -1 -1 -1 -1 -1, -1 -1 1 -1 -1 -1 -1 -1, -1 -1 1 -1 -1 -1 -1 -1, -1 -1 -1 -1 -1 -1 -1 -1, -1 -1 -1 -1 -1 -1 -1 -1.

Tindakbalas yang betul bagi corak pertama diwakilkan dengan nilai 1, manakala tindakbalas yang tidak betul bagi corak yang lain dinyatakan dengan -1. Ini bermakna bagi satu corak, misalnya huruf 'Alif', vektor output boleh diwakilkan dengan (1 -1 -1 -1 -1 -1 -1).

Algoritma

Algoritma yang akan dipaparkan di dalam kertas ini dibahagikan kepada dua bahagian iaitu *Algoritma Latihan* dan *Algoritma Aplikasi* seperti yang diutarakan oleh Fausett(1994) di bahagian berikut:

ALGORITMA LATIHAN

Secara amnya algoritma ini dibahagikan kepada 3 bahagian utama iaitu menghantar isyarat input bersih kepada lapisan yang lebih atas dalam langkah kehadapan, mengira ralat dalam perambatan-balik, dan akhir sekali kemas kini pemberat dan pincangkannya. Algoritma latihan diberikan oleh tatacara berikut:

Langkah 0. Awalkan Pemberat (mengikut keterangan 2.5.1 hingga 2.5.4).

Langkah 1. Selagi syarat berhenti masih palsu, lakukan langkah 2-9.

Langkah 2. Untuk setiap pasangan latihan, lakukan langkah 3-8.
Langkah kehadapan:

Langkah 3. Setiap unit input (X_i, $i = 1, 2, ..., n$) menerima isyarat input x_i dan menghantarkan isyarat tersebut kepada semua unit di layar yang di atasnya (unit-unit tersembunyi).

Langkah 4. Setiap unit tersembunyi (Z_j = *1, 2, ..., p*) menjumlahkan isyarat input berpemberat,

$$z\_in_j = v_{0,j} + \sum_{i=1}^{n} x_i v_{i,j},$$

menggunakan fungsi pengaktifannya untuk mendapatkan nilai isyarat output,

$$z_j = f\left(z\_in_j\right)$$

dan menghantarkan isyarat itu kepada semua unit yang berada di layar di atasnya (unit-unit output).

Langkah 5. Setiap unit output (Y_k, k = *1, 2, ..., m*) menjumlahkan isyarat input berpemberat,

$$y\_in_k = W_{0,k} + \sum_{j=1}^{p} z_i w_{j,k},$$

menggunakan fungsi pengaktifannya untuk mendapatkan nilai isyarat output,

$$y_k = f\left(y\_in_k\right)$$

RALAT PERAMBATAN BALIK

Langkah 6. Setiap unit output (Y_k, k = *1, 2, ..., m*) menerima satu corak sasaran berpasangan dengan corak latihan input, mengira ralat,

$$\delta_k = \left(t_k - y_k\right) f'\left(y\_in_k\right),$$

mengira pembetulan pemberat (digunakan untuk kemaskini pemberat W_j, k kemudian),

$$\Delta w_{j,k} = \alpha \delta_k z_j,$$

mengira pembetulan pincang (digunakan untuk kemaskini nilai pincang W_0, k kemudian),

$$\Delta w_{0,k} = \alpha \delta_k,$$

dan menghantar δ_k ke unit di layar di bawahnya.

Langkah 7. Setiap unit tersembunyi (Z_j = *1, 2, ..., p*) menjumlahkan input delta tadi (dari unit-unit di layar yang di atasnya),

$$\delta\_in_j = \sum_{k=1}^{m} \delta\_w_{j,k},$$

didarabkan dengan terbitan fungsi pengaktifannya untuk mengira ralat,

$$\delta_j = \delta\_in_j f'\left(z\_in_j\right),$$

mengira ralat pemberat (digunakan untuk kemaskini $v_{i,j}$ kemudian),

$$\Delta v_{i,j} = \alpha \delta_j x_i,$$

dan mengira pembetulan pincangnya (digunakan untuk kemaskini $v_{0,j}$ kemudian),

$$\Delta v_{0,j} = \alpha \delta_j.$$

KEMASKINI PEMBERAT DAN PINCANGNYA

Langkah 8. Setiap unit output ($Y_k = 1, 2, ..., m$) mengemaskini pincang dan pemberatnya ($j = 0, 1, 2, ..., p$):

$$w_{j,k}(baru) = w_{j,k}(lama) + \Delta w_{j,k}.$$

Setiap unit tersembunyi ($Z_j = 1, 2, ..., p$) mengemaskini pincang dan pemberatnya ($i = 0, 1, 2, ..., n$):

$$v_{i,j}(baru) = v_{i,j}(lama) + \Delta v_{i,j}.$$

Langkah 9. Uji syarat berhenti.

Algoritma Aplikasi

Algoritma aplikasi diberikan oleh tatacara berikut:

Langkah 0. Awalkan Pemberat (diperoleh daripada Algoritma Latihan).

Langkah 1. Untuk setiap vektor input, lakukan langkah 2-4.

Langkah 2. Setiap unit input (X_i, $i = 1, 2, ..., n$) menerima isyarat input dan menghantarkan isyarat tersebut kepada semua unit di layar yang di atasnya (unit-unit tersembunyi).

Langkah 3. Setiap unit tersembunyi ($Z_j = 1, 2, ..., p$) menjumlahkan isyarat input berpemberat,

$$z\_in_j = v_{0,j} + \sum_{i=1}^{n} x_i v_{i,j},$$

menggunakan fungsi pengaktifannya untuk mendapatkan nilai isyarat output,

$$z_j = f(z\_in_j),$$

dan menghantarkan isyarat itu kepada semua unit yang berada di layar di atasnya (unit-unit output).

Langkah 4. Setiap unit output (Y_k, $k = 1, 2, ..., m$) menjumlahkan isyarat input berpemberat,

$$y\_in_k = w_{0,k} + \sum_{j=1}^{p} z_j w_{j,k},$$

menggunakan fungsi pengaktifannya untuk mendapatkan nilai isyarat output,

$$y_k = f(y\_in_k)$$

Hasil-Perbandingan Prestasi

Senibina rangkaian ini telah diimplemenkan pada mikrokumputer 486 serasi IBM dan dilarikan menggunakan bahasa C++. Tiga ujikaji telah dijalankan berdasarkan kepada bilangan unit tersembunyi (UT). Bilangan UT yang digunakan ialah (i) 4, (ii) 8, dan (iii) 12 untuk diaplikasikan kepada beberapa huruf Jawi. Huruf jawi yang dipilih *ialah Alif, Ba, Ta, Sa, Jim, Ha, dan Kho,* ini menjadikan bilangan pasangan corak input output ialah sebanyak 7. Kadar latihan yang digunakan untuk kesemua latihan ialah bernilai 0.2. Faktor momentum tidak dipertimbangkan dalam kajian ini. Latihan diteruskan sehingga mencapai 50,000 kitar dan *jumlah ralat kuasa-dua* untuk kesemua latihan diuji supaya menghampiri sifar. Berikut adalah keterangan hasil perbandingan di antara tiga kaedah nilai awal pemberat.

PEMBERAT SIFAR

Berpandukan kepada Rajah 3, latihan dengan menggunakan nilai awal pemberat sifar tidak dapat mengecam corak yang dipertimbangkan tadi. Untuk kes ini walaupun latihan telah mencecah 50,000 kitaran, senibina rangkaian masih belum dapat mengenali corak tadi. Untuk kes 4-UT, *jumlah kuasa-dua ralat* bernilai 21.00 dari permulaan latihan sehinggalah ke kitaran 50,000, manakala untuk 8-UT ralat kuasa dua berkurangan (iaitu bernilai 6.0 sehinggalah ke kitaran 26,000 dan bertambah sebanyak 1.0 menjadi 7.0 pada kitaran 27,000) tetapi masih gagal mengecam corak tadi. Bagi 12-UT pula penumpuan bertambah buruk dan nilai kuasa dua ralat menjadi 24.0 dari mula latihan sehinggalah tamat latihan. Fenomena ini menunjukkan ia terperangkap di dalam minimum tempatan.

PEMBERAT RAWAK

Berpandukan kepada Rajah 4, latihan menggunakan nilai awal rawak juga didapati tidak dapat mengecam corak yang dipertimbangkan tadi. Bagi ketiga-tiga jenis UT, secara relatifnya sangat perlahan untuk menumpu. Bagi 4-UT nilai ralat kuasa-duanya bermula dengan 18.0 dan meningkat sedikit pada kitar 6,000 dan beransur-ansur menyusut sehinggalah kepada kitaran ke 37,000 dan kemudian sesudah itu meningkat semula dan kembali menyusut pada

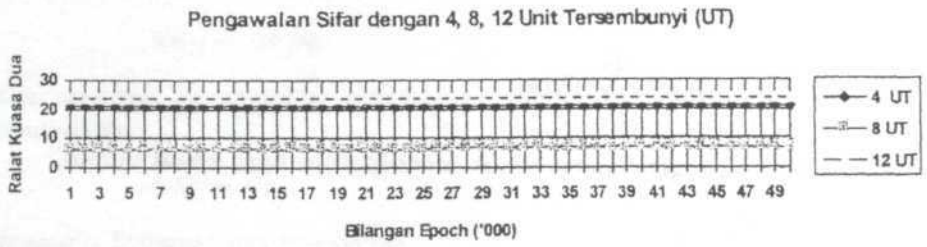

Rajah 3. Hasil dari pengawalan nilai pemberat sifar

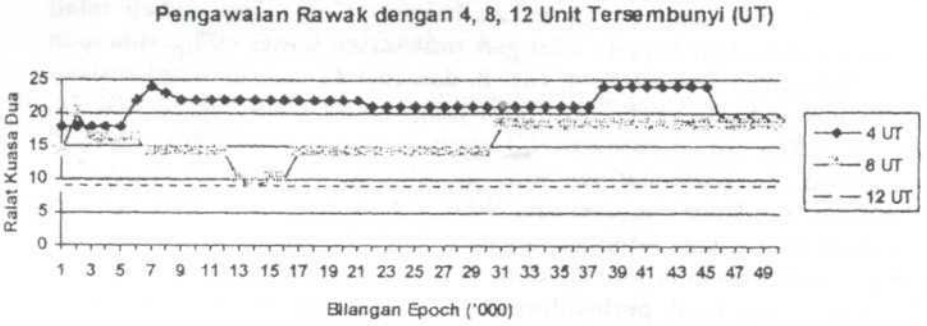

Rajah 4. Hasil Dari pengawalan nilai pemberat rawak

kitaran ke 46,000. Keadaan ini tidak jauh berbeza dengan senibina 8-UT tetapi ralat kuasaduanya sedikit berkurangan daripada senibina 4-UT. Bermula dengan nilai 14.0 dan menokok secara mendadak pada kitaran ke 2,000 dan kembali menyusut kepada nilai 9.0 pada kitaran ke 14,000. Sesudah itu kembali menokok sehingga kepada nilai 14.0 tanpa perubahan. Nilai ralat itu semakin bertambah kepada nilai 18.0 pada kitaran ke 31,000 dan terus tidak mengalami perubahan sehinggalah ke kitaran 50,000. Berbeza untuk senibina 12-UT, jumlah ralat kuasa-duanya semakin berkurang iaitu bernilai 9.0 dan terus kekal tanpa sebarang perubahan sehingga kitaran ke 50,000. Terperangkap di dalam minimum tempatan.

Pemberat Rawak Nguyen-Widrow

Berpandukan kepada Rajah 5, latihan menggunakan nilai awal rawak Nguyen-Widrow lebih mudah mencapai ralat minimum, (Fausett, 1994). Penumpuannya sangat baik kecuali bagi senibina 4-UT. Senibina 4-UT secara relatifnya tidak boleh mengecam corak. Senibina 8-UT dan 12-UT dengan begitu konsisten mencapai ralat minimum sifar sepanjang latihan kecuali bagi senibina 12-UT dengan sedikit ralat pada permulaan latihan. Dengan itu senibina 8-UT dan 12-UT telah berjaya mengecam corak dengan sangat baik.

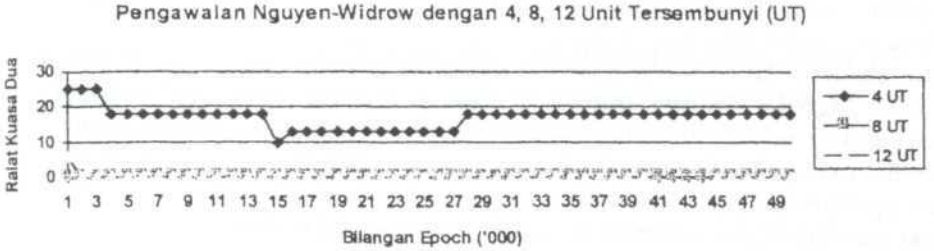

Rajah 5. Hasil dari pengawalan nilai pemberat nguyen-Widrow

PERBINCANGAN

Pemilihan pengawalan pemberat sangat mempengaruhi jumlah *ralat kuasadua minimum sejagat* dan jika berlaku ia akan memberi kesan kepada berapa cepatkah ia menumpu. Ubahsuai nilai pemberat di antara dua unit neuron bergantung *kepada terbitan fungsi pengaktifan* bagi unit-unit di paras atas (lapisan tersembunyi atau output) dan di paras bawah (lapisan input). Oleh kerana itu pemilihan pemberat yang dibuat itu perlulah sebaik mungkin supaya tidak menghasillkan nilai pengaktifan atau terbitan pengaktifan yang sifar. Nilai awal pemberat mestilah tidak terlalu besar, atau isyarat input awal kepada unit tersembunyi atau nilai output hendaklah berada dalam julat yang terbitan *fungsi sigmoid*nya mempunyai nilai yang tidak terlalu kecil (dikenali sebagai *julat penumpuan*). Dengan perkataan lain, jika nilai awal pemberat terlalu kecil, input bersih kepada unit tersembunyi atau output akan hampir kepada sifar, yang menyebabkan *kadar pembelajaran*nya terlalu perlahan. Perkara ini dapat dilihat dengan jelas untuk senibina yang nilai awal pemberatnya sifar, seperti yang dijelaskan dalam 3.3.1 di atas. Sungguhpun bilangan kitar yang dipilih itu iaitu 50,000 kitar namun senibina yang ini masih gagal mengecam corak yang dipilih. Begitu juga bagi nilai awal rawak walaupun nilai yang dipilih itu berada di antara julat -0.5 dengan 0.5 tetapi nilai awal input corak pula mempengaruhi nilai input bersih kepada unit tersembunyi. Berbeza dengan senibina pemberat awal Nguyen-Widrow, pemberatnya telah diskalarkan, oleh itu, pemberat yang diperoleh mempunyai ukuran $0.7\sqrt[n]{p}$ di mana n itu ialah bilangan input dan p bilangan unit tersembunyi. Pemberat pincangnya telah di skalarkan supaya berada di antara julat $-0.7\sqrt[n]{p}$ dan $0.7\sqrt[n]{p}$ dengan n=64, dan p=4, 8, dan 12. Nilai pemberat yang diperoleh dari senibina 8-UT pada kitar ke 1,000 telah diuji kepada beberapa pasangan corak input output sama ada yang berlaku sedikit hingar atau bebas hingar. Hasilnya dapat mengecam kesemua corak tersebut dengan ketepatan 100%.

KESIMPULAN

Kesimpulan yang boleh dibuat ialah ketepatan hasil pengecaman senibina rangkaian Perambatan-Balik untuk mengecam sesuatu corak sangat bergantung

kepada nilai awal pemberat dan telah dibuktikan melalui contoh-contoh yang telah dipaparkan didalam kertas ini.

Hasil eksperimen menunjukkan pengawalan pemberat menggunakan pendekatan Nguyen-Widrow untuk melatih *perseptron multi-lapis* berjaya mempercepatkan penumpuan dan mencapai *ralat minimum* sifar. Ini sekaligus menghasilkan keupayaan pengecaman corak ke takat 100 %. Namun demikian bilangan nod-nod yang perlu didalam senibina RN hendaklah dipilih dengan teliti agar ketepatan pengecaman yang baik ini dapat diperoleh.

RUJUKAN

FAUSETT L. 1994. *Fundamental of Neural Networks: Architectures, Algorithms, & Applications.* New Jersey: Prentice-Hall.

RAMLAN BIN MAHMOD dan KHAIRUDDIN BIN OMAR, 1996. Rangkaian Neural: Satu Tinjauan Ringkas. Laporan Teknik Jabatan Sains Komputer, Universiti Pertanian. ***SAK/TR-010/96.***

RUCK D. W., S. K. ROGERS, M. KABRISKY, P. S. MAYBECK, M. E. OXLEY, 1992. Comparative analysis of backpropagation & the extended kalman filter for training multilayer perceptrons. *IEEE Transactions on Pattern Analysis & Machine Intelligence.* 14(6): 686-691.

TSOI, AH CHUNG. 1994. Constructive Algorithms. A Course on Artificial Neural Networks. Jointly Organised by MIMOS & Computer Centre, University of Malaya, 4-8 July 1994.

Pertanika J. Sci. & Technol. 8(1): 55 - 72 (2000)
ISSN: 0128-7680

Monthly and Annual Distribution of Both the Frequency of Rainy Days and Rainfall Intensity in Peninsular Malaysia

Alejandro Livio Camerlengo and Nhakhorn Somchit
Faculty of Applied Sciences and Technology
Universiti Putra Malaysia Terengganu
Mengabang Telipot
21030 Kuala Terengganu
e-mail: alex@uct.edu.my

Received 7 December 1998

ABSTRAK

Tujuan kajian ini adalah untuk menganalisa frekuensi bilangan hari hujan serta keamatan hujan (rainfall intensity) secara bulanan serta secara berpenggal (annual). Secara ringkas kajian ini mendapati bahawa: (a) agihan frekuensi bilangan hari hujan menyerupai agihan bulanan taburan hujan di bahagian barat banjaran utama; (b) terdapat gradien penting pada kedua-dua frekuensi taburan hari hujan dan keamatan hujan di kawasan banjaran Titiwangsa dengan nilai maksima diperhatikan di sebelah barat dan minima di sebelah timur; (c) Taburan kedua-dua frekuensi hari hujan dan keamatan hujan adalah homogen untuk sebelah timur banjaran utama sehingga 50 km dari pantai timur; dan (d) nilai minuma frekuensi hari hujan dan keamatan hujan dicatatkan di kawasan barat laut semenanjung semasa musim sejuk hemesfera utara (boreal winter).

ABSTRACT

The aim of this study is to analyze both the monthly and the annual distributions of both the frequency of rainy days and the rainfall intensity in Peninsular Malaysia. The most relevant findings of this study may be summarized as: (a) the monthly distribution of the frequency of rainy days is similar to the monthly rainfall distribution at the western side of the principal mountain range; (b) an important gradient of both the frequency of rainy days and the rainfall intensity is recorded at the Titiwangsa mountain range where a maximum is observed at its western side and a minimum at its eastern side; (c) the distribution of both the frequency of rainy days and the rainfall intensity is very homogeneous from the eastern side of the mountain range up to a distance of 50 km from the east coast; and (d) minimum of both the frequency of rainy days and intensity rainfall is recorded in the northwestern sector of the Peninsula during the boreal winter.

Keywords: convergence area, northeast monsoon, southwest monsoon, rainy days, rainfall intensity

INTRODUCTION

A rainy day may be defined as a day that rains more than 0.1 mm, while the intensity of rainfall may be defined as the quotient between the monthly precipitation and the number of rainy days of that particular month.

The only attempt to study both the annual distribution of rainy days and rainfall intensity has been done in the late fifties (Dale 1959). No other attempt has been made since then in Peninsular Malaysia. It is our feeling that with a more complete data set an actualization of both the monthly (and the annual distribution) of rainy days and rainfall intensity is timely and pertinent.

There is a significant difference in the way data have been handled in our study as compared with Dale's (1959) investigation. This is explained in a companion publication (Camerlengo and Somchit 2000). The interested reader is referred to that particular work.

DATA

The meteorological data have been obtained from the "Monthly Summary of Meteorological Observations" published by the Malaysian Meteorological Service (1982-96). The location of the stations as well as the name of each station are shown in *Fig. 1* and Table 1 of the companion paper (Camerlengo and Somchit 2000).

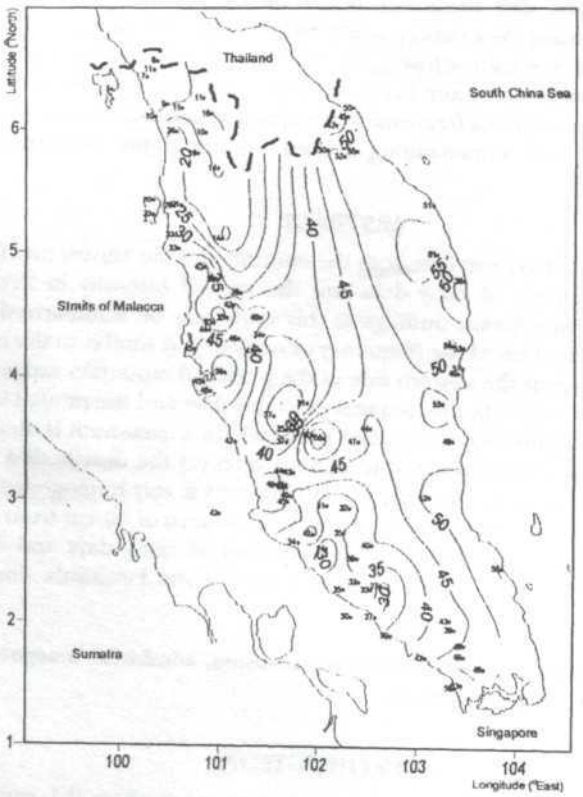

Fig 1. Percentage of rainy days in Peninsular Malaysia during January

RESULTS AND DISCUSSION

Monthly and annual distribution of rainy days

Greater number of rainy days are recorded at the east coast in January, where the largest amount of rainfall occurs in its southern half during this particular month (*Fig. 1*). On the other hand, lower number of rainy days are observed in the northwestern sector of the Peninsula where minimum precipitation occurs in that part of the country (Camerlengo *et al.* 1996)

The largest gradient of frequency of rainy days is observed between Teluk Intan, 56 %, and Kuala Kubu Baru, 25 %. This may be attributed to the fact that: (1) the northeast (NE) monsoon winds are still relatively strong in January (with the consequent discharge of humidity from the east coast towards the eastern side of the principal mountain range), and (2) that the former station is at the windward side of the mountain range while the latter one is at the leeward side.

A considerable decrease of the number of rainy days is observed all across the peninsula during the following month (*Fig. 2*). In particular, the number of rainy days is larger in the western half than in the eastern half where no gradient of rainy days is observed.

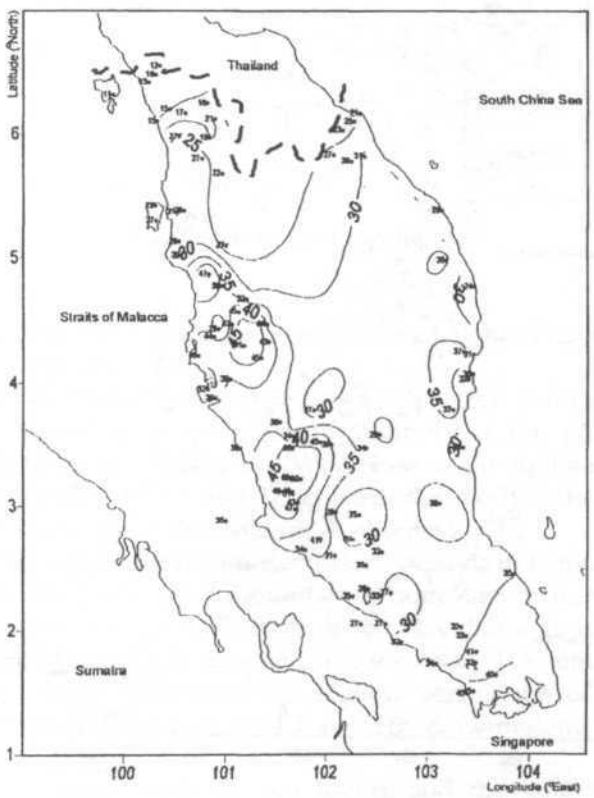

Fig 2. Idem as fig. 1, but for February

As in January, minimum number of rainy days (attributed to the same effect as in the previous month) is observed in February in the northwestern part of the peninsula. On the other hand, the largest number of rainy days is found at the western side of the mountain range. This may largely be attributed to the discharge of humidity from the air mass moving further inland due to the (early afternoon) sea breeze effect. This same maximum is observed from March to May.

March rainfall average is larger than the precedent month. This is reflected in the larger percentage of rainy days (*Fig. 3*). On the other hand, minimum number of rainy days is observed in the northern part of the peninsula in March. In particular, this includes both the states of Kelantan and Terengganu.

Larger number of rainy days is detected in Bukit Maxwell (Larut), Cameron Highlands and in the Kuala Lumpur area during April (*Fig. 4*). Maximum rainfall is precisely recorded in the first two stations during this particular month. This may largely be attributed to the fact that the maximum belt of

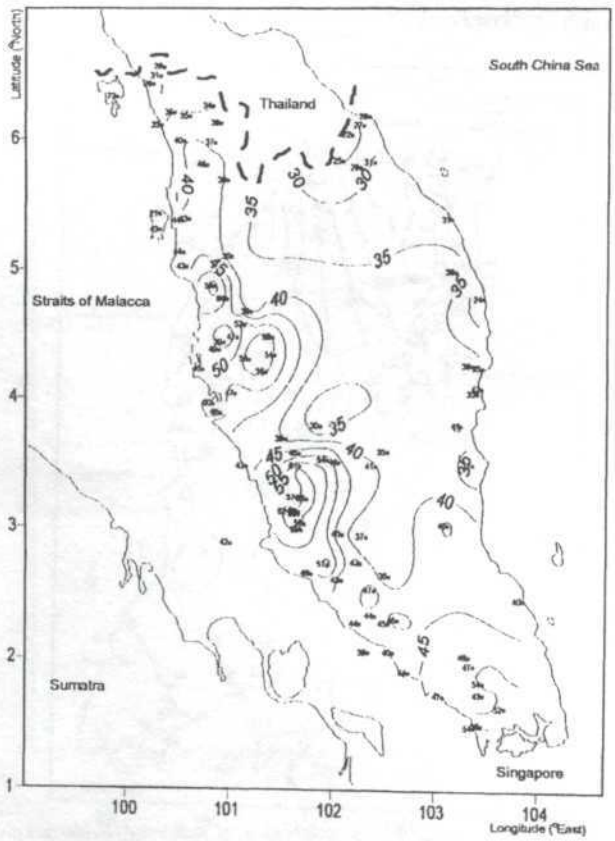

Fig 3. Idem as fig. 1, but for March

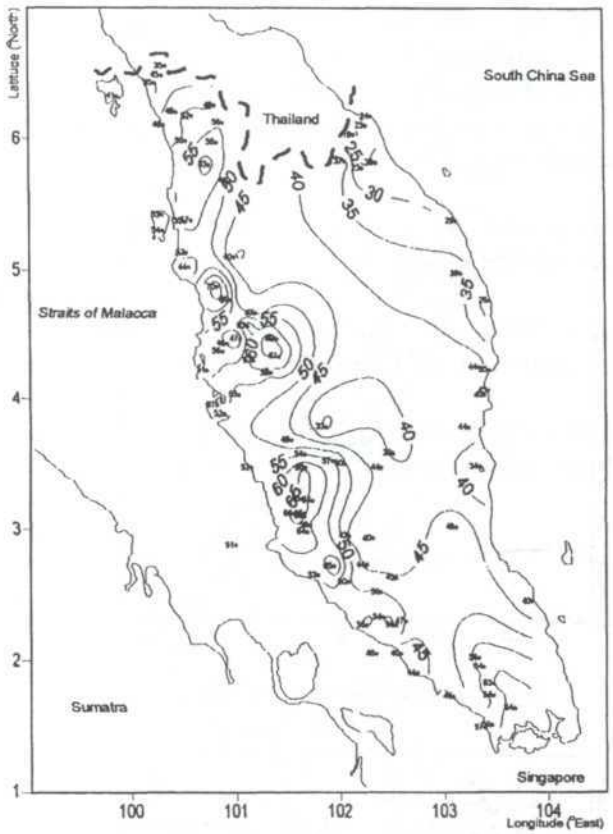

Fig 4. Idem as fig. 1, but for April

precipitation in Peninsular Malaysia is located at a height of approximately 950 meters (Camerlengo *et al.* 1998).

One of the two monthly maximums of precipitation is recorded either in April or May (according to the particular latitude of the analyzed station) (Nieuwolt 1981). This is reflected by the increase in the number of rainy days all across the peninsula (*Figs. 4* and *5*). In particular, both in the northern part and at the east coast of the peninsula it is observed.

June probably represents one of the "driest" months in Peninsular Malaysia. The decrease in the percentage of number of rainy days in June compared to May is attributed to this effect. In spite of the fact that a considerable lesser amount of monthly rainfall is recorded in Alor Setar, 128 mm, compared to Bukit Maxwell (Larut), 332 mm; the highest percentage of rainy days is observed in the former station during June (*Fig. 6.* Camerlengo and Somchit 2000).

In tropical latitudes, both the sea breeze and the land breeze have a considerable larger horizontal length scale influence than at mid-latitudes

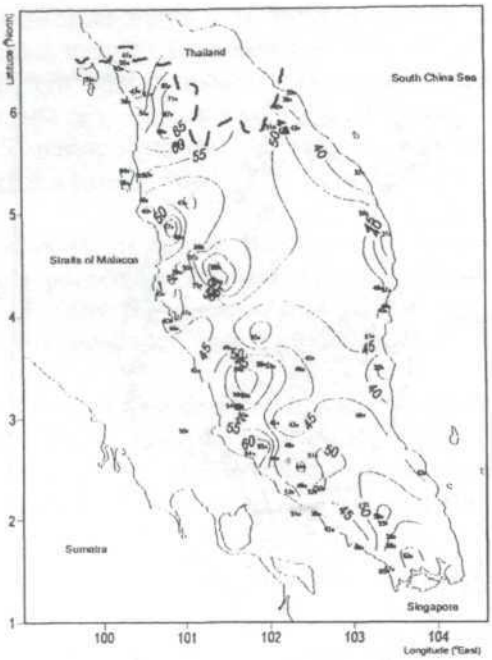

Fig 5. Idem as fig. 1, but for May

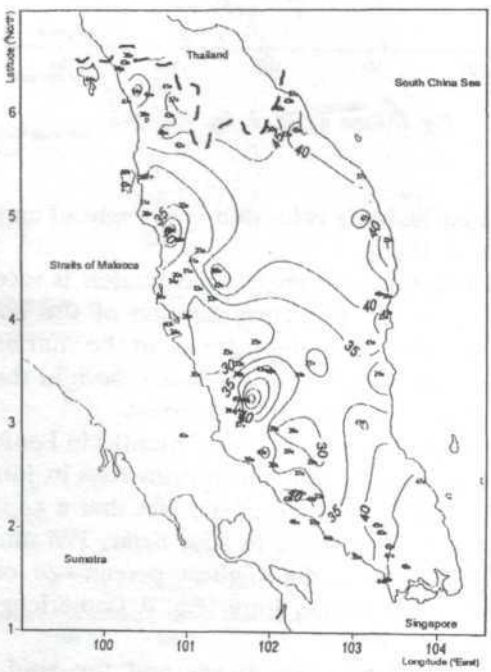

Fig 6. Idem as fig. 1, but for June

(Hastenrath 1990). As such, the sea breeze in unison with the SW monsoon winds may help explain the fact that the larger number of rainy days is observed further inland from the west coast. For example, at Alor Setar, Pusat Pertanian Charuk Padang, the Kuala Lumpur area, Johor Bahru and at Bukit Maxwell (Larut) the percentage of rainy days is higher in July than the antecedent month (*Fig. 7*).

The increase of the percentage of rainy days at the east coast recorded in July may solely be attributable to the convergence of the sea breeze effect and the SW monsoon winds.

A larger (lesser) percentage of rainy days is recorded in the northwestern sector of the peninsula (at the leeward side of the mountain range) in August (*Fig. 8*).

It is interesting to notice that a larger percentage of rainy days is observed both in the northern and in the southern parts of the peninsula compared to its central part in August.

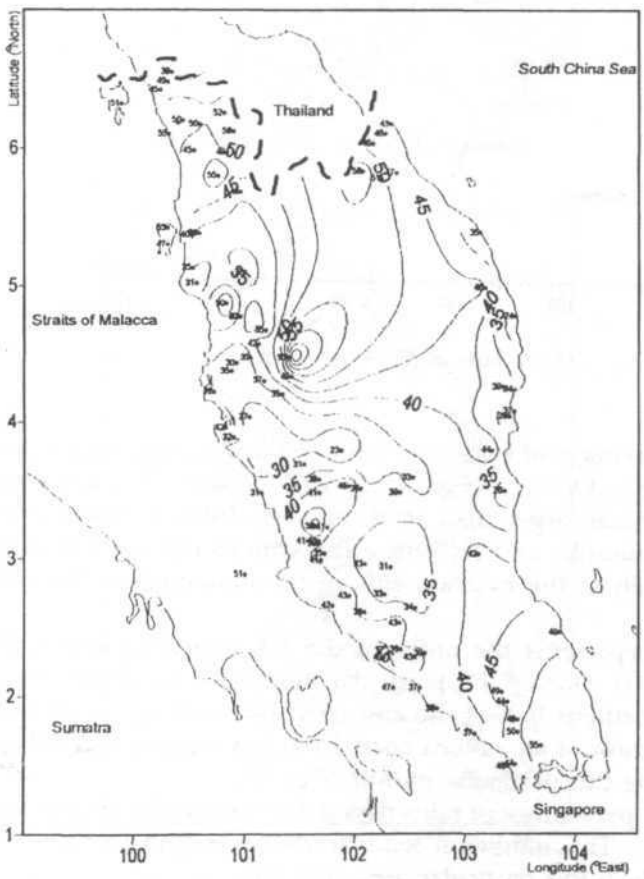

Fig 7. Idem as fig. 1, but for July

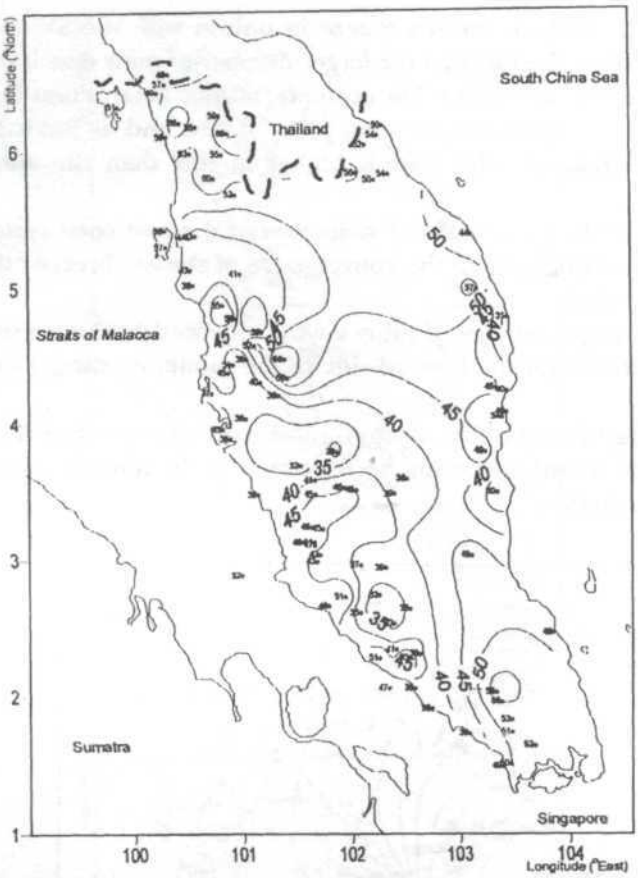

Fig 8. Idem as fig. 1, but for August

A larger percentage of rainy days is recorded all across the peninsula either in September or in October (*Figs. 9* and *10*). In particular, it is interesting to note that: (1) values larger than 70 % may be observed in the northwestern sector of the peninsula, and (2) only a few stations register less than 45 % of rainy days (usually at the eastward side of the mountain range) during both months.

November represents the onset of the NE monsoon season (Nasir and Camerlengo 1997). During this particular month, 30 % of the annual rainfall occurs in the northern half of the east coast (Camerlengo *et al.* 1996).

Therefore, most of all eastern coastal stations register more than 75 % of rainy days during this particular month (*Fig. 11*).

A minimum percentage of rainy days is detected in the northwestern sector of the Peninsula. This minimum tends to decrease (substantially) during the following month in this particular area (*Fig. 12*).

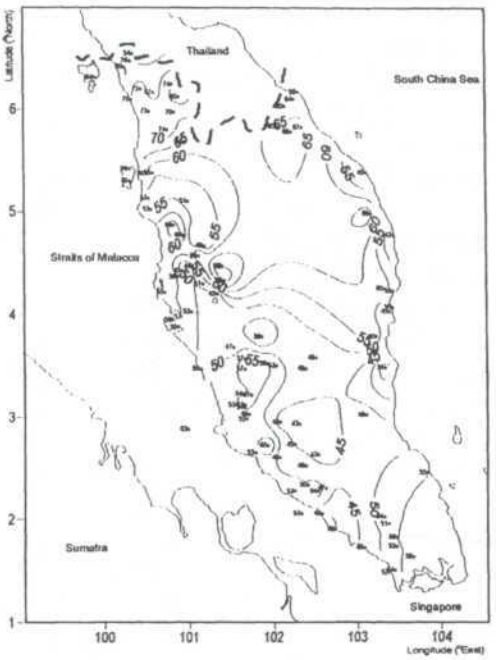

Fig 9. Idem as fig. 1, but for September

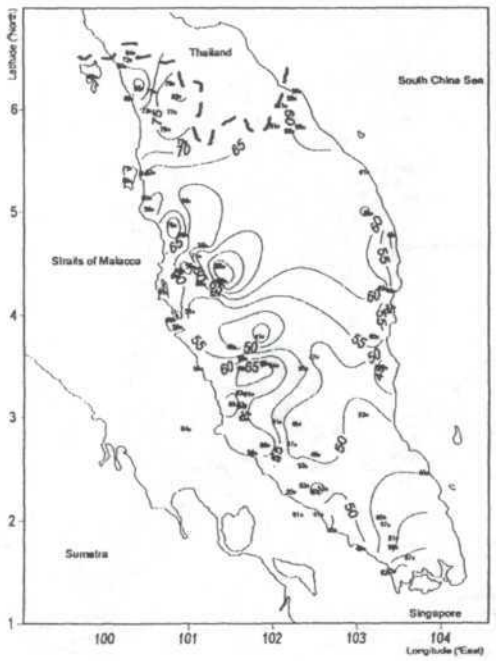

Fig 10. Idem as fig. 1, but for October

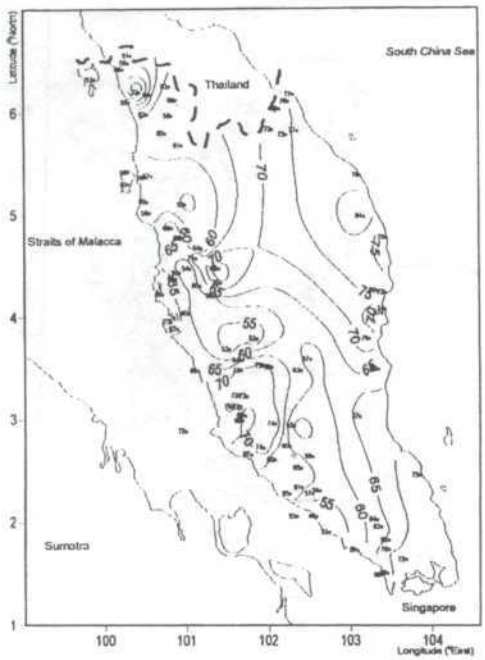

Fig 11. Idem as fig. 1, but for November

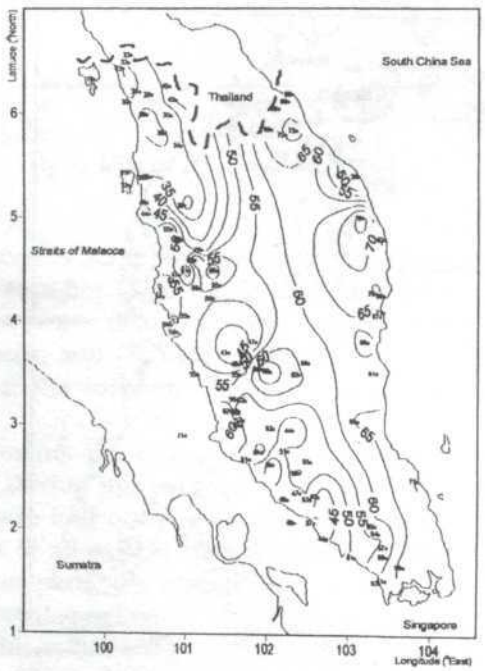

Fig 12. Idem as fig. 1, but for December

The slight decrease of the number of rainy days at the northern half at the east coast observed in December may be attributed to the equatorward migration of the leading edge of the NE monsoon.

A lower number of rainy days is usually recorded at the eastern side of the mountain range. The NE monsoon winds tend to reverse this phenomenon. As a consequence of this, the number of rainy days is higher than 50 % during November and December in this particular area.

The annual distribution of the percentage of rainy days shows that a larger percentage of rainy days is recorded further inland from the east coast i.e. around 50 km inwards from this particular coast (*Fig. 13*). Maximum number of rainy days is observed in Cameron Highlands, Bukit Maxwell (Larut) and within a radius of 50 km of Kuala Lumpur. This phenomenon is mainly due to the relief effect (Nieuwolt 1981; Camerlengo and Somchit 1998).

Minimum number of rainy days is annualy recorded in the northwestern part (as compared to the southern part) of the Peninsula.

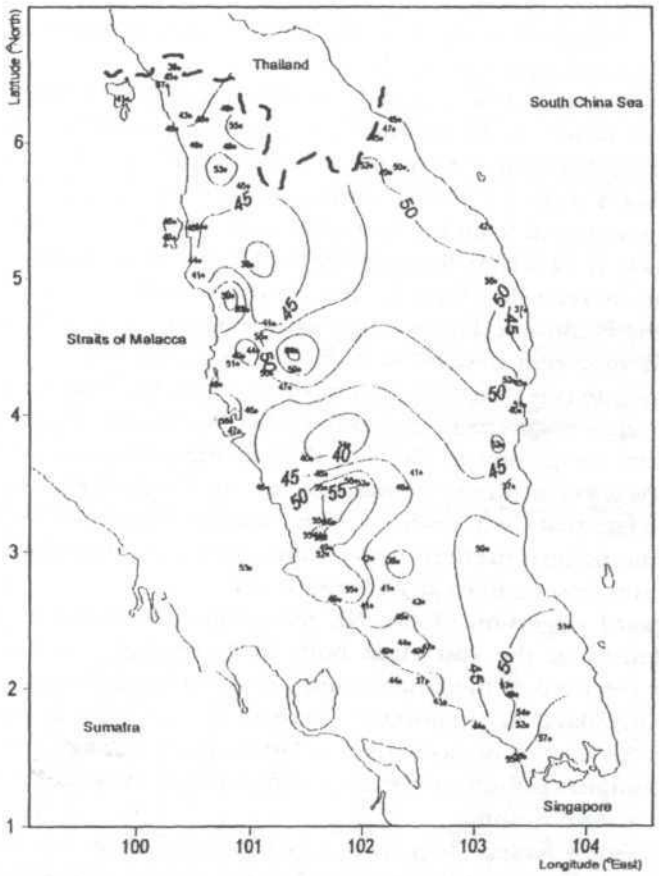

Fig 13. Annual percentage of rainy days in Peninsular Malaysia

Monthly and annual distribution of average rainfall intensity

A principal maximum (minimum) of rainfall intensity is recorded in the southern half at the east coast (extreme northern part) of the peninsula, during January, while a secondary maximum (minimum) is observed at the western side (eastern side) of the mountain range (Table 1).

The retreat of the NE monsoon may help explain the sharp drop in intensity at the east coast in February while a (relative) maximum is observed at the western side of the mountain range.

The situation at the western side of the peninsula remains unchanged in March, whereas an increase of intensity is recorded at the east coast.

The poleward migration of the convergence area during April and the first half of May causes an increase in rainfall intensity (observed in these two months as compared to March) on the western side of the peninsula. In particular, a maximum intensity is clearly distinguishable at the windward side of the mountain range. No similar increase of intensity is observed in the eastern half during these two months.

In spite of the fact that June represents a "relative" dry month, no significant change is observed in the intensity pattern when compared with the previous month (Camerlengo *et al.* 1996).

A large intensity gradient is observed across the mountain range, where larger values are recorded at the windward side of the mountain range and lesser values at its leeward side. No significant change of intensity is observed between the leeward side of the mountain range up to a distance of approximately 50 km inland from the east coast. From this point, a significant increase of intensity is observed towards the east coast in its southern half. Minimum intensity is recorded both in the northern part and the extreme southern part of the Peninsula. These main characteristics are prevalent during the rest of the SW monsoon season i.e. from July to September.

The increase of intensity observed in October all across the Peninsula may be attributable to the equatorward migration of the other broad area of convergence. Also, intensity values are greater in October than in April/May due to the fact that convergence is lesser in the latter months than in the former one.

In spite of the fact that the intensity has increased in October all across the peninsula, the same pattern prevails: larger values at the windward side of the mountain range and lesser values at its leeward side.

The equatorward migration of the NE monsoon determines a principal maximum of intensity at the east coast both in November and December. Higher values are reported in the latter month. In a similar fashion as with the percentage of rainy days, an important decrease of intensity is noticeable further inland of the east coast, towards the Titiwangsa mountain range.

A principal minimum of intensity is observed at the northwestern sector of the country during both months.

Another interesting feature to perceive is represented by the secondary maximum (minimum) located at the windward (leeward) side of the Titiwangsa mountain range.

TABLE 1
Monthly and annual rainfall intensity in Peninsular Malaysia

Station	Jan	Feb	Mar	Apr	May	Jun	Jul	Aug	Sep	Oct	Nov	Dec	Annual
Kota Baharu	4.2	5.4	16.2	12.7	9.7	10.3	11.1	11.2	10.4	14.3	29.5	24.9	14.7
Mardi Jeram Pasu	8.2	9.0	15.4	2.7	14.2	14.6	15.4	14.1	16.0	17.2	27.1	31.2	17.7
Pusat Pertanian Lundang	5.8	5.0	16.7	13.2	9.7	10.8	12.7	12.4	12.2	14.8	30.3	26.6	15.9
Pusat Pertanian Pasir Mas	6.7	5.4	13.9	11.4	12.4	15.2	15.4	17.1	15.1	13.7	28.5	25.3	16.7
Pusat Penternakan Haiwan Tanah Merah	11.0	10.3	15.5	10.0	15.8	15.7	12.1	14.4	15.1	17.5	23.5	23.6	16.2
Pejabat Haiwan Jajahan Machang	9.5	7.4	15.9	10.2	11.3	15.9	15.2	15.1	15.5	18.9	26.9	32.9	17.9
Kuala Terengganu	6.9	5.8	15.8	10.4	10.7	10.8	10.5	10.5	13.9	11.8	30.0	47.3	16.3
Dungun	13.6	12.2	21.5	15.2	17.1	13.9	16.6	15.6	18.0	14.6	31.2	35.3	21.0
Kemaman	14.0	11.1	16.9	13.5	13.7	16.2	11.3	14.5	14.2	13.2	27.8	35.0	18.5
Mardi Jerangau	13.1	10.0	15.9	12.9	14.4	14.1	13.3	12.3	14.5	14.3	21.2	30.3	16.7
Mardi Kemaman	13.6	11.3	17.6	12.5	11.4	12.4	11.2	12.1	13.4	14.8	26.1	29.3	16.6
Kuantan	16.7	10.0	16.9	11.1	12.2	12.6	10.9	20.3	12.6	13.8	20.4	26.7	16.1
Temerloh	8.8	10.8	13.4	14.7	11.9	12.6	8.6	13.5	12.4	11.8	13.2	9.8	11.8
Cameron Highlands	5.9	9.6	10.9	12.7	12.6	10.4	9.9	11.1	12.2	15.1	12.6	9.1	11.4
FELDA Kampong Sterik	7.1	9.5	13.8	12.3	10.3	10.9	13.1	9.5	9.8	12.2	12.3	9.4	10.8
FELDA Padang Piol	11.4	10.9	14.6	14.4	14.7	16.0	14.9	13.4	14.7	16.1	15.2	13.0	14.1
Bentong	8.2	9.6	12.0	11.3	9.8	10.1	10.1	9.5	9.6	11.4	12.2	11.3	10.5
MARDI Sungai Baging	12.7	10.7	15.0	12.5	11.3	13.6	11.1	11.5	15.5	11.2	24.8	24.4	15.4
MARDI Bukit Riden	16.2	10.8	14.8	12.3	10.7	11.1	8.8	9.7	10.1	12.5	13.9	20.6	13.0
MARDI Cameron Highlands	6.6	10.6	11.4	13.7	14.0	10.9	6.2	10.5	11.8	13.6	11.9	10.3	11.0
NEB Jor	6.5	8.9	10.9	9.5	9.8	10.1	10.0	9.3	10.8	11.6	10.9	7.9	9.9
Pusat Pengeluaran Tanaman Kg Awan	9.2	9.4	13.4	14.0	14.8	13.1	9.6	9.9	14.3	15.0	14.5	12.8	12.7
Pusat Pertanian Gali, Raub	10.3	12.5	14.1	19.4	14.4	16.9	14.1	11.9	10.9	14.4	14.3	12.6	13.8
Pekan	22.8	14.4	23.0	14.5	15.5	20.0	12.0	12.3	20.0	21.3	25.8	25.0	20.1

Table 1 Continued

Station	Jan	Feb	Mar	Apr	May	Jun	Jul	Aug	Sep	Oct	Nov	Dec	Annual
Johor Bahru	11.9	12.9	12.6	19.3	12.5	10.2	10.7	11.9	12.2	11.1	11.5	12.0	5.8
Mersing	23.4	15.1	10.4	9.8	10.8	9.9	10.4	12.8	11.9	10.5	17.3	27.5	15.0
Kluang	12.5	14.6	14.0	13.2	10.4	10.0	9.5	8.1	9.5	10.8	11.7	15.0	11.5
Cemara Research	12.0	14.8	12.9	12.5	11.3	10.1	10.3	12.3	11.0	10.4	13.4	14.4	12.1
Layang-layang													
Kota Tinggi	17.0	16.0	15.1	11.4	12.7	12.8	11.2	12.7	12.8	11.8	13.4	21.2	13.9
Tangkak	9.3	11.1	12.1	13.0	11.2	8.8	10.2	10.1	10.6	10.8	12.4	9.1	10.8
Muar	13.6	18.1	13.7	17.5	17.1	16.0	15.2	17.6	19.0	17.1	17.4	12.3	16.3
Pontian	10.9	10.6	13.9	13.4	10.8	11.6	14.0	11.6	14.0	10.8	14.2	10.5	12.2
MARDI Alor Bukit, Pontian	11.8	15.0	15.5	12.5	14.2	11.5	13.2	10.4	13.2	10.3	14.0	11.6	12.7
MARDI Kluang	14.0	17.2	15.4	14.3	11.7	10.1	9.3	9.4	10.5	9.5	10.9	16.2	12.2
Pusat Pertanian Parit Botak	12.2	17.3	16.0	14.7	13.7	15.0	17.4	16.1	13.2	11.6	14.6	13.8	14.5
Pusat Pertanian Sungai Sudah	11.7	14.7	15.3	15.5	15.4	16.6	20.2	17.6	17.4	15.1	16.0	14.2	15.8
Segil Estate	12.3	15.5	13.3	14.6	11.2	10.7	12.6	12.0	12.5	12.0	13.2	12.7	12.7
Cuping	4.5	12.7	10.8	12.3	11.1	8.6	11.7	10.8	11.5	10.8	9.4	7.9	10.5
Felda Cuping A	5.4	11.8	14.4	13.2	11.2	10.4	13.0	11.6	13.0	13.7	10.9	9.4	12.0
Kangar	8.8	7.6	13.2	14.5	15.8	12.7	14.5	13.7	14.9	13.2	11.4	11.0	13.4
Penang International Airport	8.3	12.8	11.8	12.3	12.8	12.1	13.7	14.8	16.9	15.7	11.2	8.3	13.1
Hospital Bukit Mertajam	12.1	11.9	13.1	13.3	11.4	10.9	14.0	11.6	15.4	13.6	14.4	11.0	13.0
Pusat Kesihatan Bukit Bendera	10.0	12.0	27.4	17.7	16.3	17.8	16.0	16.9	21.2	16.7	16.9	12.5	17.1
Malacca	6.6	9.0	12.9	12.8	12.8	11.8	11.9	10.4	13.3	11.3	12.9	9.1	11.5
Chemara Research Serkam, Jasin	8.9	11.6	11.9	11.2	11.0	10.8	8.8	10.8	10.0	12.6	12.2	10.1	10.9
Rumah Api Pulau Undan	7.5	8.6	12.0	11.9	14.8	15.8	15.4	15.9	15.1	13.1	11.9	9.6	13.1
Alor Setar Airport	9.5	11.3	11.2	12.5	17.4	8.0	11.3	9.6	12.3	16.9	19.5	8.2	12.4
DID Muda	7.5	7.7	13.0	11.8	13.0	10.7	10.9	12.4	12.7	12.2	13.6	8.5	11.8
DID Pedu	4.1	12.0	15.0	16.9	13.7	11.5	12.6	12.2	12.7	15.0	13.3	10.6	13.2
Baling	7.2	10.3	15.1	15.8	16.3	13.0	14.7	13.8	16.3	15.5	14.2	11.3	14.4
Kulim	13.1	14.8	15.8	17.9	16.1	17.0	15.0	14.2	16.3	18.8	17.1	16.1	16.3
Pulau Langkawi	9.1	16.1	12.0	14.9	14.9	16.9	17.4	15.7	21.0	16.8	13.2	8.9	15.9

Table 1 Continued

Station	Jan	Feb	Mar	Apr	May	Jun	Jul	Aug	Sep	Oct	Nov	Dec	Annual
Sungai Petani	7.8	9.8	10.2	13.0	10.1	10.9	11.1	13.0	14.0	13.7	10.8	10.2	11.7
MARDI Gajah Mati	8.8	11.1	10.6	15.1	11.2	9.1	11.4	11.4	13.2	12.7	11.9	9.1	11.8
Pusat Pertanian Batu Seketol	7.3	9.7	16.7	15.3	15.2	14.9	16.7	16.7	15.2	16.6	16.5	12.2	15.4
Pusat Pertanian Charuk Padang	7.3	11.2	14.9	14.6	15.1	12.6	13.9	13.7	16.5	15.8	13.9	9.7	14.0
Pusat Pertanian Teluk Chengai	8.0	7.6	11.6	12.3	15.4	12.9	15.5	13.1	15.6	14.3	11.9	6.8	13.5
Ipoh	9.1	11.5	11.6	14.8	12.4	11.0	13.3	10.1	10.8	14.2	12.4	14.4	12.3
Setiawan	10.7	10.6	10.9	11.5	10.0	9.3	11.5	10.5	10.0	8.9	11.7	12.7	10.7
Bukit Maxwell (Larut)	13.6	15.5	16.9	19.6	21.5	22.9	23.0	23.0	24.2	23.2	22.8	14.9	20.4
FELDA Trolak Utara	11.5	15.7	13.3	17.1	15.3	16.4	12.9	13.1	12.5	15.2	16.1	13.5	14.5
Ulu Kinta	10.9	15.4	15.3	14.9	15.5	15.3	15.2	13.4	14.4	17.7	17.4	13.4	15.1
Batu Gajah	17.1	11.2	16.9	18.5	13.7	12.4	13.4	13.6	15.0	14.2	17.0	24.1	15.7
Kampar	14.1	16.4	17.9	20.3	17.6	17.9	18.7	16.0	17.8	19.8	20.1	18.8	18.1
Kuala Kangsar	11.7	13.5	13.7	13.8	11.6	10.1	11.2	10.1	11.6	11.5	11.2	11.9	11.9
Lenggong	11.9	11.6	14.5	13.0	13.6	10.3	11.0	11.1	13.2	12.2	13.3	12.3	12.7
Parit Buntar	11.5	12.7	23.2	13.3	12.2	10.5	10.2	11.6	13.1	12.1	12.0	11.7	12.9
Tanjung Malim	12.8	18.6	19.8	21.4	19.5	20.8	16.1	18.9	17.5	20.2	19.4	17.2	18.7
Tapah	19.8	23.7	17.1	18.5	18.8	17.4	20.2	16.2	18.7	18.9	19.1	18.6	18.9
Teluk Intan	11.1	14.5	14.6	15.1	13.0	11.7	14.4	15.2	12.1	14.5	16.0	17.6	14.2
MARDI Hilir Perak	9.8	12.5	10.1	10.6	8.8	8.4	11.4	9.2	9.4	11.8	11.8	12.1	10.6
MARDI Kuala Kangsar	10.0	13.1	10.6	11.4	9.3	9.2	9.1	8.5	9.3	10.2	11.2	10.1	10.2
MARDI Parit	18.4	17.4	14.2	14.9	15.5	11.0	11.2	13.3	14.3	13.1	15.1	15.1	14.5
Pusat Pertanian Titi Gantong	11.9	11.5	12.7	13.3	10.4	8.7	10.0	11.1	11.1	10.1	14.3	12.6	11.7
JKR Bagan Serai	14.5	12.3	15.1	13.5	14.0	12.1	13.6	10.9	14.2	13.9	16.2	12.9	13.8
Kuala Lumpur	10.9	12.7	14.3	12.3	14.3	12.1	9.5	11.4	12.3	11.6	13.0	14.1	12.5
Universiti Malaya	12.6	15.6	13.4	17.1	14.2	8.4	10.2	11.5	13.8	13.4	15.1	16.3	13.6
Kolej Tunku Abdul Rahman	9.9	12.9	13.8	14.6	14.6	14.3	11.9	13.8	15.2	14.2	13.0	12.9	13.6

Table 1 Continued

Station	Jan	Feb	Mar	Apr	May	Jun	Jul	Aug	Sep	Oct	Nov	Dec	Annual
Petaling Jaya	13.0	15.3	14.0	16.2	14.0	11.9	11.1	11.6	12.3	14.6	14.9	16.0	14.0
FRI Kepong	7.2	13.0	14.2	14.3	14.6	12.5	9.5	12.6	15.0	13.4	14.8	12.0	13.0
Hospital Kuala Kubu Baru	11.1	13.6	13.2	17.1	18.0	14.7	14.1	14.1	16.1	14.9	14.7	13.9	14.9
MARDI Serdang	11.2	13.7	14.3	13.5	13.8	10.3	9.9	10.3	11.8	11.5	12.3	14.0	12.4
MARDI Tanjung Karang	10.3	10.6	11.8	11.5	8.9	10.0	9.8	10.8	11.0	11.9	12.5	13.6	11.2
Pusat Pertanian Batang Kali	10.7	11.7	13.5	14.6	15.3	12.3	12.4	14.5	14.1	13.8	15.6	12.4	13.7
Rumah Api One Fathom Bank	10.8	11.2	11.3	12.6	13.9	13.0	13.8	12.9	14.5	16.7	13.5	14.8	13.5
Universiti Putra Malaysia Serdang	12.5	12.2	15.3	13.4	13.8	10.7	12.7	10.3	12.6	11.2	13.4	13.6	12.8
Cemara Research Tanah Merah	10.3	9.0	11.4	10.1	8.4	11.9	4.4	9.9	13.4	13.6	11.7	12.2	6.6
FELDA Pasoh Dua	9.6	14.3	14.8	13.2	11.5	15.2	12.1	10.2	14.4	13.3	14.8	12.7	13.0
Haiwan Jelai, Gemas	9.5	11.8	16.9	12.6	10.4	11.2	10.0	7.8	11.3	13.5	13.4	11.7	11.7
Jelebu	7.8	8.8	10.0	10.5	7.9	9.7	7.8	8.3	9.8	8.7	9.9	9.4	8.8
Kuala Pilah	8.6	12.9	13.0	11.6	10.1	7.5	10.0	7.9	10.3	10.6	11.9	9.5	10.4
Seremban	7.7	12.0	11.6	11.7	10.3	10.0	9.8	9.6	11.6	12.9	13.0	12.2	11.2
Pusat Pertanian Chembong	11.9	15.3	18.8	17.8	14.6	14.7	14.5	12.7	16.4	15.5	15.8	12.2	15.3
Pusat Pertanian Gemencheh	9.3	10.0	13.8	11.5	12.4	9.2	7.0	9.3	8.4	10.8	10.7	10.6	10.4

The annual distribution of rainfall intensity shows two maximums: one at the east coast and the other one at the western side of the mountain range. On the other hand, three minimums of rainfall intensity are recorded: (1) at the northwestern sector of the peninsula, (2) at the extreme southern tip of the country, and (3) at the eastern side of the mountain range.

CONCLUSION

The main conclusions of this investigation are:

- The pattern of the frequency of rainy days is similar to the monthly (average) rainfall pattern at the western side of the Titiwangsa mountain range.
- A large gradient of both the frequency of rainy days and the rainfall intensity is recorded at the principal mountain range where a maximum is observed at the western side and a minimum at its eastern side. The minimum of frequency of rainy days disappears during both November and December.
- The patterns of both the number of rainy days and the rainfall intensity are very homogeneous from the eastern side of the mountain range up to 50 km inwards of the east coast.
- Minimum (Maximum) percentage of rainy days is recorded in the northwestern sector of the peninsula during the boreal winter (September and October).

ACKNOWLEDGMENTS

The study was supported by an IRPA grant. The authors gratefully acknowledge this support. Our thanks are extended to the Malaysian Meteorological Service for providing us the necessary data to carry out this investigation.

Comments made by anonymous reviewers contributed to the improvement of this manuscript. The authors gratefully acknowledge their contribution.

REFERENCES

CAMERLENGO, A. L., M. HISHAM R and M. NASIR S. 1996. On the passage on the Intertropical Convergence Zone in Peninsular Malaysia. *Malay. J. of Physics* **17(4)**: 155-162.

CAMERLENGO, A. L., and N. SOMCHIT. 2000. Monthly and annual rainfall variability in Peninsular Malaysia. *Pertanika J. Sci. & Technol.* (in Press).

CAMERLENGO, A. L., N. SOMCHIT and M. NASIR S., 1998. Determination of the level of the belt of maximum precipitation in Peninsular Malaysia. *Malay. J. of Physics* (in Press).

DALE, W. L. 1959. The rainfall in Malaya, Part I. *J. Trop. Geogr.* **13**: 23-37.

HASTENRATH, S. 1990. *Climate Dynamics of the tropics.* p.488. Kluwer Academic Publishers.

Malaysian Meteorological Service: Monthly Summary of Meteorological Observations (1982-96). Issued under the authority of the Director General, Malaysian Meteorlogical Service, Petaling Jaya, Malaysia.

NASIR, M. S. and A. L. CAMERLENGO. 1997. Response of the ocean mixed layer, off the east coast of peninsular Malaysia during the north-east and the south-west monsoon. *Geoacta* **22**: 122-133.

NIEUWOLT, S. 1981. The climates of Continental Southeast Asia, Chapter 1. In *World Survey of Climatology.* ed. Takahasi and Arakawa. Elsevier Scientific Publishing Co.

Pertanika J. Sci. & Technol. 8(1): 73 - 83 (2000)
ISSN: 0128-7680

Monthly and Annual Rainfall Variability in Peninsular Malaysia

Alejandro Livio Camerlengo and Nhakhorn Somchit
Faculty of Applied Sciences and Technology
Universiti Putra Malaysia Terengganu
Mengabang Telipot
21030 Kuala Terengganu
e-mail: alex@uct.edu.my

Received 7 December 1998

ABSTRAK

Kajian ini meneliti semula variasi taburan hujan di Semenanjung Malaysia. Satu kajian awal telah dijalankan 40 tahun yang lalu. Memandangkan: (1) kehadiran lebih banyak stesen kaji cuaca kini, (2) kesan pemanasan bumi 'global warming' keatas taburan hujan. Kami berpendapat kajian baru mengenai variasi taburan hujan adalah sesuai dan bertepatan. Jadi ini merupakan objektif utama kajian yang dijalankan. Keputusan yang diperolehi menunjukkan bahawa nilai yang tinggi bagi variasi taburan hujan tidak (jarang) berlaku apabila jumlah hujan paling rendah.

ABSTRACT

This paper re-addresses the study of the rainfall variability in Peninsular Malaysia. An earlier investigation has been conducted forty years ago. Due to the fact that: (1) a larger and more sophisticated number of meteorological stations is nowadays in place, and (2) the effect that global warming has on precipitation, we feel that a new study of rainfall variability is both timely and pertinent. This is, therefore, the aim of this particular study. Our results show that larger variability does not (always) occur whenever lowest rainfall is recorded.

Keywords: North-east monsoon, South-west monsoon, inter-monsoon season, Peninsular Malaysia, precipitation

INTRODUCTION

The aim of this study is to gain some understanding about the monthly rainfall variability in Peninsular Malaysia. In this regard, to the authors' knowledge, only a single previous attempt has been made (back in the late fifties). In that particular study, all analysed stations did not have the same number of years of data. As a consequence of this, the resulting rainfall variability is highly distorted due to the fact that it is affected by distinct meteorological events (for example, different El Niños or La Niñas events).

Our approach is fundamentally different from the one mentioned above, as we have chosen a considerable larger number of stations than in that particular study (Dale 1959). Furthermore, all our stations were selected in order to have the same period of time: fifteen years (from 1982 to 1996). Therefore, all stations are affected by similar meteorological events (e.g. the 1991-93 El Niño event and the 1988 La Niña event).

We strongly believe that our approach gives a far better and a more accurate resolution of the rainfall variability than previously attained. In particular, a considerable departure from earlier results is obtained.

DATA

Precipitation data of 94 stations were obtained from the "Monthly Summary of Meteorological Observations" published by the Malaysian Meteorological Service (1982-96). The location as well as the name of each station is shown in *Fig. 1* and Table 1, respectively.

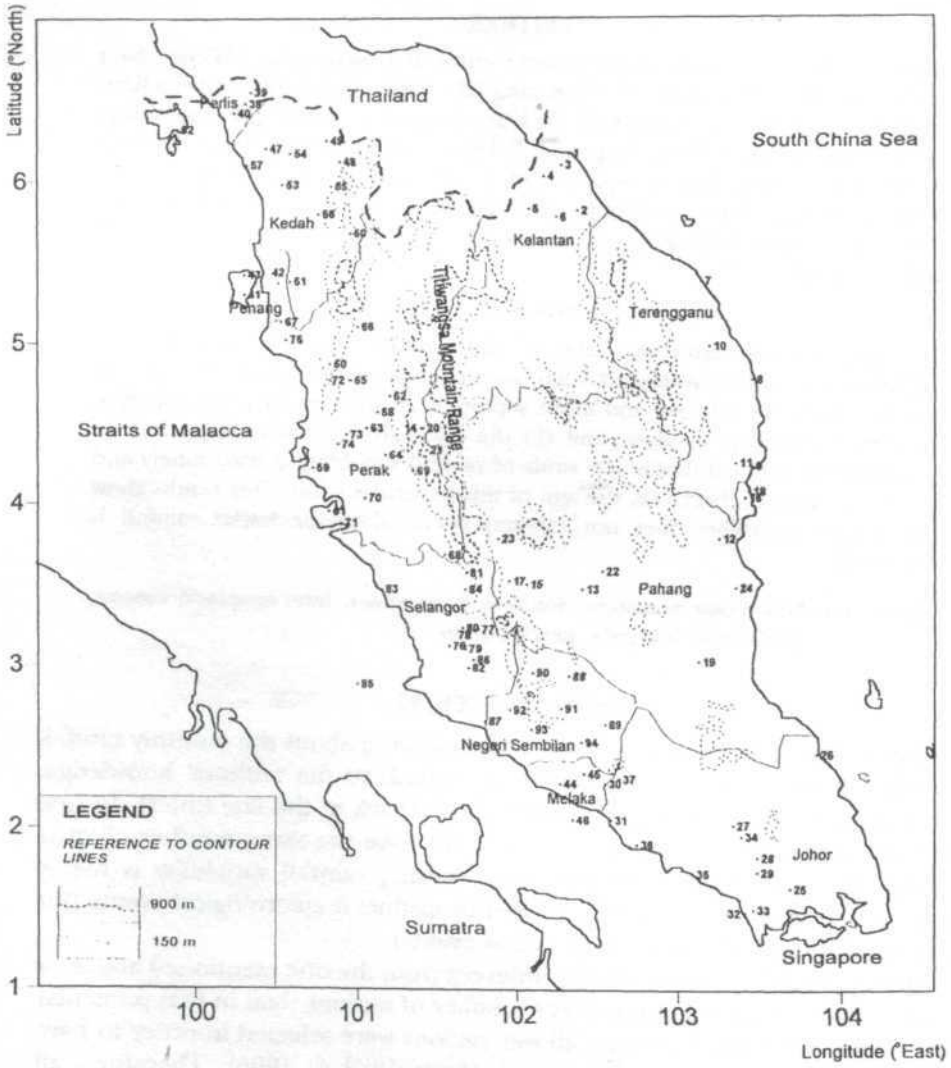

Fig 1. Location of the stations analysed in this investigation

TABLE 1
Names of stations used in the investigation

No	Station	Latitude (°N)	Longitude (°E)	Elevation (m)
1	Kota Baharu	6° 17'	102° 17'	5
2	Mardi Jeram Pasu	5° 49'	102° 20'	31
3	Pusat Pertanian Lundang	6° 06'	102° 14'	6
4	Pusat Pertanian Pasir Mas	6° 18'	102° 07'	9
5	Pusat Penternakan Haiwan Tanah Merah	5° 50'	102° 02'	0
6	Pejabat Haiwan Jajahan Machang	5° 47'	102° 12'	31
7	Kuala Terengganu	5° 23'	103° 06'	5
8	Dungun	4° 46'	103° 25'	3
9	Kemaman	4° 14'	103° 25'	3
10	Mardi Jerangau	4° 59'	103° 09'	15
11	Mardi Kemaman	4° 15'	103° 19'	50
12	Kuantan	3° 47'	103° 13'	15
13	Temerloh	3° 28'	102° 23'	39
14	Cameron Hinghland	4° 28'	101° 22'	1545
15	FELDA Kampong Sterik	3° 30'	102° 02'	70
16	FELDA Padang Piol	4° 18'	103° 23'	0
17	Bentong	3° 31'	105° 55'	97
18	MARDI Sungai Baging	4° 04'	103° 25'	4
19	MARDI Bukit Riden	3° 01'	103° 06'	26
20	Mardi Cameron Hinghland	4° 28'	101° 23'	1449
21	NEB Jor	4° 20'	101° 24'	607
22	Pusat Pengeluaran Tanaman Kampung Awan	3° 35'	102° 30'	31 159
23	Pusat Pertanian Gali, Raub	3° 47'	101° 51'	
24	Pekan	3° 29'	103° 02'	4
25	Johor Baharu	1° 39'	103° 40'	38
26	Mering	2° 27'	103° 50'	44
27	Kluang	2° 01'	103° 20'	88
28	Camara Research Layang-layang	1° 52'	103° 28'	31
29	Kota Tinggi	1° 44'	103° 28'	31
30	Tangkak	2° 16'	102° 32'	31
31	Muar	2° 03'	102° 34'	6
32	Pontian	1° 28'	103° 23'	5
33	MARDI Alor Bukit, Pontian	1° 30'	103° 27'	3
34	MARDI Kluang	1° 11'	103° 22'	107
35	Pusat Pertanian Parit Botak	1° 43'	103° 04'	2
36	Pusat Pertanian Sungai Sudah	1° 54'	104° 44'	2
37	Segi Estet	2° 18'	102° 37'	77
38	Cuping	6° 30'	100° 16'	22
39	Felda Cuping A	6° 33'	100° 18'	53
40	Kangar	6° 25'	100° 12'	3
41	Penang International Airport	5° 18'	100° 16'	2
42	Hospital Bukit Mertajam	5° 22'	100° 29'	14
43	Pusat Kesihatan Bukit Bendera	5° 25'	100° 16'	732
44	Malacca	2° 16'	102° 15'	9
45	Chemara Research Serkam, Jasin	2° 20'	102° 24'	27
46	Rumah Api Pulau Undan	2° 03'	102° 20'	53
47	Alor Setar Airport	6° 12'	100° 24'	4

Table 1 cont'd

No	Station	Latitude (°N)	Longitude (°E)	Elevation (m)
48	DID Muda	6° 07'	100° 51'	110
49	DID Pedu	6° 15'	100° 46'	59
50	Baling	5° 41'	100° 55'	52
51	Kulim	5° 23'	100° 33'	32
52	Pulau Langkawi	6° 20'	99° 51'	4
53	Sugai Petani	5° 59'	100° 30'	8
54	Mardi Gajah Mati	6° 10'	100° 33'	15
55	Pusat Pertanian Batu Seketol	5° 58'	100° 48'	71
56	Pusat Pertanian Charuk Padang	5° 48'	100° 43'	31
57	Pusat Pertanian Teluk Chengai	6° 06'	100° 17'	1
58	Ipoh	4° 34'	101° 06'	40
59	Setiawan	4° 13'	100° 42'	7
60	Bukit Maxwell (Larut)	4° 52'	100° 48'	1037
61	FELDA Terolak	3° 57'	100° 48'	0
62	Ulu Kinta	4° 40'	101° 10'	70
63	Batu Gajah	4° 28'	101° 02'	34
64	Kampar	4° 18'	101° 09'	38
65	Kuala Kangsar	4° 46'	100° 56'	39
66	Lenggong	5° 12'	100° 58'	101
67	Parit Buntar	5° 08'	100° 30'	3
68	Tanjung Malim	3° 41'	101° 31'	43
69	Tapah	4° 12'	101° 19'	35
70	Teluk Intan	4° 02'	101° 01'	3
71	Mardi Hilir Perak	3° 53'	100° 52}	9
72	Mardi Kuala Kangsar	4° 46'	100° 55'	66
73	Mardi Parit	4° 26'	100° 54'	5
74	Pusat Pertanian Titi Gantong	4° 22'	100° 51'	0
75	JKR Bagan Serai	5° 01'	100° 32'	3
76	Kuala Lumpur	3° 07'	101° 33'	17
77	Universiti Malaya	3° 13'	101° 44'	104
78	Kolej Tunku Abdul Rahman	3° 07'	101° 39'	0
79	Petaling Jaya	3° 06'	101° 39'	46
80	FRI Kepong	3° 14'	101° 38'	97
81	Hospital Kuala Kubu Baru	3° 34'	101° 39	61
82	MARDI Serdang	2° 59'	101° 40	38
83	Mardi Tanjung Karang	3° 28'	101° 01'	3
84	Pusat Pertanian Batang Kali	3° 28'	101° 39'	46
85	Rumah Api One Fathom Bank	2° 53'	100° 59'	21
86	Universiti Putra Malaysia Serdang	3° 02'	101° 42'	40
87	Cemara Research Tanah Merah	3° 39'	101° 47'	5
88	FELDA Pasoh 2	2° 56'	102° 18'	0
89	Haiwan Jelai, Gemas	2° 38'	102° 32'	46
90	Jelebu	2° 57'	102° 04'	137
91	Kuala Pilah	2° 44'	102° 15'	107
92	Seremban	2° 43'	101° 56'	64
93	Pusat Pertanian Cembong	2° 36'	102° 04'	61
94	Pusat Pertanian Gemencheh	2° 31'	102° 23'	70

The coefficient of variability is defined as:

$$C.\ V. = (SD_i/R_i)\ 100,$$

where SD represents the monthly standard deviation; R, the monthly rainfall average and; the subindex i (ranging from 1 to 12), the particular month of the year. For the sake of comparison with previous results we have chosen to use the same coefficient of variability.

RESULTS AND DISCUSSION

A principal maximum rainfall variability is recorded in the northwestern sector of the peninsula both in January (*Fig. 2*) and in February (not shown), while a secondary maximum is observed in the southern part of Terengganu. The former maximum may be attributed to the relative dryness observed in that part of the country during both months. The secondary maximum observed in the east coast during February may also be attributable to the same effect (Camerlengo *et al.*, 1996). On the other hand, the larger variability observed in the southern part of Terengganu during January may solely be attributed to the variations of the annual retreat of the leading edge of the North-east (NE) monsoon (Camerlengo and Somchit, 1998).

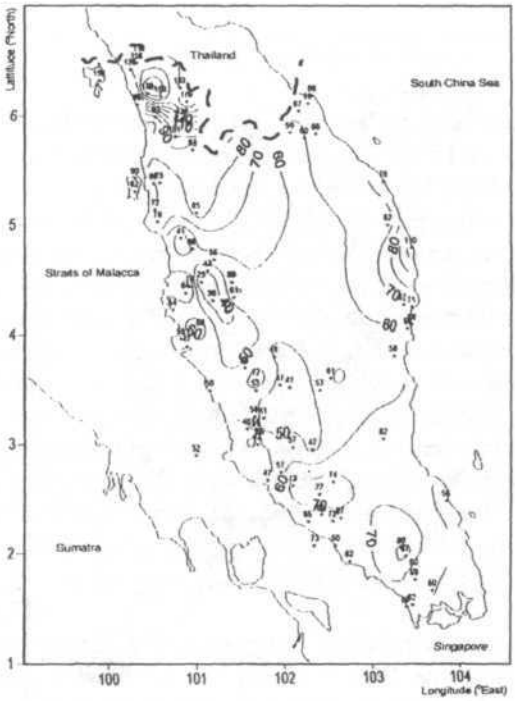

Fig 2. January coefficient of variability of precipitation (in %)

Table 1 cont'd

No	Station	Latitude (°N)	Longitude (°E)	Elevation (m)
48	DID Muda	6° 07'	100° 51'	110
49	DID Pedu	6° 15'	100° 46'	59
50	Baling	5° 41'	100° 55'	52
51	Kulim	5° 23'	100° 33'	32
52	Pulau Langkawi	6° 20'	99° 51'	4
53	Sugai Petani	5° 59'	100° 30'	8
54	Mardi Gajah Mati	6° 10'	100° 33'	15
55	Pusat Pertanian Batu Seketol	5° 58'	100° 48'	71
56	Pusat Pertanian Charuk Padang	5° 48'	100° 43'	31
57	Pusat Pertanian Teluk Chengai	6° 06'	100° 17'	1
58	Ipoh	4° 34'	101° 06'	40
59	Setiawan	4° 13'	100° 42'	7
60	Bukit Maxwell (Larut)	4° 52'	100° 48'	1037
61	FELDA Terolak	3° 57'	100° 48'	0
62	Ulu Kinta	4° 40'	101° 10'	70
63	Batu Gajah	4° 28'	101° 02'	34
64	Kampar	4° 18'	101° 09'	38
65	Kuala Kangsar	4° 46'	100° 56'	39
66	Lenggong	5° 12'	100° 58'	101
67	Parit Buntar	5° 08'	100° 30'	3
68	Tanjung Malim	3° 41'	101° 31'	43
69	Tapah	4° 12'	101° 19'	35
70	Teluk Intan	4° 02'	101° 01'	3
71	Mardi Hilir Perak	3° 53'	100° 52'	9
72	Mardi Kuala Kangsar	4° 46'	100° 55'	66
73	Mardi Parit	4° 26'	100° 54'	5
74	Pusat Pertanian Titi Gantong	4° 22'	100° 51'	0
75	JKR Bagan Serai	5° 01'	100° 32'	3
76	Kuala Lumpur	3° 07'	101° 33'	17
77	Universiti Malaya	3° 13'	101° 44'	104
78	Kolej Tunku Abdul Rahman	3° 07'	101° 39'	0
79	Petaling Jaya	3° 06'	101° 39'	46
80	FRI Kepong	3° 14'	101° 38'	97
81	Hospital Kuala Kubu Baru	3° 34'	101° 39	61
82	MARDI Serdang	2° 59'	101° 40	38
83	Mardi Tanjung Karang	3° 28'	101° 01'	3
84	Pusat Pertanian Batang Kali	3° 28'	101° 39'	46
85	Rumah Api One Fathom Bank	2° 53'	100° 59'	21
86	Universiti Putra Malaysia Serdang	3° 02'	101° 42'	40
87	Cemara Research Tanah Merah	3° 39'	101° 47'	5
88	FELDA Pasoh 2	2° 56'	102° 18'	0
89	Haiwan Jelai, Gemas	2° 38'	102° 32'	46
90	Jelebu	2° 57'	102° 04'	137
91	Kuala Pilah	2° 44'	102° 15'	107
92	Seremban	2° 43'	101° 56'	64
93	Pusat Pertanian Cembong	2° 36'	102° 04'	61
94	Pusat Pertanian Gemencheh	2° 31'	102° 23'	70

The coefficient of variability is defined as:

$$C.\ V. = (SD_i/R_i)\ 100,$$

where SD represents the monthly standard deviation; R, the monthly rainfall average and; the subindex i (ranging from 1 to 12), the particular month of the year. For the sake of comparison with previous results we have chosen to use the same coefficient of variability.

RESULTS AND DISCUSSION

A principal maximum rainfall variability is recorded in the northwestern sector of the peninsula both in January (*Fig. 2*) and in February (not shown), while a secondary maximum is observed in the southern part of Terengganu. The former maximum may be attributed to the relative dryness observed in that part of the country during both months. The secondary maximum observed in the east coast during February may also be attributable to the same effect (Camerlengo *et al.*, 1996). On the other hand, the larger variability observed in the southern part of Terengganu during January may solely be attributed to the variations of the annual retreat of the leading edge of the North-east (NE) monsoon (Camerlengo and Somchit, 1998).

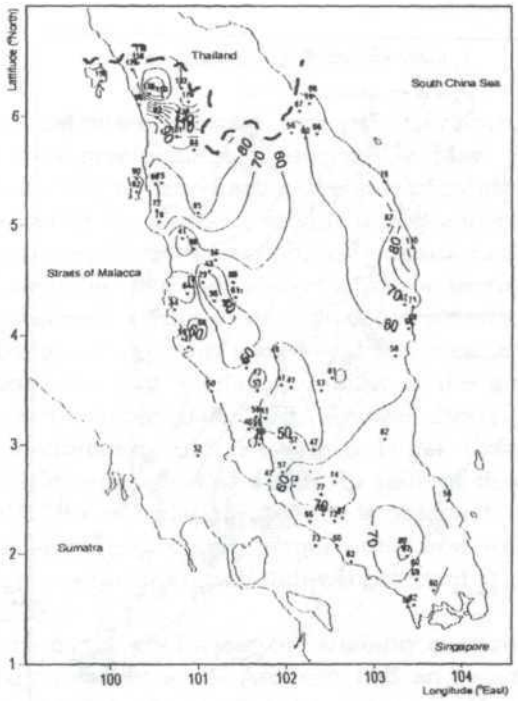

Fig 2. January coefficient of variability of precipitation (in %)

Maximum variability, of a slightly lesser magnitude than the one observed in Terengganu, is observed in the third southern part of the peninsula. This may also be attributed to the variations of the yearly retreat of the NE monsoon.

Minimum variability is recorded at the windward side of the Titiwangsa mountain range in January. However, a larger variation is recorded in this same area during the following month. This is found in spite of the fact that the February monthly rainfall is larger compared to the January one. It contradicts previous results in the sense that the largest variability is observed whenever lesser rainfall is recorded at Peninsular Malaysia' s west coast (Dale, 1959).

Larger variability is recorded in the eastern half of the peninsula as opposed to the western half during March (*Fig. 3*). In particular, maximum variability is observed in the state of Kelantan. On the other hand, minimum variability is recorded at the windward side of the Titiwangsa mountain range where maximum rainfall is observed in this particular month.

Similar pattern of rainfall variability as in March (larger at the eastern half and lesser at the western half) is observed in April (not shown). However, values of rainfall variability observed in this latter month are considerably lesser than in the former month.

The rainfall pattern at the western half is slightly larger in May compared with the previous month (*Fig. 4*). There is also a considerable increase of precipitation at the eastern half (Camerlengo and Somchit 1998). May represents

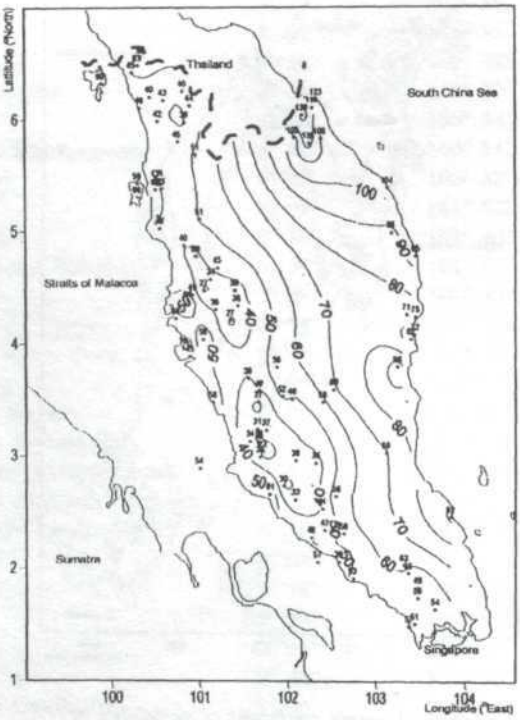

Fig 3. Idem as Fig 2, but for March

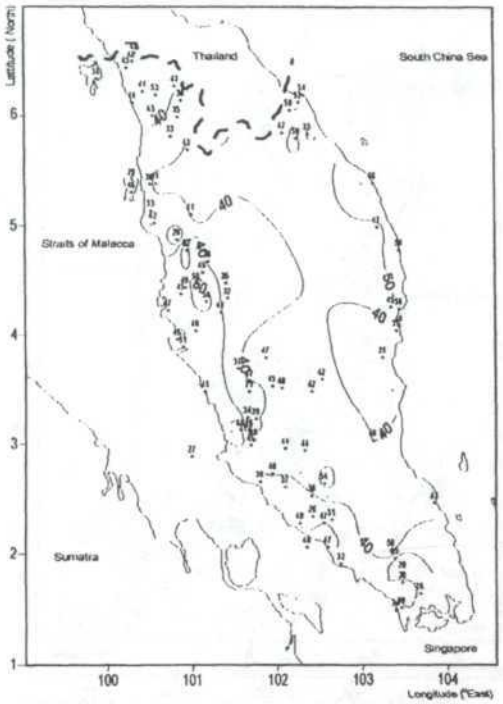

Fig 4. Idem as Fig 2, but for May

one of the transitional inter-monsoon seasons. Therefore, one of the two monthly maximums of precipitation is observed in May. (The other one is observed in October). Due to this effect, a decrease of rainfall variability in the eastern half compared to the previous month is noticeable.

June (not shown) represents the second driest month in Peninsular Malaysia (Camerlengo and Somchit 1998). However, a minor increase in the rainfall variability is only observed at the western half compared to the preceeding month while no change of variability is observed at the eastern half. This result contradicts the statement that rainfall variability is the greatest during the month with the lowest rainfall (Dale 1959; Nieuwolt 1981).

July average precipitation (not shown) is larger than the one of the antecedent month (Camerlengo *et al.* 1996). In spite of this, not a significant change in the coefficient of variability pattern is observed

August rainfall average is slightly larger compared to July. Contrary to expectations, a larger coefficient of variability is observed at the western half of the peninsula (*Fig. 5*).

A similar pattern of the coefficient of variability compared with the prior month (namely, larger values at the western half and smaller values at the eastern half) is observed in September (not shown). However, the rainfall variability in September is lower than the one recorded in the previous month. This may be attributable to the retreat of the South-west (SW) monsoon.

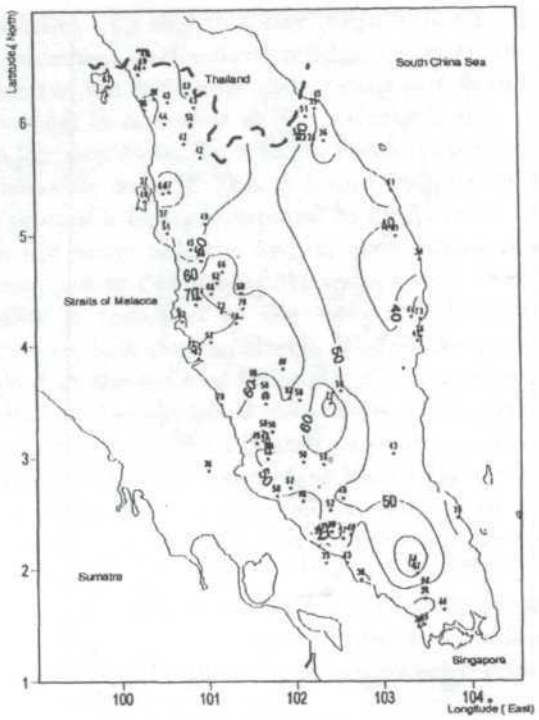

Fig 5. Idem as Fig 2, but for August

The retreat of the SW monsoon as well as the equatorward migration of the NE monsoon enhances the formation of a broad area of convergence, which in turn favours convection. October represents the other inter-monsoon transitional period. This may help explain the fact that October has the lowest rainfall variability all across the peninsula (*Fig. 6*).

There is a sharp contrast between our results at the eastern half of the peninsula, for this particular month, from previous ones. We strongly believe that this is due to the fact that we are analyzing a larger number of stations for the same period of time.

November represents the onset of the NE monsoon (Nasir and Camerlengo 1997). Our results show a considerable larger variability (than previously recorded) at the east coast (*Fig. 7*). This may be explained by the annual variation of the equatorward migration of the NE monsoon.

Thirty percent of the annual precipitation in the states of Kelantan and Terengganu is recorded in November (Camerlengo *et al.* 1996). Larger variability is observed in these two states during November. Our results are in sharp contradiction with previous ones. This is due to the fact that we are analysing a larger number of stations. We feel that our results represent a better resolution of the November variability than earlier ones.

In spite of the fact that larger amounts of precipitation are recorded in December in the eastern half of the Peninsula compared with the western half,

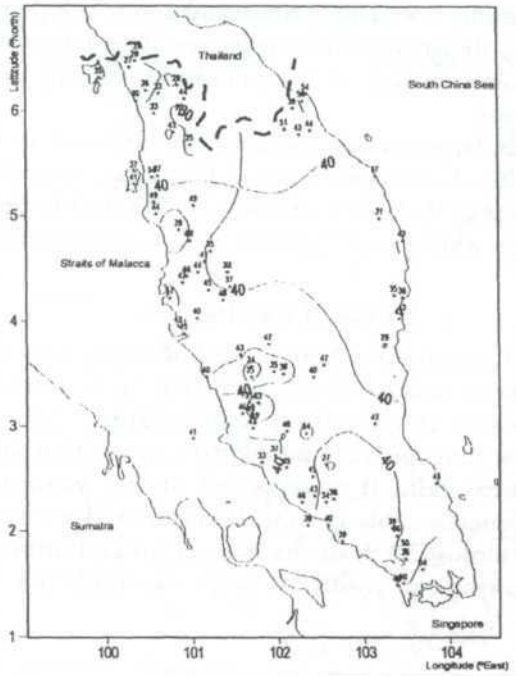

Fig 6. Idem as Fig 2, but for October

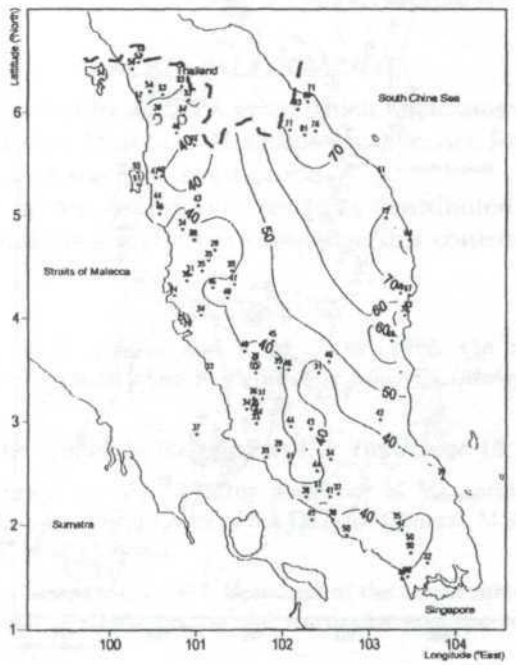

Fig 7. Idem as Fig 2, but for November

the coefficient of variability is strikingly similar all across the peninsula (*Fig. 8*). This represents a sharp departure from earlier results; a larger departure from normal values at the eastern half of the peninsular during December (Dale 1959) has been observed.

On an annual basis, larger values of rainfall are observed at the eastern half (Camerlengo *et al.* 1996). As a consequence of this, larger variability is observed in that particular area (*Fig. 9*). Lesser variability is observed in the northwestern sector of the peninsula where lesser rainfall is also observed annually.

CONCLUSION

Using a different and (we feel) a better methodology, previous results are confirmed while others had to be disregarded. It is confirmed that the annual rainfall variability at the eastern half is larger than at the western half. Our results show that the statement in the sense that larger variability occurs whenever lowest rainfall is recorded at the western side (of the peninsula) is rather questionable at best. It certainly does not hold true for the east coast where almost 30 % of the annual precipitation is recorded in November and (following our results) a large variability is attained for that particular month.

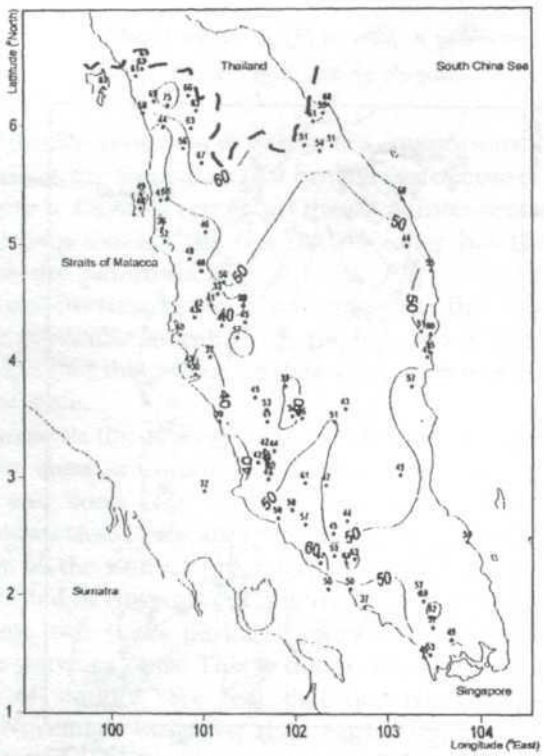

Fig 8. Idem as fig 2, but for December

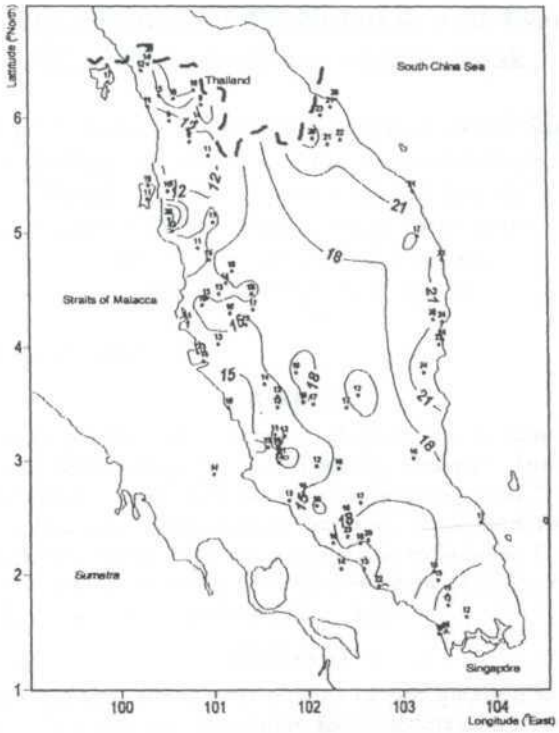

Fig 9. Annual coefficient of variability of precipitation (in %)

ACKNOWLEDGMENTS

This study was supported by an IRPA grant which we acknowledge. Our thanks are also extended to the Malaysian Meteorological Service for providing us the necessary data to carry out this investigation.

Comments made by an anonymous reviewer contributed to improve this manuscript. The authors gratefully acknowledge this contribution.

REFERENCES

CAMERLENGO, A,. L., M. R. HISHAM and S. M. NASIR. 1996. On the passage on the Intertropical Convergence Zone in Peninsular Malaysia. *Malay. J. of Physics* **17(4)**: 155-162.

DALE, W. L. 1959. The rainfall in Malaya, Part I. *J. Trop. Geogr.* **13**: 23-37.

Malaysian Meteorological Service: Monthly Summary of Meteorological Observations (1982-96) issued under the authority of the Director General, Malaysian Meteorlogical Service, Petaling Jaya, Malaysia.

NASIR, M. S. and A. L. CAMERLENGO. 1997. Response of the ocean mixed layer, off the east coast of peninsular Malaysia during the north-east and the south-west monsoon. *Geoacta* **22**: 122-133.

NIEUWOLT, S. 1981. The climates of Continental Southeast Asia, chapter 1. *In World Survey of Climatology*, ed. Takahasi & Arakawa, p. 1-37. Elsevier Scientific Publishing Co.

Pertanika J. Sci. & Technol. **8(1)**: 85 - 91 (2000)
ISSN: 0128-7680

Monthly Distribution of Preciptation and Evaporation Difference in Sabah and Sarawak

Alejandro Livio Camerlengo and Mohd. Nasir Saadon
Department of Marine and Environmental Sciences
Faculty of Applied Sciences and Technology
Universiti Putra Malaysia Mengabang Telipot
21030 Kuala Terengganu Malaysia
e-mail: Alex@upmt.edu.my

Received 31 March 1997

ABSTRAK

Corak perbezaan kerdasan dan sejatan tahunan, P - E, sangat berbeza di Malaysia Timur berbanding di Semenanjung Malaysia. Ditunjukkan juga perbezaan ini adalah positif di Sabah dan di Sarawak. Nilai P - E yang lebih tinggi diperhatikan dibahagian selatan Sarawak, sementara nilai yang lebih rendah dicatakkan di utara. Peranan utama (taburan bulanan P - E) dimainkan oleh laluan dua kali Zon Penumpuan Intertropika (ITCZ). Peranan kedua dimainkan oleh angin timur laut dan barat daya.

ABSTRACT

In spite of the fact that the annual pattern of precipitation and evaporation difference, P - E, is completely different in East Malaysia compared to Peninsular Malaysia. It is shown that this difference is also positive in both Sabah and Sarawak. Higher values of P - E are observed in the southern part of Sarawak, while lower values are registered further north. The principal role of the monthly distribution of P - E is given by the double passage of the Intertropical Convergence Zone (ITCZ). The secondary role is given by both the NE and the SW monsoon winds.

Keywords: Intertropical Convergence Zone, Southeast monsoon, Northeast monsoon, inter-monsoon period

INTRODUCTION

El Niño represents the warm phase of the Southern Oscillation. This process is known by the acronym of ENSO (El Niño Southern Oscillation) events. Whenever ENSO events occur, droughts in Indonesia, Sri Lanka and southern India happen. During the 1982-83, the 1986-87 and the 1991-93 ENSO events, a significant distortion of the precipitation pattern has been registered in Peninsular Malaysia (Camerlengo *et al.* 1998). It is believed that local effects, such as monsoon winds and sea breeze, tend to mask the deficit of precipitation that occurs in this area during ENSO events. On the other hand, East Malaysia registers an important deficit of precipitation during the above three mentioned ENSO events (Camerlengo *et al.* 1997). Further investigation is needed to determine the variability of parameters other than precipitation, such as insolation, evaporation, incoming short wave solar radiation, sea surface

temperature anomalies. To accomplish this task, a comparison between monthly climatological values of the above mentioned parameters and their monthly anomaly during ENSO events needs to be done.

A comprehensive knowledge of the climate of Malaysia is mandatory. The aim of our research is to gain a better knowledge of the principal dynamic aspects of the climatic pattern of Malaysia. In particular, the aim of the present study is to gain a better understanding of the monthly distribution of P - E in Sabah and Sarawak. No similar undertaking has been done before. Thus, this work represents the first of such an attempt. For this purpose, monthly records of ten stations are analyzed.

Our results are quite conclusive. It is established that the total amount of rainfall is greater than the total amount of evaporation. (In particular, P - E in Sarawak is higher than in Sabah.) This may be attributed to the fact that East Malaysia belongs to the "Maritime Continent" of the western Pacific and southeastern Asia (Philander 1990). Due to the fact that a low pressure system is usually located in Indonesia, the "Maritime Continent" is an area characterized by convective precipitation. This effect is frequently observed by satellite measurements in the form of outgoing long-wave radiation from the top of Cumulu-nimbus clouds.

The "Maritime Continent" undergoes an eastward migration during ENSO events. As a consequence of this, the climatic pattern of Southeast Asia suffers a severe distortion. Drought in Southeast Asia follows quite naturally, as registered in Indonesia and Australia during the severe 1982-83 ENSO event. In particular, palm oil production in the Philippines declines during an ENSO event (Glantz 1994).

The ultimate aim of our research is to understand how a "canonical" ENSO event disrupts the climatic pattern of Malaysia. Once this is known, we should be able to determine the economical losses of the Malaysian economy during ENSO events.

For the sake of convenience, the monthly distribution of P – E is only shown for typical months of both the north-east (NE) and the south-west (SW) monsoon seasons, as well as for a typical month of the transitional month between both monsoon seasons. As such, maps showing the monthly distribution of P – E for January, July and October are presented.

DATA

Monthly data of precipitation and evaporation at Kuching, Sri Aman, Sibu, Miri, Labuan, Kota Kinabalu, Sandakan, Bintulu, Kudat and Tawau are obtained from the "Monthly Summary of Meteorological Observations" published by the Malaysian Meteorological Service (1964-1993). The location of the meteorological stations as well as the years of monthly records are given in *Fig. 1.*

RESULTS AND DISCUSSION

In January the monthly distribution of P - E in East Malaysia is quite similar to the one observed in the east coast of Peninsular Malaysia (Camerlengo *et al.*

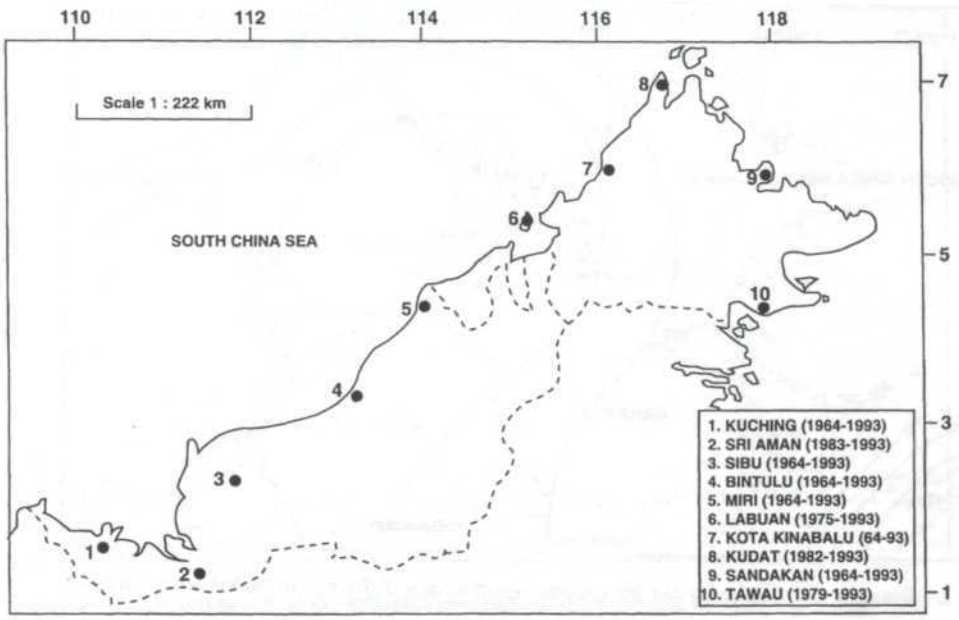

Fig 1. Location of both the precipitation and the evaporation stations being analyzed in this study. The years of records are indicated in parenthesis

1996). Higher values are registered in the southern part of East Malaysia, while lower or negative values are observed in Sabah (*Fig. 2*). The only exception is represented by Sandakan and Kudat. This may be attributed to their exposure to the NE monsoon winds. Higher values of P - E observed in Kuching, Sri Aman, Bintulu and Sibu may be explained by the southward motion of the convective area associated with the ITCZ.

The distribution of P - E has substantially lesser values in February compared to January, at all stations. This may be attributed to the fact that the ITCZ is in the southern hemisphere during February.

Negative values of P - E are observed in Sabah in March. The same situation is registered in the northern part of Peninsular Malaysia's east coast. Furthermore, Sarawak (with the single exception of Kuching) registers an increase of P - E in unison with the southern part of Peninsular Malaysia's east coast (with the single exception of Mersing (Camerlengo *et al.* 1996)). This phenomenon may largely be attributed to the fact that the sun crosses the equator on March 21st. It is well established that the ITCZ follows the motion of the sun (Necco 1980).

Negative values of P - E persist in Sabah during April. This may largely be attributed to the fact that April represents the transition period between the Northeast (NE) and the Southwest (SW) monsoon season (Nasir and Marghany 1996). Moreover, lower values are registered in Sarawak compared to the previous month. Cloudless skies prevail during the transition period. Thus, there is an increase of local evaporation values in April.

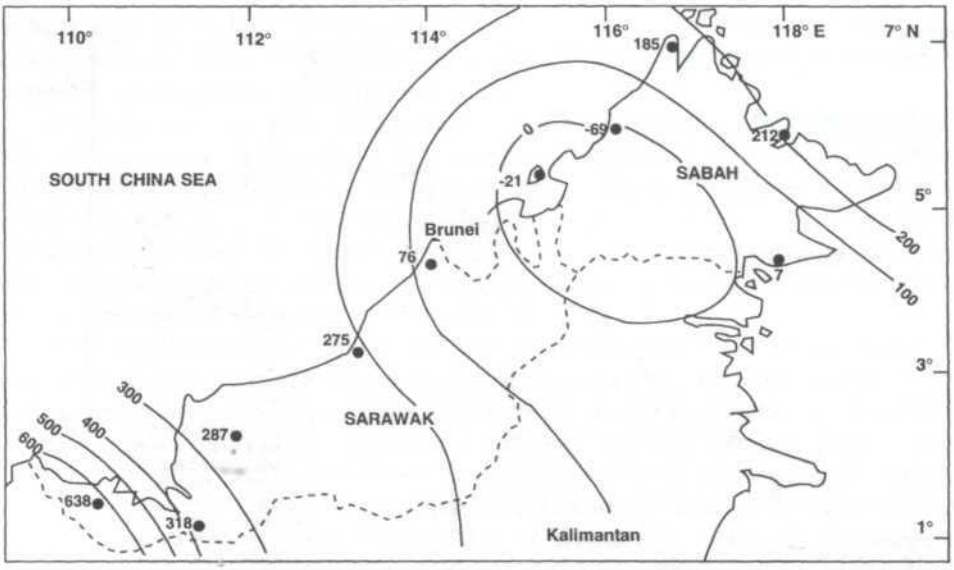

Fig 2. January distribution of the precipitation-evaporation difference in Sabah and Sarawak

From January to April, the situation in East Malaysia is strikingly similar to Peninsular Malaysia's east coast. Negative values in the northern part and positive values in the southern part exist.

May represents the onset of the SW monsoon season. Therefore, an increase of P - E values is observed in Sabah, in particular, in Labuan and Kota Kinabalu.

In June, positive values of P - E are observed, for the first time, at all stations in Sabah. At the same time, a decrease is observed in Sarawak (as compared to May). This may largely be explained by the northward motion of the ITCZ. The convective area associated with the ITCZ discharges its humidity in Sabah as it progresses northwards. Due to this same effect, precipitation in Sarawak is lesser than in the previous month.

A slight increase of P - E (with the exception of Kudat and Miri) is observed in July (*Fig. 3*). This may be attributed to the fact that precipitation values are higher (during July) due to the equatorward motion of the ITCZ, which in turn is related with the southern motion of the sun.

Due to the SW monsoon winds, the distribution of P - E is quite similar for both August and July. However, an increase of P - E is observed in September. This may largely be attributed to the fact that the sun crosses the equator on September 21st. The convective area associated with the ITCZ is responsible for the increase of precipitation being observed at all stations (with the single exception of Tawau) during September.

October P - E values are higher than in the previous month (*Fig. 4*). This should be attributed to the southward migration of the ITCZ. This effect is more obvious in the following month. Northeast monsoon winds are also responsible for larger precipitation values during November. These two combined

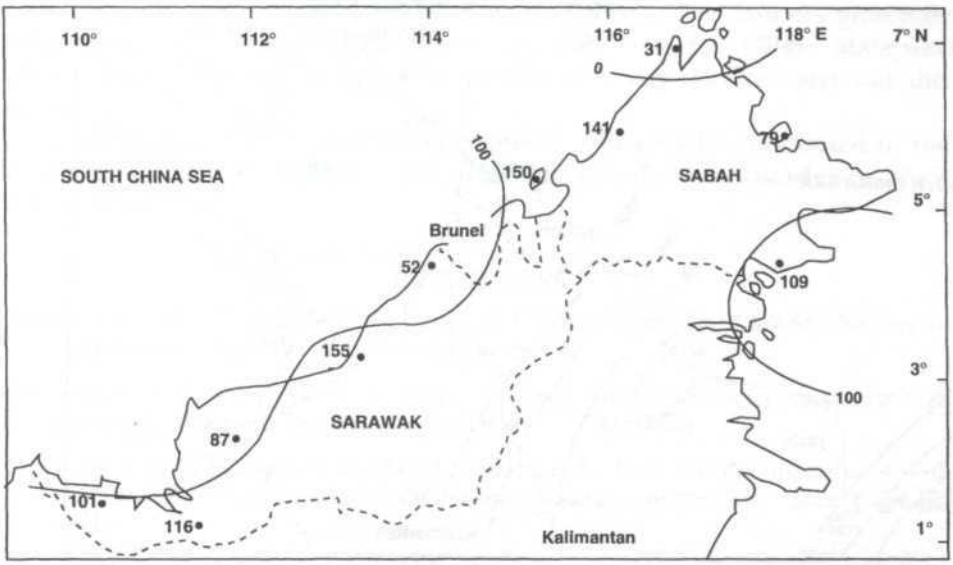

Fig 3. July distribution of the precipitation-evaporation difference in Sabah and Sarawak

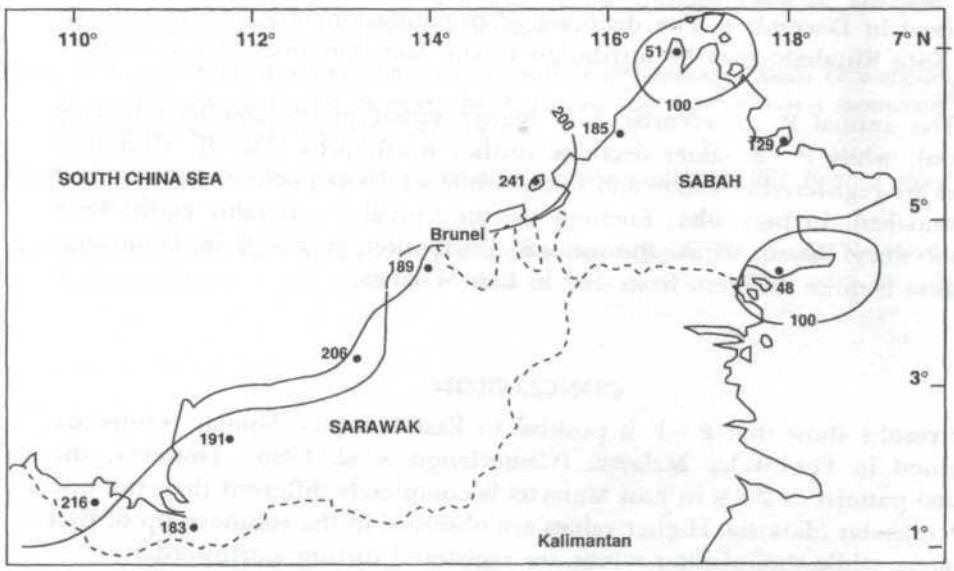

Fig 4. October distribution of the precipitation-evaporation difference in Sabah and Sarawak

effects - NE monsoon winds and the passage of the ITCZ - may be attributed to the high values of P - E observed in November.

The exposure of Sandakan, Kuching, Sibu, Miri, Bintulu, Sri Aman and Kudat to the NE monsoon winds is responsible for the increase of P - E values

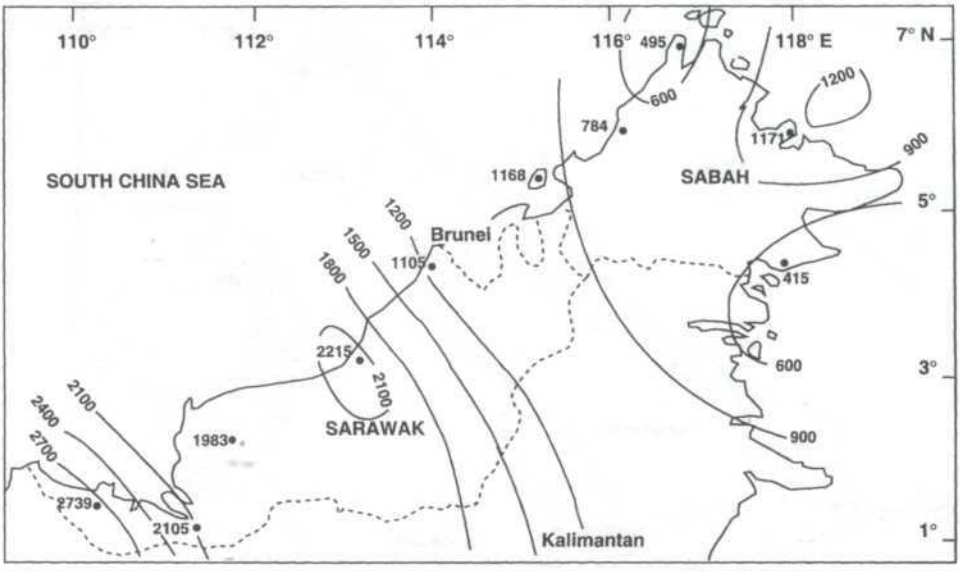

Fig 5. Annual distribution of the precipitation-evaporation difference in Sabah and Sarawak

observed in December. The decrease of precipitation observed in Labuan and Kota Kinabalu may be attributed to the fact that the ITCZ is further south.

The annual P - E records show higher values in the southern half of Sarawak, while P - E values decrease further northwards (*Fig. 4*). Minimum values are registered in Tawau and Kudat, while a relative maximum is observed in Sandakan. In particular, Kuching has an annual P - E value eight times higher than Tawau. Thus, the annual distribution of P - E in Peninsular Malaysia is quite different from that in East Malaysia.

CONCLUSION

Our results show that P - E is positive in East Malaysia. Similar results are obtained in Peninsular Malaysia (Camerlengo *et al.* 1996). However, the annual pattern of P - E in East Malaysia is completely different than the one in Peninsular Malaysia. Higher values are observed in the southern tip of East Malaysia, while diminishing values are registered further northwards.

The fact that P - E is positive verifies the fact that Malaysia is embedded in the "Maritime Continent" of Southeast Asia (Philander 1990).

The principal role of the distribution of P - E is given by the double passage of the ITCZ. The secondary role is given by both the NE and the SW monsoon winds. In this regard, previous results obtained for Peninsular Malaysia are confirmed.

ACKNOWLEDGMENTS

This research was supported by UPM in its entirety. The authors gratefully acknowledge this support. Our thanks are also extended to the Malaysian Meteorological Service for providing us the necessary data to carry out this investigation.

Comments made by anonymous reviewers substantially contributed to the improvement of this paper. The authors gratefully acknowledge their contribution.

REFERENCES

CAMERLENGO, A. L., M. NASIR S., K. C. JALAL and T. YANAGI. 1998. The 1982-83 ENSO event in Peninsular Malaysia. *Ultra Scientist* (in Press).

CAMERLENGO, A. L., M. NASIR S. A. SHAZILI A. 1996. Precipitation-evaporation ratio in Peninsular Malaysia. *Meteorologica* (in Press).

CAMERLENGO, A. L, M. NASIR S. and M. MAHATIR M. b. O. 1997. On the influence of both the 1982-83 and the 1986-87 ENSO events in Sabah and Sarawak. *Malay. J. Sci.* (in Press).

GLANTZ, M. H. 1994. Forecasting El Niño: Science's gift to the 21st century. *Ecodecision*. 78-81.

Malaysian Meteorological Service (1964-1993): Monthly Summary of Meteorological Observations. Issued under the authority of the Director General. Malaysian Meteorological Service, Petaling Jaya, Malaysia.

NASIR, M. S. and M. M. MARGHANY. 1996. On the surface circulation of Kuala Terengganu in the transitional period between the Northeast and the Southwest monsoons. *Pertanika J. Sci & Technol.* **4(1)**: 141-148.

NECCO, G. 1980. Curso de cinematica y dinamica de la atmosfera. p. 287. Buenos Aires: EUDEBA.

PHILANDER, S.G. 1990. El Niño, La Niña and the Southern Oscillation. p. 289. New York: Academic Press.

Pertanika J. Sci. & Technol. 8(1): 93 - 104 (2000)
ISSN: 0128-7680

Microcomputer-Based Data Acquisition System for Crop Production

Wan Ishak Wan Ismail, Azmi Yahya, and Mohd. Zohadie Bardaie
Department of Biological and Agricultural Engineering
Faculty of Engineering
Universiti Putra Malaysia
43400 UPM Serdang, Selangor, Malaysia

Received 31 December 1999

ABSTRAK

Sistem perolehan data asas mikrokomputer telah direkabentuk dan dibangunkan di Michigan State University, USA untuk mengendalikan pengajian data di ladang. Rekabentuk sistem untuk penyelidikan ini dijalankan menggunakan mikrokomputer Apple IIe yang dipasang di atas traktor bagi tujuan mengumpul data. Penukar A113 Analog kepada Digit (A/D) telah dipilih untuk antara muka setiap isyarat analog kepada mikrokomputer. Dj TPM II yang didapati dipasaran telah digunakan untuk mempamirkan maklumat seperti laju enjin, laju traktor, kegelinciran roda pemacu, jarak perjalanan dan luas kawasan diliputi sejam. Pengeluaran frekuensi dari unit radar telah disalurkan melalui penukar frekuensi kepada voltan (F/V), supaya penukar AI13 Analog kepada Digit (A/D) boleh membacanya. Penggunaan bahanapi diukur menggunakan meter pengalir bahanapi EMCO pdp-1 yang dipasang pada saluran bahanapi enjin. Daya penarikan pembajak dan alat seret ditentukan oleh tolok tarikan yang dipasang pada bar penarik traktor. Sistem ini dibangunkan untuk mengumpul daya penarikan dan keperluan bahanapi untuk pelbagai alat pertanian di tanah yang pelbagai. Pada masa ini, Universiti Putra Malaysia telah membeli sebuah sistem 'Autotronic' yang dipasang atas traktor. Sistem tersebut berupaya mengukur laju enjin, jarak perjalanan, kelajuan hadapan, penggunaan bahanapi, kapasiti ladang, kegelinciran roda, daya mengufuk pada titik bar penarik dan daya daya penarikan pada sangkutan 3 mata. Dinamometer sangkutan 3 mata telah direkabentuk dan dibangunkan untuk mendapatkan maklumat ciri tarikan traktor dan ciri penarikan peralatan khusus untuk keadaan di Malaysia.

ABSTRACT

A Microcomputer-based data acquisition system was design and developed at Michigan State University, USA, to conduct field data studies. The system designed for the research carried out used an Apple IIe microcomputer for collecting data on-board the tractor. An AI13 Analog to Digital (A/D) convertor was chosen to interface each analog signal to the microcomputer. A commercially available Dj TPM II was employed to display information such as engine speed, ground speed, drive wheel slip, distance travelled and area covered per hour. The frequency output from the radar unit was channelled through a frequency to voltage (F/V) convertor, so that AI13 Analog to Digital (A/D) convertor could read it. The fuel consumption was measured using an EMCO pdp-1 fuel flow meter attached to the engine fuel line. The draft of the tillage and other drag equipment was determined using strain gauges attached to the drawbar of

the tractor. The system was developed to collect the draft and fuel requirements for various farm equipments on different kind of soils. Apparently, Universiti Putra Malaysia has purchased the available system on-board the tractor (Autotronic). The system is capable of measuring engine speed, distance travelled, forward speed, fuel consumption, field capacity, wheel slip, horizontal force at drawbar point and draft forces at the 3-point hitch. A 3-point hitch dynamometer was designed and developed to obtain information on tractive characteristics and implement draft characteristics that are typical for Malaysian conditions.

Keywords: data acquisition system, autotronic, draft requirement, energy requirement, crop production systems

INTRODUCTION

Energy limitations have directed agricultural engineering researchers to study and improve the efficiency of field machines through field data studies. Information needs to be collected to adequately evaluate crop production and to be able to choose alternative crop production or tillage systems. Among the information is the draft and fuel requirements on different soils of major crop production systems. Soil types, soil conditions, operation depths, operation speed and type and size of implements will determine the draft and fuel required and the traction ability of the tractor in the field. Implement draft requirement is an important consideration in selecting implements, tillage systems and tractor size that is compatible with the operation. In addition to the required tractor size, implement draft will also be used to determine the fuel consumption of operation.

Microcomputers were increasingly utilized in the acquisition and processing of implement-tractor performance data. Thomson and Shinners (1987) reported using a portable instrument system to measure draft and speed of tillage implements. Measurements were taken and stored using a data logger, then transferred via magnetic cassette tape to a microcomputer for further processing. Carnegie *et al.* (1983), Clark and Adsit (1985), Bowers (1986), and Grogan et al. (1987), were examples of researchers who developed microcomputer-based data acquisition systems for measuring in field-tractor performance.

The system designed for the research carried out at Michigan State University, USA, used an Apple IIe microcomputer for collecting data on-board the tractor and an IBM microcomputer for data processing. The Apple IIe data acquisition system was developed by earlier researchers (Tembo 1986; Guo 1987; Mah 1990 and Wan Ishak 1991) at Michigan State University. The Apple IIe was chosen for its compactness and durability in adverse physical conditions as observed by Carnagie *et al.* (1983) and reported by Tembo (1986).

This paper discusses the instrumentation developed by the authors at Michigan State University, USA. The knowledge and experience of the authors were then applied to the system on-board the tractor (Autotronic) which was available at Universiti Putra Malaysia, Malaysia. A 3-point hitch dynamometer

was designed and developed and was used together with Autotronic to obtain draft and fuel information.

INSTRUMENTATION

Research carried out at Michigan State University, USA utilized a Ford 7610, 68.8 kw (86.95 hp) tractor. The tractor-on-board data acquisition system was developed for the infield data collection. The data acquisition system consists of Dickey John Tractor Performance Monitor II (DjTPM II) to measure the engine speed, ground speed and tractor front and rear wheels rotation speeds; an EMCO pdp-1 fuel flow transducer to measure the fuel consumption; and strain gauges to measure the draft of implements. The data obtained from the transducers were then recorded directly by the data acquisition system.

Speed Measurement

The Dickey-John Tractor Performance Monitor II (DjTPMII) consists of a Doppler radar unit, an engine rpm sensor, a magnetic pickup sensor used for determining drive wheel speed, an implement status switch, and a computerized console which displays information from the sensors.

Radar ground speed measurement was obtained by using the frequency signal generated from the DjTPMII radar unit. The radar unit and mounting bracket were installed so that the face of the unit projects onto an unobstructed view of the ground when facing rearwards. The nominal angle setting of the radar unit which determines the accuracy speed measurement was set and checked with a calibrated face plate and plumb bob. The frequency output from the radar unit was channelled through a Frequency to Voltage (F/V) converter, so that AI13 Analog to Digital (A/D) converter could read it. The F/V converter applied was an M1080 10 KHz converter.

Engine speed was obtained using the frequency signal generated by the DjTPMII engine rpm sensor. The engine rpm sensor fits between the existing mechanical drive sender and the tachometer cable leading to the operator's console. The sensor contained a separate keyed drive pin that was inserted into the tachometer drive sender. As the sender rotates, the sensor generates a frequency proportional to engine speed. The frequency signal from the sensor was routed through an M1080, 10KHz F/V converter, so it could be read by the AI13 A/D converter.

To measure the front and rear wheel rotational speeds, magnetic pickups supplied by Wabash Inc., Huntington, Indiana were used. In tachometry applications such as these, magnetic pickups produce an output frequency from an actuating gear in direct proportion to the rotational speed. The frequency produced was then converted directly to wheel rpm by means of a frequency-to-voltage converter (M1080). The signal produced in this mode was given as:

$$\text{Frequency (Hz)} = (\text{Number of sprocket teeth} * \text{wheel rpm})/60$$

The front wheel rotational speed sensor in the 2WD mode of the tractor used for the test served as the ground speed measuring sensor. The front wheel rotational speed sensor consisted of a 60 tooth sprocket mounted on the inner hub of the front wheel and a cylindrical pole piece magnetic pickup was mounted perpendicular to the sprocket teeth.

The rear wheel rotational speed measurement was used primarily for determining the drive wheel slip, in the 2WD mode. The rear wheel rotational speed sensor consisted of an 80 tooth sprocket mounted on the inner hub of the rear wheel and a Wabash Inc. cylindrical pole piece magnetic pickup was mounted in the same manner as the front wheel speed sensor.

Fuel Flow Measurement

The fuel consumption was measured using an EMCO pdp-1 fuel flow water meter attached to the engine fuel line. It was necessary to insert a three-way valve in the return line to bring the injector surplus fuel back into the line downstream from the flow meter. The magnetic flow counter of the flow meter generates an electric current pulse with a frequency directly proportional to the flow rate. The output of the flow meter was amplified before input to a Frequency-to-Voltage (M1080 F/V) converter. The amount of fuel and time consumed was captured directly by the data acquisition system.

Drawbar Draft Measurement

The draft of the tillage and planting equipment was determined using strain gauges attached to the drawbar of the tractor. Signals from the strain gauges were transferred to the signal conditioner. To enable the AI13 A/D converter to read the output signal from the strain gauges, a strain gauge signal conditional model M1060 was employed. The M1060 consists of a high quality difference amplifier with a variable stage gain, adjustable transducer excitation voltage (range : 3 to 12 volts) and provision to lower the excitation voltage to a value less than 3 volts. By applying the M1060 strain gauge conditioner, the low level millivolt strain gauge signal was amplified to the standard voltages (-5 to +5 volts), which is detectable by the AI13 A/D converter.

Calibration of Transducers

Calibration of the strain gauges for draft measurement was done using a Universal Testing Machine with a maximum load of 4627 kg (10200 lb). The calibration of the other transducers were carried out using a frequency function generator. Regression equations for each transducer were obtained.

The method used to arrive at the calibration equations was through estimating the maximum load expected for each of the transducers. The maximum expected loads (i.e. engine rpm, fuel consumption, ground speed, rear wheel speed and front wheel speed) were converted into frequencies. A frequency function generator was used to generate the maximum frequencies for their respective transducers which were later fed into the signal conditioner to obtain analogous voltages.

The calibration of the fuel flow meter was done using a custom-made frequency simulator that was designed to expand the narrow signal obtained from the sensor to one that the conditioner could display. The frequency simulator had four preset frequency levels of 100 Hz, 250 Hz, 500 Hz, and 1000 Hz. These were used to determine the calibration equation for the fuel consumption. The respective equations and the coefficients of determination for each channel are listed in Table 1.

The Data Acquisition Hardware

The data acquisition system is capable of operating at high speeds, collecting up to 16 channels of data sequentially and storing the data into RANDOM-ACCESS-MEMORY (RAM) space in the microcomputer. The system consists of an AI13 Analog to Digital (A/D) converter (Interactive Structures Inc.) and a 65C02 microprocessor based microcomputer (Apple Ile, Apple Computer Co.). The analogue to digital conversion is the heart of the data acquisition system. It is the interface between the analog and digital domains. Analog signals were sampled, quantized and encoded into digital format. An M1000 series (Data Capture Technology) signal conditioner provided the required conditioning of all signals from the transducers to the A/D converter. *Fig. 1* shows how the transducer were connected to the data acquisition system.

The data acquisition system is powered by a 12VDC-120VAC, 60 Hz, 500 watt sinusoidal voltage converter. Input power to the converter is supplied by a 12 VDC battery with free floating ground. The signal from each sensor is passed through a signal conditioner and through an analog-to-digital converter. The data were stored as ASCII code in the Random Access Memory (RAM)of a microcomputer which was later transferred to a floppy disk. A second computer was used to convert the data from ASCII code to numerical values for analysis.

Model Equations

The equations for the draft and fuel consumption used in the model were obtained from ASAE D230.4 (ASAE 1990) and Machinery Management (FMO 1987). The implement draft was estimated based on the operation speed, operation depth and implement width. The operation speed and depth used

TABLE 1
Regression equation for the transducers

Channel	Gain Code	Transducer	Equations	R^2
6	0	Engine Rpm	Hz = v*0.08914+1.6936	0.9998
7	0	Ground Speed	Hz = mv*0.0978+2.2774	0.9992
8	0	Rear Wheel Rpm	Hz = mv*0.0835+2.7575	0.9988
9	0	Front Wheel Rpm	Hz = mv*0.0902+1.1103	0.9986
10	0	Draft	N = v*24000.664-12.857	0.9991
11	0	Fuel Consumption	Hz = mv*0.2036 + 0.8803	0.9999

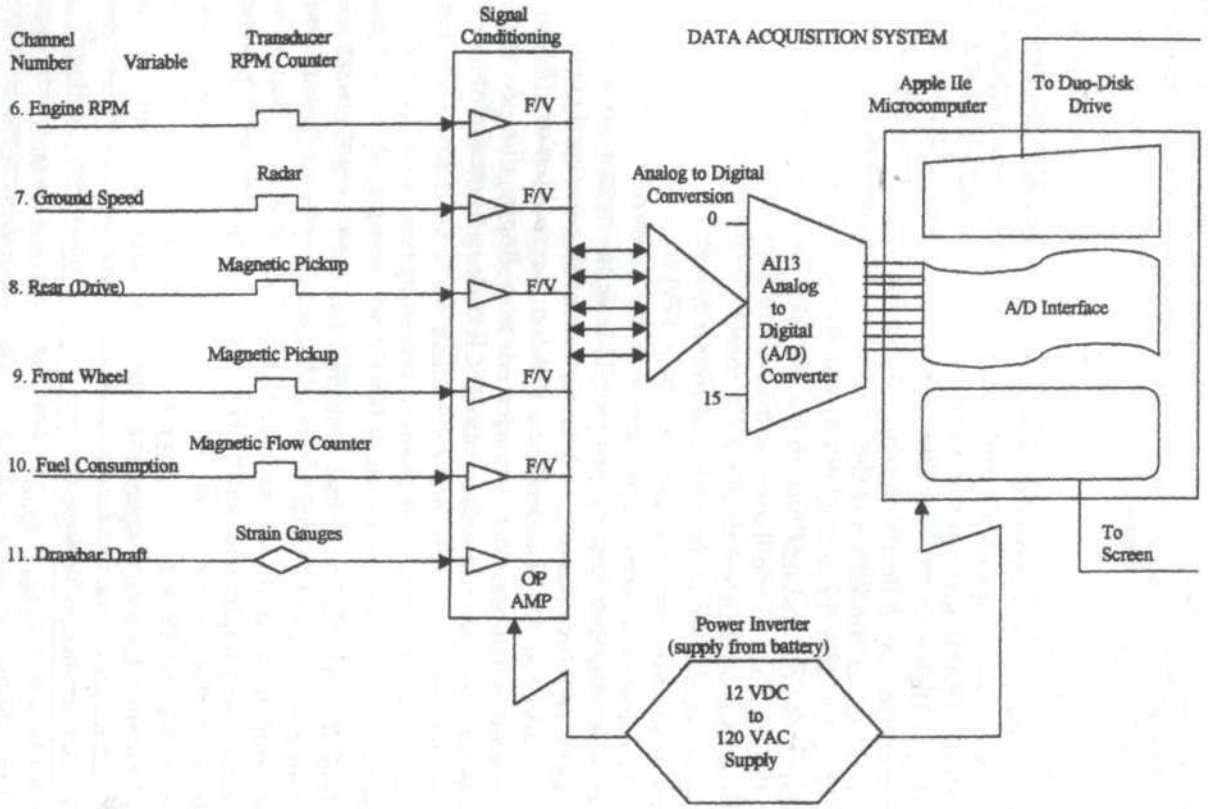

Fig 1. Block diagram of the data acquisition system hardware

were obtained from the experiment. The fuel required by each implement operation was estimated based on the implement equivalent power take-off power (EPTOP) and the tractor available power take-off power (APTOP). The implement EPTOP was calculated using the drawbar power and tractive efficiency. The implement drawbar power was calculated using the implement draft and operation speed. The tractive efficiency was estimated from the wheel slippage and soil cone index obtained from the field experiments. The tractor used in the experiment produced an APTOP of 64.1 kW.

Field Experiments

The field experiments were carried out on a farm at Michigan State University (MSU) and in Clinton county, Michigan. The implements used for the field experiments were a moldboard plow, chisel plow, tandem disk harrow, field cultivators, row crop planters, and grain drills. Experiments were carried out on different soils at different speeds and depths of operation. Data were also obtained and recorded on previously tilled areas.

Special care was taken to provide a stable source of electrical power during operation. The data collected were stored temporarily in RAM memory during each experimental run of the tractor. The data were stored as an ASCII file so that they can be easily transferred to other computers of analysis. About 500 to 1000 data sets at 20 Hz frequency sampling were obtained for each experimental run. Each data set contained one data point for each of the six measured parameters. These data sets were used to calculate the engine rpm, ground speed, rear wheel revolution, front wheel revolution, wheel slip, implement draft, implement power requirement and fuel consumption. The data recorded using the on-board data acquisition system were then retrieved and transferred to an IBM personal computer. The fuel consumption, draft and drawbar power required by the implement are compared with the values computed by the computer model. Table 2 shows an example of the experimental and model draft and fuel requirements for chisel plow on Capac Loam Soil.

TABLE 2
Experiment and model draft and fuel requirements for chisel plow on Capac Loam soil

Speed, km/h	Depth, cm	Expt. Draft, KN	Expt. Fuel, L/h	Model Draft, KN	Model Fuel, L/h
3.68	25.00	22.06	13.32	15.97	14.28
5.26	25.00	16.37	10.92	13.88	13.27
5.39	25.00	20.56	16.31	17.47	14.81
4.69	25.00	22.26	17.86	16.86	15.04
5.01	20.00	16.92	11.03	13.71	13.24
5.34	20.00	17.47	11.86	13.94	14.00
6.82	20.00	18.38	16.23	14.98	13.78
8.44	13.00	11.39	12.84	10.47	10.92
8.20	10.00	8.44	8.43	7.97	9.58

RESEARCH IN MALAYSIA

A similar research was recently carried out at Universiti Putra Malaysia, in Malaysia. The ultimate objective of the research work was to develop an information database on the draft and energy requirements of various field operations that are involved in the agricultural production in Malaysia. A 3-point hitch dynamometer was designed and developed by Azmi *et al.* (1994) to obtain information on tractive characteristics and implement draft characteristics that are typical for Malaysian conditions. Work was also currently underway to develop a data acquisition system for a tractor with the capability of measuring and recording performance data of the tractor-implement operating in the field. Apparently, the available system on-board the tractor is capable of measuring engine speed, pto speed, distance travelled, forward speed, fuel consumption, field capability, wheel slip, horizontal force at drawbar point and draft foresat the 3-point hitch.

Data Acquisition System

The employed data acquisition system was the product of Data Electronics (Australia) Pty. Ltd. The whole system consists of Datataker 605 unit, a Channel Expansion Module, a Memory Card Reader-Programmer and a Compact Contura 3/25c Notebook.

The Datataker 605 unit is a microprocessor based data logger that can be either internally powered by a 6 volt cell or externally powered from any 8-28 Volt AC/DC source. It has a 64 K bytes of internal battery backed RAM that is capable of storing in excess of 16,000 readings at a sampling rate of 25 samples per second, and at the same time supports optional plug in credit card sized in 1 M byte memory card for additional data storage up to 330,000 readings. Each bridge circuitary on the beam transducer is independently wired to the individual channels of the Datataker 605 unit. The constant current bridge configuration was employed for strain-gauges on the centilever beam transducers for the reason of obtaining better measurement accuracy. The bridge sensivity with such a configuration is known to be independent of the cable length. Apparently six of the 10 available channels on the Datataker 605 unit are being utilized for the transducer's circuitary. Additional two channels are wired individually to two toggle switches. The first toggle-type switch is used to trigger the Datataker 605 unit for taking initial readings while the second switch is for the actual data collections and recordings.

The compact Contura 3/25c notebook with in-house Decipher Plus software is used as the host computer. The Datataker 605 unit can be executed directly from the host computer or by the programme commands that has been earlier pre-recorded into the memory card. The command programme will be automatically executed whenever the memory card is inserted to the Datataker 605 unit. The Memory Card Reader-Programmer is used with the host computer to log the programme commands into the memory card. The communications between the host computer with the Memory Card Reader-Programmer and the Datataker 605 unit were made via the RS232 COMMS

serial interface. *Fig. 2* shows the block diagram of the complete datatronic instrumentation and data acquisition system for the tractor.

System Command Program

Field operation of the 3-pont hitch dynamometer was conducted with the Datataker 605 running under the prerecorded programme command in the memory card. As for the purpose, a command programme was written from the Datataker 605 to scan, sample and receive the signals from the available circuitary channels of the beam transducers, and logged all measured signals into the memory card. Upon the completion of the field operation test, all the stored data in the memory card would be downloaded to the storage medium of the host computer with the use of the memory card Reader-Programmer at the laboratory. The stored data were in standard ASCII character strings and could be imported into any available text editors, word processors, spreadsheets and graphical packages.

The command programme structure began with the conditional tests on the status of the two available external toggle switches marked as SWITCH-1 and SWITCH-2. The switches were individually wired to the digital input signal of the Datataker 605 unit. Triggering SWITCH-1 would indirectly execute the subcommand programme from taking the initial force readings. This subcommand programme was written to scan and record input signals at channel 1 to 6 of the Datataker 605 unit at 1 second sampling interval, 30 seconds averaging and recording interval, and for the total duration of 15

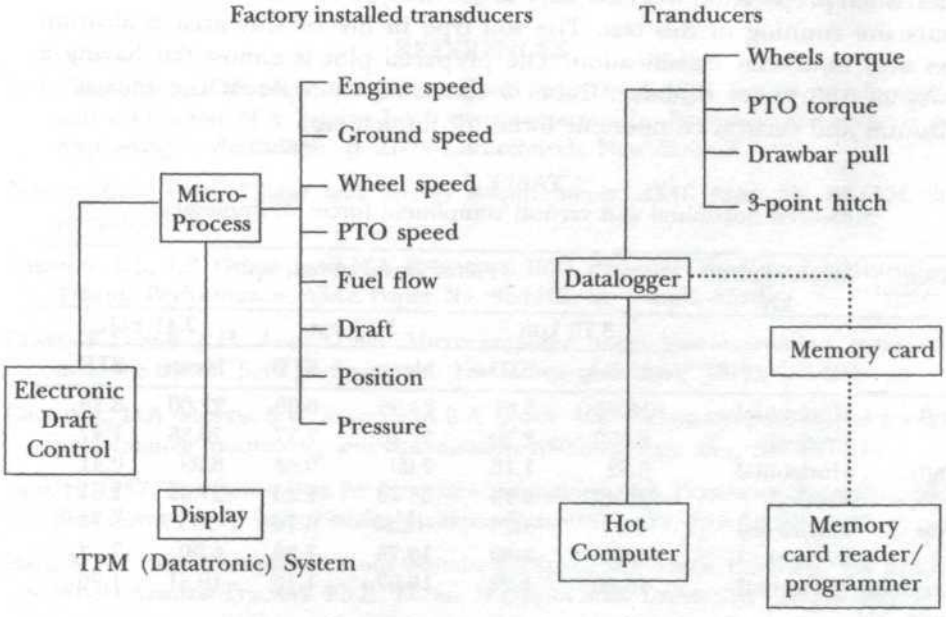

Fig 2. Block diagram of the tractor instrumentation system

minutes. Average reading from each channel was computed to give the initial value for the vertical and horizontal force measurements. Activating SWITCH-2 would indirectly execute the sub-command for the actual force measurements. Consequently, this sub-command programme was written to scan and record the six input channels at 1 second sampling interval, 1 minute averaging and recording interval, and for the duration of time SWITCH-2 was left activated. The collected data would be stored in accordance to the specified format and units with the earlier initial values taken care of.

Field Experiments

A field demonstration test was conducted to observe the performance of the 3-point linkage dynamometer and its data acquisition system in measuring and recording the implement forces during actual operation. A 2-654 disk plow was mounted to the tractor together with the 3-point linkage dynamometer. Two specially made steel DAS boxes were made to house the Datataker 605 unit together with the Channel Expansion Module and the COMPAC Contura 3/25c Notebook. These two boxes were then securely bolted to a rigid made frame rack located beside the operator seat in the tractor cab. The available auxiliary 12 DC volt point source inside the cab was employed to run the set-up data acquisition system.

The demonstration test was conducted at the closed-by University Research Farm of University Putra Malaysia. The test was conducted at three different gear combinations with specified travelled speeds of 3.70, 5.37 and 7.41 kph, respectively. The acquired field plot for the test was once rotovated a day earlier. Such preparation was necessary to get the type of terrain conditions that favours the running of this test. The soil type in the locality area is aluvium series with sandy-clay classification. The prepared plot is almost flat having a runway of 100 meter distance. Table 3 shows an example of the measured horizontal and vertical component forces of implement.

TABLE 3
Measured horizontal and vertical component forces of implement

Beam	Measurement, kN	Tractor travel speed, kph					
		3.70 kph		5.37 kph		7.41 kph	
		Mean	STD	Mean	STD	Mean	STD
Left	Horizontal	18.75	5.61	24.95	6.99	22.00	8.78
	Vertical	22.20	2.70	27.26	2.77	26.38	1.47
Right	Horizontal	6.62	1.15	7.09	0.58	8.09	0.41
	Vertical	23.45	4.15	25.73	2.23	27.59	1.61
Top	Horizontal	-9.17	5.26	-12.37	6.70	-10.27	8.78
	Vertical	6.00	3.39	10.75	2.58	6.00	7.12
Resultant horizontal force, kN		15.80	1.72	19.67	1.16	19.81	1.96
Resultant vertical force, kN		51.65	3.37	63.74	2.67	59.96	4.98

On the day of the test, the already pre-recorded command programme in the memory card was entered into the data acquisition system on-board the tractor at the laboratory. Once this was entered, the system was set on halt and set ready to begin the data initiation or collection task upon triggering and activating the respective switches on the DAS box. The sampling and recording of the initial reading were taken prior to the beginning of the test run when the tractor was stationary with its disk plow being slightly raised off the ground at the field plot. The tractor was then set for the plowing operation at its rated engine speed in the selected test gear combinations.

CONCLUSION

Information database on the energy requirements of various field operations that are involved in crop production is very important for the machine design and farm managers. Computer data acquisition systems have been the most significant tools in the development of agriculture. Researchers at Michigan State University, USA have successfully developed the Tractor-on-board data acquisition system, able to measure the draft and fuel requirements. The draft and fuel consumptions were used to determine the size and number of tractors and implements to be used for a particular farm size. Researchers at University Putra Malaysia are developing an information database on various field operation using the available Tractor-on-board system (Autotronic). The data acquisition system on-board the tractor for the dynamometer was able to receive and record the signal inputs from the transducers. The system has demonstrated to perform excellently under the present tractor noise and vibration levels at the field.

REFERENCES

AZMI YAHYA, Mohd Z. Bardaie, Koh J. Hoong and Peter David. 1994. Design, development and calibration of a 3-point hitch dynamometer. In *Proceedings of Conference on Engineering in Agriculture.* p. 21-24 Christchurch, New Zealand.

BOWERS, C.G. 1986. Tillage and Energy Requirements. *ASAE Paper No. 86-1524.* St. Joseph: ASAE.

CARNEGIE, E.J., R.R. GRINNEL and N.A. RICHARSON. 1983. Personal Computer for Measuring Tractor Performance. ASAE Paper No. 83-1165. St. Joseph: ASAE.

CLARK. R.L and A.H. ADSIT. 1985. Microcomputer based instrumentation system to measure tractor field performance. *Transaction of the ASAE* **28(2):** 393-396.

GROGAN J., D.A. MORRIS, S.W. SEARCY and B.A. STOUT. 1987. Microcomputer-based tractor performance monitoring and optimization system. *J. Agri. Eng. Res.* 227-243.

GUO, H. 1987. The Power Disk Performance Evaluation - Disk Trajectory Simulation and Side Force Study. M.S. Thesis, Michigan State University, East Lansing, MI.

MAH, M.M. 1990. Analysis of Front Mounted Three-Point Hitch Geometry on Front-Wheel Assisted Tractors. Ph.D. Thesis, Michigan State University, East Lansing, MI.

TEMBO, S. 1986. Performance Evaluation of the Power-DISK-a PTO Driven Disk Tiller. M.S. Thesis, Michigan State University, East Lansing, MI.

THOMSON, N.P., AND K.J. SHINNERS. 1987. A Portable Instrumentation System for Measuring Tillage Draft and Speed. *ASAE paper No. 87-1521.* St. Joseph: ASAE.

WAN ISHAK WAN ISMAIL, 1991. Simulation Model for Field Crop Production Machinery System. Ph.D Thesis, Michigan State University, East Lansing, MI.

ISSN: 0128-7680
Pertanika J. Sci. & Technol. **8(1)**: 105 - 115 (2000)

Drying Characteristics of Malaysian Padi

Wan Ramli Wan Daud, Muhammad Niazul Haque Sarker and Meor Zainal Meor Talib

Department of Chemical & Process Engineering
Universiti Kebangsaan Malaysia
43600 UKM Bangi, Selangor, Malaysia

Received: 15 April 1998

ABSTRAK

Dalam karya ini, kelakuan pengeringan padi Malaysia dikaji dengan menggunakan kaedah lapisan nipis. Lengkung pengeringan cirian padi ditentukan dengan menggunakan kebuk sekitaran. Uji kaji meliputi suhu udara antara 30°C hingga 70°C, kelembapan udara 30% hingga 80% dan halaju udara 0.12 hingga 1 m/s. Tempoh kadar malar tidak dicerap. Kehilangan jisim, suhu, kelembapan nisbi, dan halaju udara diawasi melalui komputer peribadi. Lengkung pengeringan menunjukkan dua tempoh kadar menurun, iaitu tempoh pengeringan awal yang laju dan seterusnya tempoh pengeringan yang perlahan. Kadar pengeringan ternormal melawan kandungan lembapan ternormal diregresikan dengan kaedah ganda dua terkecil untuk memadankan model polinomial baru untuk tempoh kadar menurun pertama dan model linear untuk tempoh kadar menurun kedua Model-model ini menganggar kedua-dua tempoh kadar menurun dengan baik.

ABSTRACT

In this paper, the drying behaviour of Malaysian padi was studied using the thin layer method. Characteristic drying curves of padi were determined using an environmental chamber. The experiments were conducted over a temperature range of between 30°C to 70°C, air relative humidity from 30% to 80% and air velocity from 0.12 to 1 m/s. No constant rate periods was observed. Mass loss, temperature, relative humidity and air velocity were monitored on a personal computer. From the drying curves, two falling rate periods were observed, namely an initial rapid drying period and a subsequent gradual drying period. The normalised drying rate versus normalised moisture content was regressed by least square method to fit a new polynomial model for the first falling rate period and a linear model for the second falling rate period. Both the polynomial and linear models estimate the falling rate periods quite well.

Keywords: Drying kinetics; thin layer method, characteristic drying curve

INTRODUCTION

Artificial drying of biological products such as padi, is one of the common methods of preservation. Proper drying procedures can eliminate the potential of spoilage during subsequent storage and the product quality can thus be improved. However rapid drying can increase brittleness and induce internal cracks which predispose the product to breakage during subsequent handling, and reducing its quality. The drying process must be understood and controlled

so that design guidelines which reduce and minimise drying damage to such products can be established or improved. This requires an accurate account of the drying process.

SEMI-EMPIRICAL AND EMPIRICAL DRYING CURVES OF CEREAL GRAINS

Most early workers such as Becker and Sallans (1955), Pabis and Henderson (1962) and Hustrulid (1963), used the solution the diffusion equation given by Crank (1969) directly:

$$\frac{X - X_e}{X_{cr} - X_e} = \frac{6}{\pi^2} \sum_{q=1}^{\infty} \frac{1}{q^2} \exp\left(-\frac{Dq^2\pi^2 t}{R^2}\right) \quad (1)$$

where X is the mean moisture content, X_{cr} is the critical moisture content, X_e is the equilibrium moisture content, D is the diffusion coefficient, R the diameter of cereal grain.

Other workers such as Thompson *et al.* (1968), Flood *et al.* (1972), and Noomhorn and Verma (1986) used the solution the diffusion equation to formulate a semi empirical drying equation of the form:

$$\frac{X - X_e}{X_{cr} - X_e} = \sum_{q=1}^{Q} K_q \exp\left(-k_q t\right) \quad (2)$$

The value of the coefficient Kq and exponent $_q$ vary with the authors.

The main problem with these types of equation is that drying is not simply controlled by diffusion alone. At the beginning of drying where the grain is fully saturated with water, the drying rate is controlled only by the evaporation rate at the surface. As drying progresses and surface water disappears, the drying rate is controlled by diffusion of water. In certain cases, further drying is controlled by a mixture of diffusion of water, evaporation and diffusion by vapour.

Freshly harvested padi has an average moisture content of 25 to 36% dry basis (d.b.). For safe storage, the padi must be dried to between 12 to 13%(d.b.). Early kinetic study by Keey (1978) has identified three distinct periods in padi drying, namely a short constant rate period, followed by a rapid first falling rate period and a much slower second falling rate period at the end. A more recent study by Kiyohiko Toyoda (1988) identified the two falling rate periods but did not observe a constant rate period.

There is therefore a need to use a more general drying equation to account for at least two periods of drying in padi.

THE CHARACTERISTIC DRYING CURVE

The characteristic drying curve is a simple model for extrapolating the drying behaviour of a material for different operating conditions. The model, whereby the drying rate and free moisture level are normalised by the constant drying

rate and critical moisture content respectively, was introduced by Van Meel (1958). A general form of the curve for the penetration falling rate period is normally given by the power law model:

$$f = f(\phi) \tag{3}$$

where, f is the normalised drying rate, ϕ is the normalised moisture content, $\phi = (X - X_e)/(X_{cr} - X_e)$. Langrish *et al.* (1991) used a three parameter set of equations to describe materials that exhibit both a penetration period and a regular regime:

$$f = \phi^n \qquad B < \phi < 1 \tag{4}$$

$$f = B^{(m-n)}\ \phi^m \qquad 0 < \phi < B \tag{5}$$

where B is the second critical moisture content, and m and n are constants that can be fitted from experimental data. Langrish *et al.* (1991) developed a technique to determine the parameters of the characteristic drying curve from flow drying experiments on thin layers of material. For materials that do not show any constant rate period of drying, the experimental curve may be divided into two periods, the induction period and falling rate period. In *Fig. 1*, point A is the transition between the two periods. In *Fig. 2*, the corresponding point A is also shown. The maximum average drying rate N_{max} and the average moisture content X_{ind} are defined at A. From *Fig. 1*, it is clear that no constant rate period of drying was observed. So we may define new functions:

$$g = \frac{f}{f_1} \tag{6}$$

$$\mu = \frac{\phi}{\phi_1} \tag{7}$$

where

$$f_1 = \frac{\dfrac{dX}{dt_{ind}}}{\dfrac{dX}{dt_{cr}}} \tag{8}$$

$$\phi_1 = \frac{X_{ind} - X_e}{X_{cr} - X_e} \tag{9}$$

where, X_{ind} is the moisture content at induction period.

The difficulty with the Langrish model is that it is only valid if the drying curves for both periods intersect the origin. In the case where the curve for the first period does not intersect the origin as in the case of padi drying, a new

model is proposed. The general polynomial given by the following equations is proposed as the new form of the curve:

$$g = \sum_{n=0}^{n} A_n \mu^n \qquad B < \mu < 1 \tag{10}$$

$$g = C\ \mu^m \qquad 0 < \mu < B \tag{11}$$

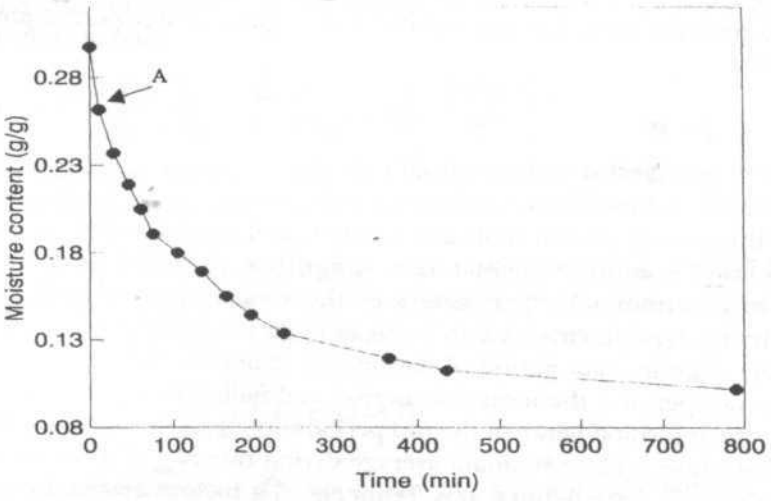

Fig 1. Time versus mass loss for padi at condition A1 indicating initial moisture content X_0 = 0.2969 (g/g), temperature T= 40°C, relative humidity RH = 45% and air velocity u = 0.96 m/s

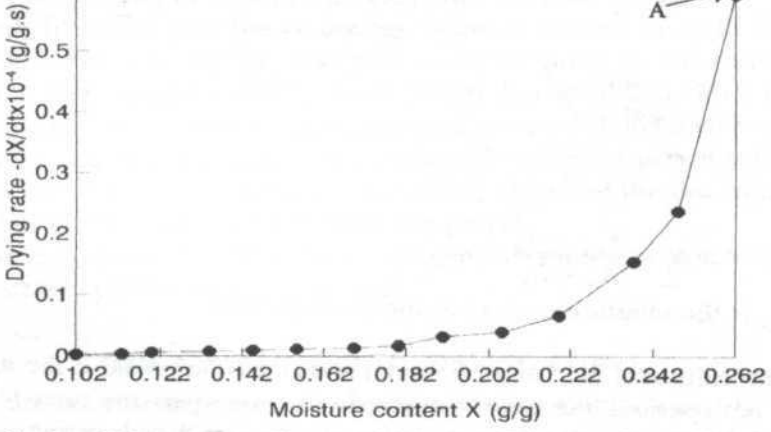

Fig 2. Moisture content (X) versus drying rate (-dX/dt) for padi at condition A1. X_{ind} = 0.2969

MATERIALS AND METHODS

Freshly harvested padi was collected from Tanjung Karang, Selangor, Malaysia. The sample was preserved in a container at 0°C temperature until used. No appreciable loss in mass was detected after the sample was thawed before use. The initial moisture content of the sample ranged from 23.6 % to 35.93 % (dry basis). The drying data were measured using an environmental chamber (μ-Isuzu). The environmental chamber can produce air velocity ranging from 0.12 m/s to 0.96 m/s, humidity range of 20 to 90% and temperature range of 20°C to 70°C. The actual operating conditions for the various experimental runs are given in Table 1. The variation of temperature and relative humidity in the chamber were ± 0.5°C and ± 3.0% respectively. A single layer padi was suspended by a balance from a Mettler AT250 electronic balance in the test section. Mass loss of the balance was monitored on a microcomputer connected to the balance via RS port, by using a data acquisition software. The temperature, relative humidity and velocity of the air were monitored on a microcomputer using a software SOLOMAT 4000 data acquisition system. Initial moisture content of the samples was determined according to the IDRC-053e, where two to five grams of the sample were grounded and weighed in a weighing bottle. The powdered sample was placed in an electric oven for 5 hours at a temperature of 130°C. It was then allowed to cool inside a dessiccator before weighing.

TABLE 1
Operating conditions of environmental chamber

Run No.	Initial Moisture content (g/g)	Air Temperature (°C)	Relative Humidity (%)	Air Velocity (m/s)
A1	0.2969	40	45	0.96
A2	0.2905	50	35	0.96
A3	0.2945	50	40	0.96
A4	0.2579	60	30	0.96
A5	0.2753	60	43	0.96
A6	0.2377	70	32	0.96
A7	0.2510	70	41	0.96
A8	0.2361	70	50	0.96
B1	0.3213	50	40	0.46
B2	0.2875	60	30	0.46
B3	0.2360	70	50	0.46
C1	0.2904	40	51	0.12
C2	0.3593	50	44	0.12
C3	0.3059	60	35	0.12
C4	0.3007	60	50	0.12

RESULTS AND DISCUSSION

One set of the experimental results is shown in *Figs. 1* and *2*. It is clearly evident from *Fig. 2* that the whole drying process is a falling rate drying period. The constant rate period is non-existent and the falling rate period can be divided into two. Period I is the shortest period and during this period, the drying rate decreases sharply. In period II, drying advances very slowly and the grains reach the equilibrium moisture content at the end of the drying.

The drying data are normalised using X_e value derived from padi desorption data. The normalised data are regressed by least square method according to Equation (8) up to third order and Equation (9) with the exponent m equal to unity to account for the linearity of the regular regime period. The results of the normalisation and regression are shown in Table 2 and in *Figs. 3, 4, 5, 6, 7* and *8*. The polynomial model estimates the characteristic drying curve quite well whereas the regular regime is found to be linear.

Once the data have been normalised and fitted to Equations (8) and (9) as described above, the reduced characteristic curves all fall into a tight band, indicating that the effect of variation in different conditions is small over the range tested. This trend is shown clearly in *Fig. 3* to *8*. The location of the second critical point in the normalised moisture content is determined by a discontinuity in slope and ranges from $B = 0.242$ to $B = 0.732$. The slope of the regular regime increases slightly with air velocity indicating a faster drying rate for higher velocities. The minimum effects of operating conditions on the

TABLE 2
Regression analysis of the characteristic drying curves of padi

Run No.	Induction drying rate ($x10^{-4}$ kg/kg dry matter s)	A_o	A_1	A_2	Regression Coefficient R^2	Second Critical Point (kg/kg)	Second Critical Point B	C	Regression Coefficient R^2
A1	0.598	1.9525	-6.5031	5.5176	0.982	0.192	0.732	0.0617	0.9640
A2	1.010	2.2213	-5.6785	5.9876	0.9721	0.179	0.688	0.0338	0.9430
A3	0.799	2.3106	-7.1934	5.8464	0.9231	0.135	0.573	0.0617	0.9150
A4	1.575	1.1869	-6.3791	5.4405	0.9627	0.130	0.607	0.0437	0.8796
A5	1.033	1.1464	-4.4938	4.2605	0.9610	0.130	0.527	0.0391	0.912
A6	1.280	0.4696	-2.0252	2.5533	0.9985	0.090	0.495	0.1105	0.9053
A7	1.240	0.7749	-3.0775	3.2854	0.9933	0.067	0.340	0.0601	0.9695
A8	1.502	0.7705	-3.1471	3.3534	0.9918	0.068	0.376	0.0685	0.8588
B1	0.775	0.6081	-2.6515	2.974	0.977	0.158	0.612	0.044	0.9548
B2	1.601	0.776	-3.3401	3.4549	0.9488	0.110	0.455	0.0299	0.9193
B3	1.302	0.5091	-2.4025	2.8537	0.9836	0.090	0.501	0.0438	0.9234
C1	0.960	0.9575	-3.9007	3.8185	0.9331	0.135	0.523	0.0205	0.8756
C2	0.803	0.5441	-2.6014	2.8933	0.9128	0.120	0.355	0.0274	0.9533
C3	1.980	0.7713	-3.2808	3.4267	0.9592	0.060	0.242	0.0327	0.9600
C4	1.240	0.442	-2.2778	2.7452	0.954	0.064	0.246	0.0273	0.9754

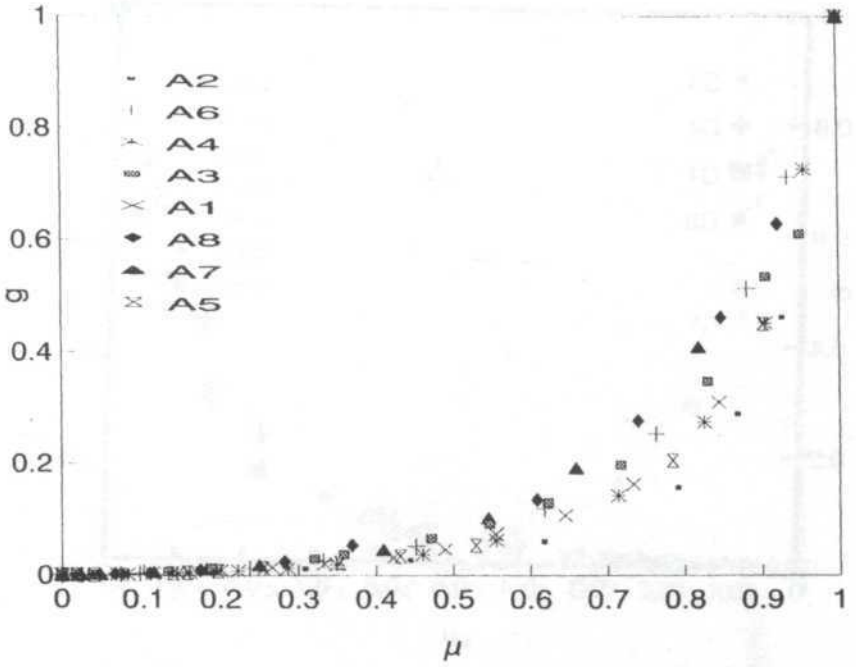

Fig 3. Normalised drying rate versus normalised moisture content for air velocity 0.96m/s

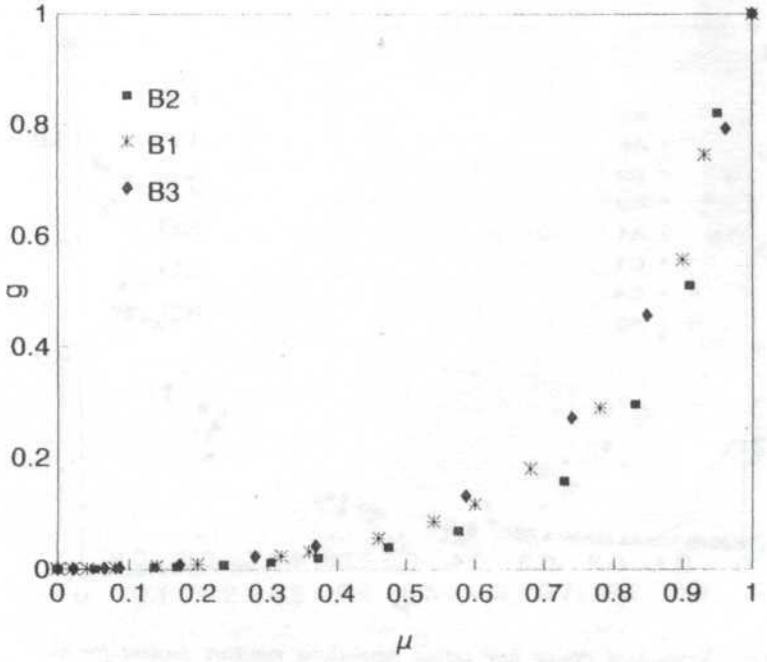

Fig 4. Normalised drying rate versus normalised moisture content for air velocity 0.46m/s

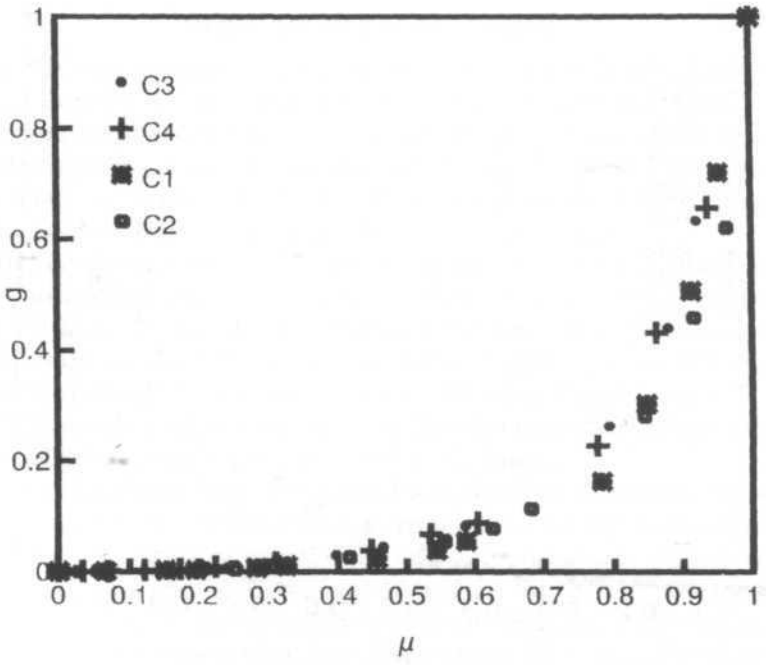

Fig 5. Normalised drying rate versus normalised moisture content for air velocity 0.12m/s

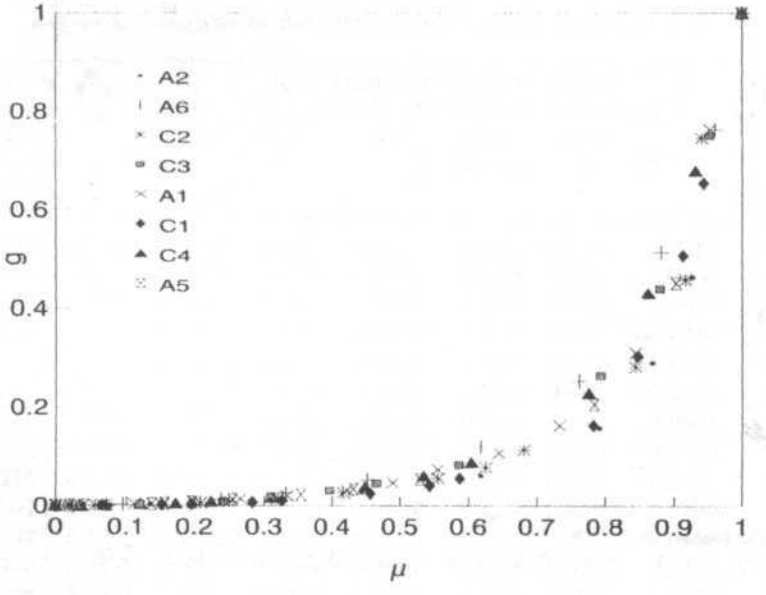

Fig 6. Normalised drying rate versus normalised moisture content for air velocity 0.96m/s and 0.12m/s.

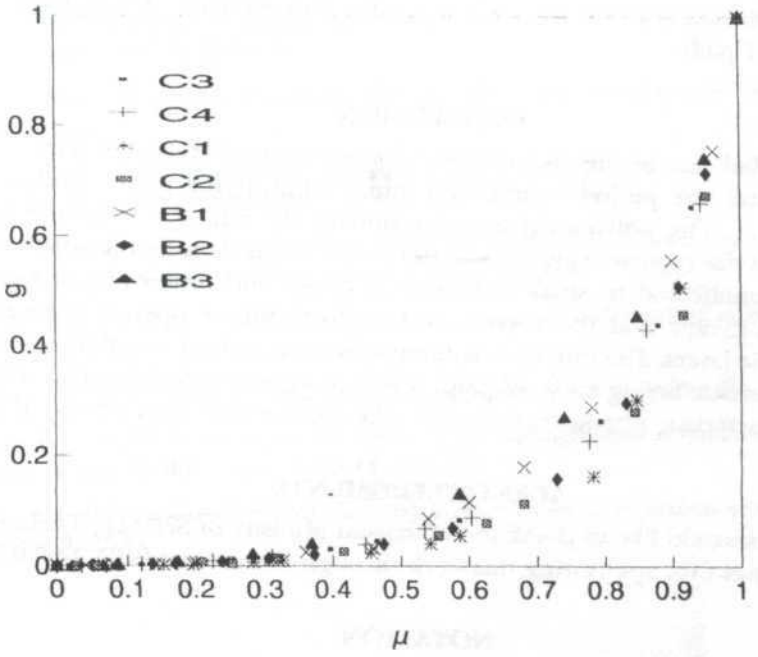

Fig 7. Normalised drying rate versus normalised moisture content for air velocity 0.46m/s and 0.12m/s.

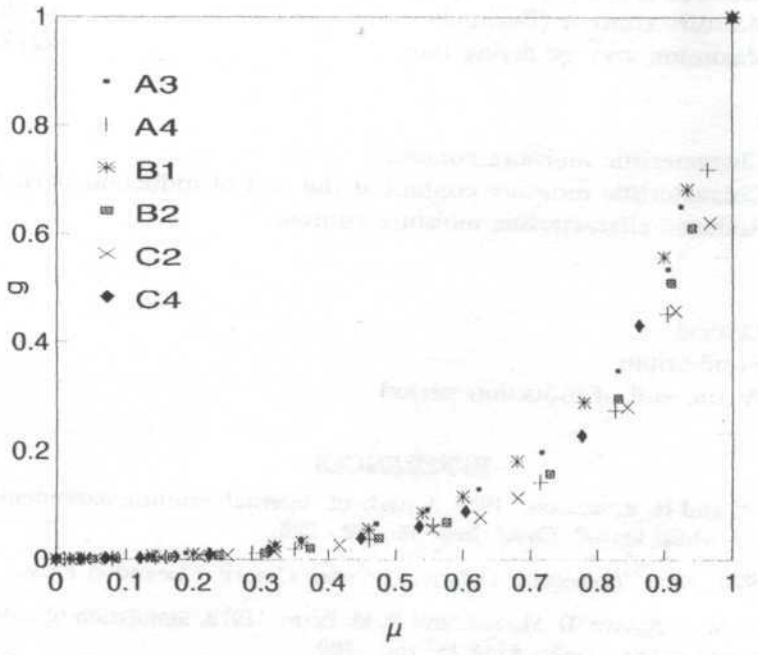

Fig 8. Normalised drying rate versus normalised moisture content for air velocity 0.96m/s , 0.46m/s and 0.12m/s

normalised curves confirm the existence of a characteristic drying curve for thin layers of padi.

CONCLUSION

It is concluded that in the characteristic drying curve of Malaysian padi, there are two falling rate periods, namely an initial rapid drying period and a slow drying period. The polynomial model estimates the falling rate period quite well whereas the regular regime was found to be linear. It is significant that the curves are unaffected by small variations in depth and uniformity of particle layers. This means that the curves are free from minor operating errors in arranging the layers. The thin layer technique is thus a robust way of determining the characteristic drying curve of padi. It is further concluded that the concept of the characteristic drying curve is also valid for the thin layer drying of padi.

ACKNOWLEDGMENTS

The authors would like to thank the Malaysian Ministry of Science, Technology & Environment for sponsoring this work through the project IRPA 1-07-03-014.

NOTATION

A, B, C	Parameters of characteristic function	
f	Characteristic drying rate	-
g	Reduced characteristic drying rate	-
X	Moisture content (Decimal)	kg/kg
N_{max}	Maximum average drying rate	kg/kg s

Greek letters

Φ	Characteristic moisture content
Φ_1	Characteristic moisture content at the end of induction period
μ	Reduced characteristic moisture content

Subscripts

cr	Critical
e	Equilibrium
ind	At the end of induction period

REFERENCES

BECKER, H. A. and H. R. SALLANS. 1955. A study of internal moisture movement in the drying of wheat kernel. *Cereal Chem.* **32**: 212 - 226.

CRANK, J. 1970. *The Mathematics of Diffusion.* 2nd edn. Oxford: Clarendon Press.

FLOOD, C. A., M. A. SABBAH. D. MECHER. and R. M. PEART. 1972. Simulation of natural air corn drying system. *Trans. ASAE* **15**: 156 - 160.

IDRC-053e. 1976. Rice: Postharvest Technology.

HUSTRULID. 1963. Comparative drying rates of naturally moist, remoistened and frozen wheat. *Trans. ASAE* **6**: 304-308.

KEEY, R.B. 1992. *Drying Loose Particulate Materials.* New York: Hemisphere Publishing Corporation.

KIYOHIKO TOYODA. 1988. Study on intermittent drying of rough rice in a recirculation dryer. In *Sixth International Drying Symposium IDS'88*, p.171-178.

LANGRISH, T.A.G., R.E. BAHU and D. REAY. 1991. Drying kinetics of particles from thin layer drying experiments, *Trans. IChemE* **69(A5)**: 417-424.

NOOMHORN, A. and L. R. VERMA. 1986. A generalized single-layer rice drying model. *ASAE Paper* **86**: 3057.

PABIS , S. and S. M. HENDERSON. 1962. Grain drying theory III. *J. Agric Eng. Res.* **7**: 21-28.

THOMPSON, T. L., R. M. PEART and G. H. FOSTER. 1968. Mathematical simulation of corn drying - a new model. *Trans. ASAE* **11**: 582-586.

VAN MEEL, D.A. 1958. Adiabatic Convection Batch Drying with recirculation of air. *Chem. Eng. Sci.* **9**: 36-44.

Preparation of Manuscript

General
The manuscript, including footnotes, tables, and captions for illustrations, should be typewritten double spaced on paper 210 x 297 mm in size, with margins of 40 mm on all sides. Three clear copies are required. Typing should be on one side of the paper only. Each page of the manuscript should be numbered, beginning with the title page.

Title page
The title of the paper, name of author and full address of the institution where the work was carried out should appear on this page. A short title not exceeding 60 characters should be provided for the running headline.

Abstract
Abstracts in Bahasa Melayu and English of not more than 200 words each are required for full articles and communications. No abbreviation should appear in the abstract. Manuscripts from outside of Malaysian may be submitted with an English abstract only.

Keywords
Up to a maximum of ten keywords are required and they should be placed directly below the abstract.

Footnotes
Footnotes to material in the text should not be used unless they are unavoidable. Where used in the text, footnotes should be designated by superscript Arabic numerals in serial order throughout the manuscript. Each footnote should be placed at the bottom of the manuscript page where reference to it is made.

Equations
These must be clearly typed, triple-spaced and should be identified by numbers in square brackets placed flush with the right margin. In numbering, no distinction is made between mathematical and chemical equations. routine structural formulae can be typeset and need not be submitted as figures for direct reproduction but they must be clearly depicted.

Tables
Tables should be numbered with Arabic numerals, have a brief title, and be referred to in the text. Columns headings and descriptive matter in tables should be brief. Vertical rules should not be used. Footnotes in tables should be designated by symbols or superscripts small italic letters. Descriptive materials not designated by a footnote may be placed under a table as a *note.*

Illustrations & Photographs
Illustration including diagrams and graphs are to be referred to in the text as 'figures' and photographs as 'plates' and numbered consecutively in Arabic numerals. All photographs (gloosy black and white prints) should be supplied with appropriate scales.

Illustrations should be of print quality; outputs from dotmatrix printers are not acceptable, Illustrations should be on separate sheets, about twice the size of the finished size in print. All letters, numbers and legends must be included on the illustration with the author's name, short title of the paper, and figure number written on the vereso. A list of captions should be provided on a separate sheet.

Unit of Measure
Metric units must be used for all measurements.

Citations and References
Items in the reference list should be referred to in the text by inserting, within parentheses, the year of publication after the author's name. If there are more than two authors, the first author should be cited followed by '*et al*'. The names of all authors, however, will appear in the reference list.

In the case of citing an author who has published more than one paper in the same year, the papers should be distinguished by addition of a small letter, e.g. Choa (1979a); Choa (1979b); Choa (1979c).

In the reference list, the names should be arranged alphabetically according to the name of the first author. Serials are to be abbreviated as in the *World List of Scientific Periodicals.*

The abbreviation for Pertanika Journal of Science and Technology is *Pertanika J. Sci. Technol.*

The following reference style is to be observed:

Monograph
Alefed, G. and J. Herzberger. 1983. *Introduction to Interval Computations.* New York: Academic Press.

Chapter in Edited Book
Muzzarell, R.A.A. 1980. Chitin. In *Polymers in Nature,* ed. E.A. MacGregor and C.T. Greenwood, p. 417-449. New York: John Wiley.

Serials
Kamaruzaman Ampon. 1991. The effect of attachment of hydrophobic imidoesters on the catalytic activity of trypsin. *Pertanika* **14(2)**: 18-185.

Proceedings
Mokhtaruddin, A.M. and L.M. Maene. 1981. Soil erosion under different crops and management practices. In *Agricultural Engineering in National Development,* ed. S.L. Choa, Mohd Zohdie Bardaie, N.C. Saxena and Van Vi Tran, p. 245-249. Serdang, Malaysia: Universiti Pertanian Malaysia Press.

Unpublished Materials (e.g. theses, reports & documents)

Sakri, 1. 1990. Proper construction set-up of Malaysian Fish Aggregating Devices (Unjam). Ph.D. Thesis, Universiti Pertanian Malaysia, Serdang, Selangor.